



universität
wien

DIPLOMARBEIT

Titel der Diplomarbeit

**„The Role of L-type Voltage-Gated Calcium-Channels in the
Discharge Activity of Primary Hippocampal Neurons“**

Verfasser

Michael Lagler

angestrebter akademischer Grad

Magister der Naturwissenschaften (Mag. rer.nat.)

Wien, 2009

Studienkennzahl lt. Studienblatt:	A 439
Studienrichtung lt. Studienblatt:	Biologie/Zoologie
Betreuerin / Betreuer:	Ao. Univ.-Prof. Karlheinz Hilber

CONTENTS

	Abstract	7
Chapter 1.	Introduction	9
Chapter 1.1.	General properties of voltage-gated Ca ²⁺ -channels (VGCCs)	10
Chapter 1.2.	Role of VGCCs in excitable cells	10
Chapter 1.3.	Classification of VGCCs	12
Chapter 1.4.	Molecular structure of VGCCs	13
Chapter 1.5.	L-type voltage-gated Ca ²⁺ -channels (LTCCs, Ca _v 1.x)	18
Chapter 1.5.1.	Expression and tissue distribution of LTCCs	18
Chapter 1.5.2.	Pharmacology of LTCCs	19
Chapter 1.5.3.	Electrophysiological properties of LTCCs	21
Chapter 1.6.	Ca ²⁺ -dependent ion channels	24
Chapter 1.6.1.	Classification and general properties of Ca ²⁺ -dependent K ⁺ -channels (K _(Ca) s)	24
Chapter 1.6.2.	Tissue distribution and different roles of K _(Ca) -channels in the neuronal discharge activity	26
Chapter 1.6.3.	Pharmacology of K _(Ca) -channels	28
Chapter 1.6.4.	Other Ca ²⁺ -dependent ion channels	30
Chapter 1.6.4.1.	Ca ²⁺ -dependent non-selective cation channels (CANs)	30
Chapter 1.6.4.2.	Transient receptor potential (TRP)M4-channels are Ca ²⁺ -activated monovalent cation channels	32
Chapter 1.6.4.3.	Ca ²⁺ -dependent Cl ⁻ -channels (Cl _(Ca) s)	33
Chapter 1.6.5.	Functional coupling of LTCC-mediated Ca ²⁺ -influx to different Ca ²⁺ -dependent ion channels	33
Chapter 1.6.5.1.	Functional coupling of LTCC to K _(Ca) 1.x	34
Chapter 1.6.5.2.	Functional coupling of LTCC to K _(Ca) 2.x, I _{mAHP} and I _{sAHP}	35
Chapter 1.6.5.3.	Functional coupling of LTCC to CAN	35
Chapter 1.7.	Specific question of this diploma thesis	37

Chapter 2.	Material and methods	39
Chapter 2.1.	Preparation of primary hippocampus culture from rats	39
Chapter 2.2.	Transformation, DNA purification and transient transfection of HEK-TSA cells	40
Chapter 2.3.	Solutions and drugs	42
Chapter 2.4.	Patch clamp set up and preparations for measurements	43
Chapter 2.5.	Correction of offset potentials	44
Chapter 2.5.1.	The liquid junction potential in whole cell experiments	47
Chapter 2.5.2.	The liquid junction potential in perforated patch experiments	48
Chapter 2.6.	Cell attached mode (gigaseal) and compensation of capacitive artifacts	49
Chapter 2.7.	Whole cell configuration, series resistance compensation and space clamp problem	50
Chapter 2.8.	The perforated patch configuration	53
Chapter 2.9.	Principles of voltage and current clamp	54
Chapter 2.10.	Filtering and digitization of signals	55
Chapter 2.11.	Leak subtraction, data analysis and statistics	56
Chapter 3.	Results	59
Chapter 3.1.	Comparison of different $Ca_v1.2$ and $Ca_v1.3$ constructs heterologously expressed in HEK-TSA cells	59
Chapter 3.2.	The role of $Ca_v1.3$ in hippocampal neurons	61
Chapter 3.2.1.	Determination of LTCC activation voltage	61
Chapter 3.3.	The regulation of hippocampal firing activity by LTCCs	63
Chapter 3.3.1.	LTCC-couplings in hippocampal neurons	63
Chapter 3.3.1.1.	Inhibition of LTCC-mediated AHPs by blocking $K_{Ca2.x}$ -channels with apamin or UCL 1684	66
Chapter 3.3.1.2.	LTCC-mediated ADPs were enhanced by blocking $K_{Ca2.x}$ -channels with apamin and inhibited by Na^+ substitution	67
Chapter 3.3.1.3.	De- and Hyperpolarizing LTCC-couplings differ in their “coupling efficiency”	69
Chapter 3.3.2.	The contribution of LTCCs to normal electrical discharge activity	71

Chapter 4.	Discussion	77
Chapter 4.1.	Ca _v 1.3long activates at more negative potentials than Ca _v 1.2α1C77	77
Chapter 4.2.	Ca _v 1.3 plays an important role in hippocampal neurons	77
Chapter 4.3.	The regulation of hippocampal firing activities by LTCCs	79
Chapter 4.3.1.	The LTCC-SK-interaction system forms sAHPs in hippocampal neurons	79
Chapter 4.3.2.	CAN-channels functionally couple to LTCCs and underlie the ADPs in hippocampal neurons	80
Chapter 4.3.3.	In hippocampal neurons the stimulus intensity determines the afterpotential modality	81
Chapter 4.3.4.	In hippocampal neurons LTCCs predominantly contribute to enhanced discharge activity	82
Chapter 5.	Bibliography	83
Chapter 6.	Appendix	97
Chapter 6.1.	Kurzfassung	97
Chapter 6.2.	Calculations of the LJP	
Chapter 6.2.1.	For whole cell configuration	99
Chapter6.2.2.	For perforated patch configuration	99
Chapter 6.3.	Statistics for chapters 3.2.1.1. and 3.2.1.2.	100
	Acknowledgements	103
	Curriculum vitae	105

ABSTRACT

L-type voltage-gated calcium channels (LTCCs) were shown to have several distinct roles in excitable cells. For example, Ca^{2+} -influx via LTCCs was shown to be an important component of the excitation-transcription coupling [West et al. 2002; Pinato et al. 2009]. Additionally, LTCC-mediated Ca^{2+} -influx can also affect membrane voltage and discharge properties, either directly or via activation of Ca^{2+} -dependent conductances, such as K^{+} - [Lima and Marrion 2007], or cation-channels [Lee and Tepper 2007].

Here I evaluated the contribution of LTCCs to the electrical activity of central neurons *in vitro*. Current-clamp experiments were performed on hippocampal neurons in culture using the perforated patch-clamp method to record the membrane voltage. The neurons were continuously superfused and LTCC-activity was modulated by application of the dihydropyridines BayK 8644 3 μM (enhanced LTCC-activity) and isradipine 3 μM (LTCC-inhibition), all in the presence of TTX. Activation of LTCCs was provoked by incremental current injections to depolarize the neurons experimentally. Doing so, LTCC-activation thresholds and LTCC-induced afterpotentials, occurring after the current pulse, were investigated.

Analysis of LTCC-activation revealed a distinct population of neurons with thresholds negative to -35 mV under control conditions. Since neuronal $\text{Ca}_v1.2$ -channel variations have never been found to activate at such negative potentials, these data argue for an important role of $\text{Ca}_v1.3$ -channels in hippocampal neurons. This findings stand in clear contrast to what has previously been concluded from results obtained with transgenic mice [Clark et al. 2003; Moosmang et al. 2005; Lacinova et al. 2008].

The afterpotential occurring as after-hyperpolarizations (AHPs) or after-depolarizations (ADPs) were typically seen already under control conditions, and increased with BayK. Using 8 s-long current pulses, in the majority (80 %) of neurons, the afterpotential was an AHP, which could be blocked by apamin 100 nM or UCL 1684 30 nM indicating the involvement of $\text{K}_{(\text{Ca})2.x}/\text{SK}$ -channels. $\text{K}_{(\text{Ca})2.x}$ -blockade also revealed that the hyperpolarizing afterpotential can either

represent a pure AHP (N = 10, afterpotential-area normalized to control under BayK: -1.37, 1.30 or BayK + apamin: 0.11, 1.00, $p < 0.001$) or an overlap of an AHP and ADP (N = 5, afterpotential-area normalized to control under BayK: -3.25, 8.05 or BayK + apamin: 18.99, 22.72, $p < 0.01$). In neurons, which showed a depolarizing afterpotential, the co-application of BayK and apamin as compared to BayK alone revealed a further enhancement of the ADP and therefore a concomitantly occurring AHP. Reduction of external $[Na^+]$ to 1.5 mM led to a significant diminishment of the ADP-area, suggesting that a Ca^{2+} -activated non selective cation (CAN) channel mediates the primary excitatory LTCC-coupling in the hippocampus (N = 7, afterpotential-area normalized to DMSO under BayK + apamin = 2.22, 3.99 or low Na^+ /BayK + apamin = 0.34, 0.68, $p < 0.01$, all values are given as median and interquartile range).

Moreover, variations of the current pulse duration (0.1 to 10 s) as well as the pulse strength indicated that LTCC-coupling to CAN- and SK-channels differs in its coupling efficiency: CAN-channels activate at weaker stimuli (shorter and/or smaller depolarization) than SK-channels and long-lasting (> 2 s) favored the SK-mediated AHP-formation. As the control discharge pattern of hippocampal neurons mainly consists of rather short-lasting (500 ms to 1 s) depolarizations, the predominant abundance of cells increasing their excitation, when I_{LTCC} is enhanced, is in accordance with the coupling-model described above.

From that, I suggest a certain balance between de- and hyperpolarizing LTCC-couplings as an important mechanism regulating the discharge activity in the hippocampus. This could include a CAN-mediated enhancement of short subthreshold potentials, such as in LTCC-dependent and NMDA-independent hippocampal LTP [Moosmang et al. 2005] as well as a SK-mediated protection against long-lasting excitotoxic LTCC-mediated plateau potentials occurring after SK-channels blockade [Ping et al. 1999]. In accordance with the latter assumption, the up-regulation of I_{CAN} is currently discussed in relation to Parkinson's disease [Lee and Tepper 2007].

To sum up, my data indicate that $Ca_v1.2$ as well as $Ca_v1.3$ contribute to hippocampal firing activities and suggest that in primary hippocampal neurons (I) LTCCs couple to both SK- and CAN-channels, (II) that in most hippocampal neurons both coupling modes operate in parallel and (III) that coupling efficiency differs among the two Ca^{2+} -dependent conductances.

1. INTRODUCTION

1.1. General properties of voltage-gated Ca²⁺-channels (VGCCs)

Voltage-gated Ca²⁺ channels are found in every excitable cell from *Paramecium sp.* to humans [Hagiwara 1983] (from [Hille 2001]) and share lots of their properties with voltage-gated Na⁺-channels (VGSCs) and voltage-gated K⁺ channels (VGKCs), such as depolarization induced opening, rapid deactivation in response to a membrane repolarization, some forms of channel inactivation and a relatively high ion selectivity [Lacinova et al. 2005]. Whereas some di(tri)valent cations permeate Ca²⁺ channels (sequence of ion permeability: Ba²⁺ > Sr²⁺ > Ca²⁺), others can block these channels at concentrations of 10 μM to 20 mM (strength of relative blocking: La³⁺ > Cd²⁺ > Co²⁺ > Mn²⁺ > Ni²⁺ (> Cd²⁺ in LVA Ca²⁺-channels) > Mg²⁺ [Hagiwara et al. 1967; Tsien et al. 1988] (from [Hille 2001])). It has been hypothesized that “blocking ions” dissociate so slowly from the channel that they hinder the permeation of rapidly moving permeating ions. Every VGCC-subfamily exhibits a characteristic profile of blocking sensitivities to different metal ions [Byerly 1988; Heinemann et al. 1992; Herrington et al. 1992; Hille 2001].

In comparison to VGSC-mediated Na⁺-currents, Ca²⁺-currents flowing through VGCCs usually exhibit a roughly 100-fold lower current density in neurons or myocytes, which lies in a range of 50 μA/cm² [Hille 2001]. The predicted equilibrium potential for Ca²⁺ (E_{Ca}) is at 124 mV, if 100 nM Ca²⁺ are at the inside and 2 mM Ca²⁺ are at the outside of the membrane. However, reversal potentials for Ca²⁺-currents are typically observed between 40 and 70 mV. This is caused by the impurity of Ca²⁺-outward currents through VGCCs contaminated with monovalent ions, such as K⁺ [Reuter et al. 1977; Fenwick et al. 1982; Lee et al. 1984; Zhou et al. 2000] (from [Hille 2001]).

1.2. Role of VGCCs in excitable cells

Besides their major roles of (I) translating electrical into chemical signals via neurotransmitter release and (II) the mediation of muscle fiber contraction as well as (III) exocytosis of endocrine cells, VGCCs also affect (IV) dendritic integration, (V) are involved in certain forms of synaptic plasticity (i.e. non-NMDA mediated LTP), (VI) modulate subthreshold potentials by opening and inactivating around the neuronal resting membrane potential and even (VII) carry the upstroke of certain action potentials (APs), known as Ca^{2+} -spike. In myocytes of arthropods, mollusks, nematodes and adult tunicates VGCCs entirely account for regenerative electrical excitation, whereas in most mammalian cell types VGCCs coexist with VGSCs and only partly contribute to the discharge behaviour. An exception is represented by APs in mammalian cardiac pacemaker cells of the sinu-atrial node and in smooth muscle cells, where no functional VGSCs are present and APs are exclusively carried by VGCCs. In ventricular myocytes, a high density of VGSCs is responsible for eliciting and propagating action potentials. However, most of these Na^+ -channels are inactivated after several milliseconds. Hence, Ca^{2+} -influx via VGCCs contributes to the plateau-phase of the ventricular action potential, which can last up to one second. To sum up, VGCCs are either able to shape AP elicited via Na^+ -currents, or induce regenerative AP-firing (for an overview see [Hille 2001]).

Moreover, VGCCs (VIII) control a variety of Ca^{2+} -dependent intracellular events including cell functions activated by Ca^{2+} as a second messenger. In the resting cell the internal $[\text{Ca}^{2+}]$ is kept at an extremely low level (between 30 and 200 nM) regulated by the combined action of various transport mechanisms, such as a Ca^{2+} -ATPase and a $\text{Na}^+/\text{Ca}^{2+}$ -antiporter both at the surface membrane and a Ca^{2+} -ATPase, a $\text{Na}^+/\text{Ca}^{2+}$ -antiporter and a $\text{H}^+/\text{Ca}^{2+}$ -exchanger in the membranes of intracellular organelles, especially of intracellular Ca^{2+} -stores like the endoplasmic and the sarcoplasmic reticulum or the mitochondrion. Due to the particularly low intracellular $[\text{Ca}^{2+}]$ the opening of Ca^{2+} -channels either in the surface membrane or in the membranes of the Ca^{2+} -loaded organelles can lead to local, yet substantial $[\text{Ca}^{2+}]$ -rises. The transient elevation of Ca^{2+} -ion concentration in the vicinity of the respective channels represents the trigger for further cellular actions and is in fundamental contrast to the situation with Na^+ or K^+ [Roberts 1994; Neher 1998] (from [Hille 2001]). Once Ca^{2+} -ions are locally accumulated in the cytoplasm, regulatory proteins with high-affinity Ca^{2+} -receptors, such as calmodulin, are activated by binding of Ca^{2+} -ions [Chin et al. 2000] (from [Hille 2001]). These proteins react very sensitively to changes in the internal $[\text{Ca}^{2+}]$ in their dynamic range between 0.1 and 10 μM . Activated Ca^{2+} -calmodulin activates enzymes like the CAM-kinase, which then causes protein-phosphorylation. The activated CAM-kinase then affects gene transcription either through direct cAMP response element-binding protein (CREB)-phosphorylation, or through indirect CREB-activation via rising the internal cAMP-level by phosphorylating the adenylyl cyclase (e.g. overviewed in [Alberts 2002]).

Coming back to one of the VGCC-functions, which is (I) the transduction of electrical excitation into the appropriate secretion of neurotransmitters at the presynaptic terminals of a neuron. If the

axon terminal is excited by a certain frequency of invading APs, its membrane gets depolarized, which therefore causes the opening of presynaptic VGCCs directly clustered at the docking site of the synaptic vesicles. Comparable to the situation discussed in the paragraph above, this is the call to action, in particular to the activation of the exocytosis-machinery including various proteins such as vesicular synaptotagmin, which is suggested to serve as the intracellular Ca^{2+} -sensor, and synaptobrevin, syntaxin and SNAP-25. Synaptobrevin, syntaxin and SNAP-25 together are termed as the so called SNARE-protein-complex, which is crucially involved in the process of pore-formation and represents the target for all known *Clostridia*-toxins (e.g. botulinum toxin and tetanospasmin). These toxins are zinc-endopeptidases, which are known to cleave SNARE-proteins and thus fully inhibit neurotransmission. Neurotransmitter secretion consists of 4 stages: (I) budding of vesicles from the Golgi apparatus, (II) targeting of vesicles in the active zone, (III) docking of vesicles at the presynaptic membrane and (IV) fusion of vesicles with the surface membrane, detectable by elevations in the cell capacitance. The whole process beginning with the arrival of APs until formation of neurotransmitter-permeable pores takes not longer than 0.1 ms. In detail, the intracellular accumulation of Ca^{2+} -ions induces CAM-kinase-activity, which leads to phosphorylation of Synapsin I. Phosphorylated synapsin I can not connect vesicles with the actinfilament any more, which therefore start to move towards the active zone of a synaptic bouton. As far as the docking of the vesicle is concerned, some SNARE-proteins act as donors (i.e. synaptobrevin) other as receptors (i.e. SNAP-25, syntaxin) interacting with each other. Furthermore, synaptotagmin interacts as a donor with neurexine, a receptor in the surface membrane. Regarding the building of the fusion-pore synaptophysin and physophilin are assumed to play an important role (for an overview see [Kandel 1996; Aktories 2009]).

Internal Ca^{2+} -concentrations also affect (IX) gating of ion channels. So far, a Ca^{2+} -dependency was reported for K^{+} -, Cl^{-} -, cation- and Ca^{2+} -channels itself, but also for the NMDA-receptor. All these ion channels have a Ca^{2+} - and/or Ca^{2+} -calmodulin-binding site on their intracellular surface in common (overviewed in [Hille 2001]). One aspect of internal $[\text{Ca}^{2+}]$ affecting VGCCs, the Ca^{2+} -dependent inactivation, will be discussed in chapter 3.3.1.3. The effect of intracellular Ca^{2+} -rises on specific K^{+} - and cation-channels is overviewed in chapter 3.3.1.4., where I will focus on L-type voltage-gated Ca^{2+} -channel (LTCC)-mediated Ca^{2+} -influx as the primary Ca^{2+} -source for activating Ca^{2+} -dependent conductances.

1.3. Classification of VGCCs

After the identification of VGSCs and VGKC and the postulation of a model for the action potential by [Hodgkin et al. 1952], VGCCs were added to the class of voltage-dependent ion channels, only later by [Fatt et al. 1953]. The initial VGCC subdivision referred to electrophysiological characteristics as well as differences in kinetic properties and pharmacology of the observed currents. As far as the voltage-dependency is concerned, Ca^{2+} currents with a high threshold of activation positive than -20 mV (high voltage activated, HVA), were separated from currents activating and inactivating near the neuronal resting potential at approximately -60 mV (low voltage activated, LVA, [Hagiwara et al. 1975; Llinas et al. 1981]). According to their small single channel conductance of about 8 pS as well as their complete and fast inactivation with a time constant of 20 to 50 ms, Tsien's group termed these channels T-type Ca^{2+} channels (TTCC, $\text{Ca}_v3.x$), while T stands for tiny and transient. Due to the fact that the first identified HVA currents exhibited large single channel conductances ($G = 25$ pS) and slow inactivation kinetics ($\tau > 500$ ms), they were called L-type (LTCC, $\text{Ca}_v1.x$) with L relating to large and long-lasting [Tsien et al. 1988; Snutch et al. 1990; Birnbaumer et al. 1994; Ertel et al. 2000] (from [Hille 2001]).

A new HVA-subdivision had to be made when it was discovered that only a subclass of HVAs is sensitive to 1,4-dihydropyridines (DHPs). Moreover, single channel recordings for the DHP-insensitive I_{HVA} revealed a conductance and inactivation rate lying between that of $\text{Ca}_v1.x$ and $\text{Ca}_v3.x$ ($G = 13$ pS, $\tau = 50 - 80$ ms [Tsien et al. 1988; Snutch et al. 1990; Birnbaumer et al. 1994; Ertel et al. 2000] (from [Hille 2001]) which was hence named N-type with N referring to "neither/nor" and "neuronal", where they were primarily detected [Nowycky et al. 1985; Fox et al. 1987]. Further pharmacological analysis using toxins from the pacific cone snails *Conus sp.* (ω -conotoxin GVIA) and from spiders like *Agelenopsis aperta* (ω -agatoxin IVA) divulged an additional inconstancy in the neuronal non-L-type class ($\text{Ca}_v2.x$), while the channels generating currents sensitive to ω -conotoxin GVIA in a low micromolar concentration kept the name of the previously formed group (NTCC, $\text{Ca}_v2.2$), whereas channels with ω -agatoxin IVA sensitivity were renamed P/Q-type (PTCC or QTCC, $\text{Ca}_v2.1$) with P as an abbreviation for Purkinje cells, where they were initially described [Llinas et al. 1989]. PTCCs and QTCCs consist of different $\alpha 1A$ -isoforms generated by alternative splicing and vary in their sensitivity to ω -agatoxin IVA (K_D for PTCC = ~ 2 nM, K_D for QTCC > 100 nM) as well as their inactivation kinetics [Bourinet et al. 1999]. A third non-L-type HVA fraction persisted, if both ω -conotoxin GVIA and ω -agatoxin IVA were applied. Henceforward this VGCC-subfamily was termed RTCC ($\text{Ca}_v2.3$, [Llinas et al. 1989]). Except for their pharmacological properties, the $\text{Ca}_v2.x$ -subfamily is functionally consistent with some form of voltage-dependent inactivation and the possible inhibition by G-protein-coupled receptors (GPCRs). The non-L-type HVA-channels are also the dominant VGCCs expressed in the presynaptic terminals, where they mediate Ca^{2+} -influx in response to invading APs and also form parts of the docking complex for synaptic vesicles [Catterall 2000].

The nomenclature distinguishing between different types of Ca^{2+} -channels bases on the one introduced by [Tsien et al. 1988], whereas the structural nomenclature using the $\text{Ca}_v x.y$ scheme concerning the individual $\alpha 1$ -subunits was established by [Ertel et al. 2000]. Cloning experiments revealed that voltage-operating Ca^{2+} -channels usually consist of 4 subunits. $\alpha 1$ is the principle one, which is pore-forming and defines the basic electrophysiological and pharmacological properties. β , $\alpha 2\delta$ and γ are so called auxiliary subunits with regulatory functions. 7 different HVA and 3 different LVA $\alpha 1$ subunits were cloned until now. Among the high voltage activated channels 4 different L-type $\alpha 1$ subunits ($\text{Ca}_v 1.1$ formerly termed $\alpha 1S$, $\text{Ca}_v 1.2$ ($\alpha 1C$), $\text{Ca}_v 1.3$ ($\alpha 1D$), $\text{Ca}_v 1.4$ ($\alpha 1F$) and one subtype each for the other three HVA Ca^{2+} -channels ($\text{Ca}_v 2.1$ ($\alpha 1A$), $\text{Ca}_v 2.2$ ($\alpha 1B$), $\text{Ca}_v 2.3$ ($\alpha 1E$)) are known to date. Concerning the T-type subfamily, three members were identified $\text{Ca}_v 3.1$ ($\alpha 1G$), $\text{Ca}_v 3.2$ ($\alpha 1H$) and $\text{Ca}_v 3.3$ ($\alpha 1I$) [Lacinova and Hofmann 2005].

Amino-acid sequence-comparisons of membrane-spanning regions of $\alpha 1$ -subunits proved the principal phylogenetic connection of channels belonging to the VGCC class. HVA and LVA Ca^{2+} channels share the lowest percentage of sequence homology (below 30 %), which represents the first separating event among voltage-gated Ca^{2+} channels. After that the HVA group split into L-type and non-L-type Ca^{2+} channels, which share about 50 % sequence homology. Members of the $\text{Ca}_v 1.x$ - and $\text{Ca}_v 2.x$ -subfamily showed more than 80 % matching of their amino-acid sequences. Finally, all known $\alpha 1$ -subunits have different splice variants with homologies higher than 95 % [Lacinova and Hofmann 2005].

1.4. Molecular structure of VGCCs

The conducting $\alpha 1$ -subunits of $\text{Ca}_v s$ and $\text{Na}_v s$ are composed of four 6-TM-domains linked via intracellular loops connecting the respective S6 and S1 segments of consecutive domains (fig. 1). This is in contrast to 6-TM- $\text{K}_v s$, where four independent $\alpha 1$ -subunits assemble to form a pore-forming tetramer. However, voltage-gated Ca^{2+} and Na^{+} -channels belong to the same multigene family as voltage-activated K^{+} -channels. Voltage-dependent ion channels are gated by alterations of the membrane potential. In general this is mediated by a voltage sensor formed by the S4 helices of the $\alpha 1$ -subunit. Due to positively charged side residues of arginines and/or lysines at every third position of the S4 helices (each has five to six gating charges), a change in the electrostatic force caused by depolarizations of the membrane potential leads to an outward movement and rotation of the voltage sensor from an internal to an external crevice of the $\alpha 1$ -subunit [Cha et al. 1999]. This movement of the S4s results in a conformational change of the S5 and S6 helices. If the channel switches from the closed into the open state, the intersecting inner ends of the S6s diverge from each other, which opens the pore. The channel is now able to conduct its charge carrier [Hille 2001]. This specific mechanism was directly proved only for K^{+} channels [Logothetis et al. 1992; Glauner et al. 1999], but a similar one is

hypothesized for VGCCs. The channel pore is primarily formed by the two segments S5 and S6, with the S5s oriented to the phospholipid bilayer and therefore building the outer helix, whereas the S6s are suggested to form the inner helix facing the aqueous pore. Furthermore, between these two segments extracellular loops can be found extending into the pore. Referring to their orientation, these loops are called pore-loops (P-loops) and mediate the ionic selectivity of a voltage-gated ion channel. Besides atomic radii and ionic charges, the substitution of the hydrate envelope is predominantly responsible for the highly selective discrimination of ions able to pass the channel or being hindered. Concerning the $\alpha 1$ -subunit both the N- and C-terminus are intracellularly localized [Lacinova and Hofmann 2005]. For $\text{Ca}_v 1.3$ and $\text{Ca}_v 1.4$ it was shown that an intrinsic distal C-terminal modulator controls activation and Ca^{2+} - as well as voltage-dependent inactivation [Singh et al. 2006, 2008]. The $\alpha 1$ -subunit sequence contains various interaction sites, as for example for the two membrane spanning auxiliary subunits $\alpha 2$ and γ as well as for the intracellular β -subunit. Moreover, it provides binding sites for DHPs and G-proteins [Lacinova and Hofmann 2005].

The $\alpha 1$ -subunit of VGCCs is typically associated with a certain composition of ancillary subunits (β , $\alpha 2\delta$ and γ), which generally regulate channel expression, membrane incorporation, drug binding and gating properties of the pore-forming subunit [Catterall 2000]. All HVA Ca^{2+} channels show coexpression of the $\alpha 1$ - and β -subunit (fig. 1). For the LVA-superfamily such coexpression has not been observed [Lacinova et al. 2000]. Four different β -subunit isoforms ($\beta 1$, $\beta 2$, $\beta 3$, $\beta 4$), and for each various splice variants are known until now [Lacinova and Hofmann 2005]. Among LTCCs $\text{Ca}_v 1.1$ is exclusively interacting with $\beta 1$ [Varadi et al. 1991], whereas $\text{Ca}_v 1.2$ interacts with all four isoforms [Wei et al. 1991; Hullin et al. 1992; Castellano et al. 1993a, b] and interaction of $\text{Ca}_v 1.3$ was shown for $\beta 2$ and $\beta 3$ [Williams et al. 1992; Koschak et al. 2001]. $\text{Ca}_v 1.4s$ interaction with β -subunits has not been investigated up to now. As far as the mentioned publications are concerned, “ β -subunit interaction” refers to the modulatory action of a specific β -subunit on currents of a given $\alpha 1$ -subunit heterologously coexpressed in *Xenopus* oocytes or in mammalian cell lines. $\beta 1$ is expressed in skeletal muscles, whereas $\beta 2$ gene expression is predominantly located in cardiac myocytes and in a lower extend in the brain. This is in contrast to $\beta 3$, which is abundant in neuronal and smooth muscle tissues [Biel et al. 1991; Hullin et al. 1992; Ludwig et al. 1997; Volsen et al. 1997]. The putative $\alpha 1$ - β -interaction sites are illustrated in and are on the one hand particularly located in the intracellular loop between the homologous domains I and II of the $\alpha 1$ -subunit termed α interaction domain (AID, [Biel et al. 1991]) and on the other hand in the loop connecting the second and third α -helix of the β -subunit termed β interaction domain (BID, [De Waard et al. 1994; De Waard 1996]). However, most recent studies from different crystallized β -subunits provide conflicting data, namely that BID lies in the core region of the crystallized protein and would therefore be inaccessible for protein-protein-interactions [Chen et al. 2004; Van Petegem et al. 2004].

The commonly supposed $\alpha 1$ - β -interaction-stoichiometry is 1:1. However, data from various authors give reason to assume that more than one β -subunit may interact with a single $\alpha 1$ -subunit [Stephens et al. 2000; Garcia et al. 2002; Stotz et al. 2004]. Regarding the modulatory

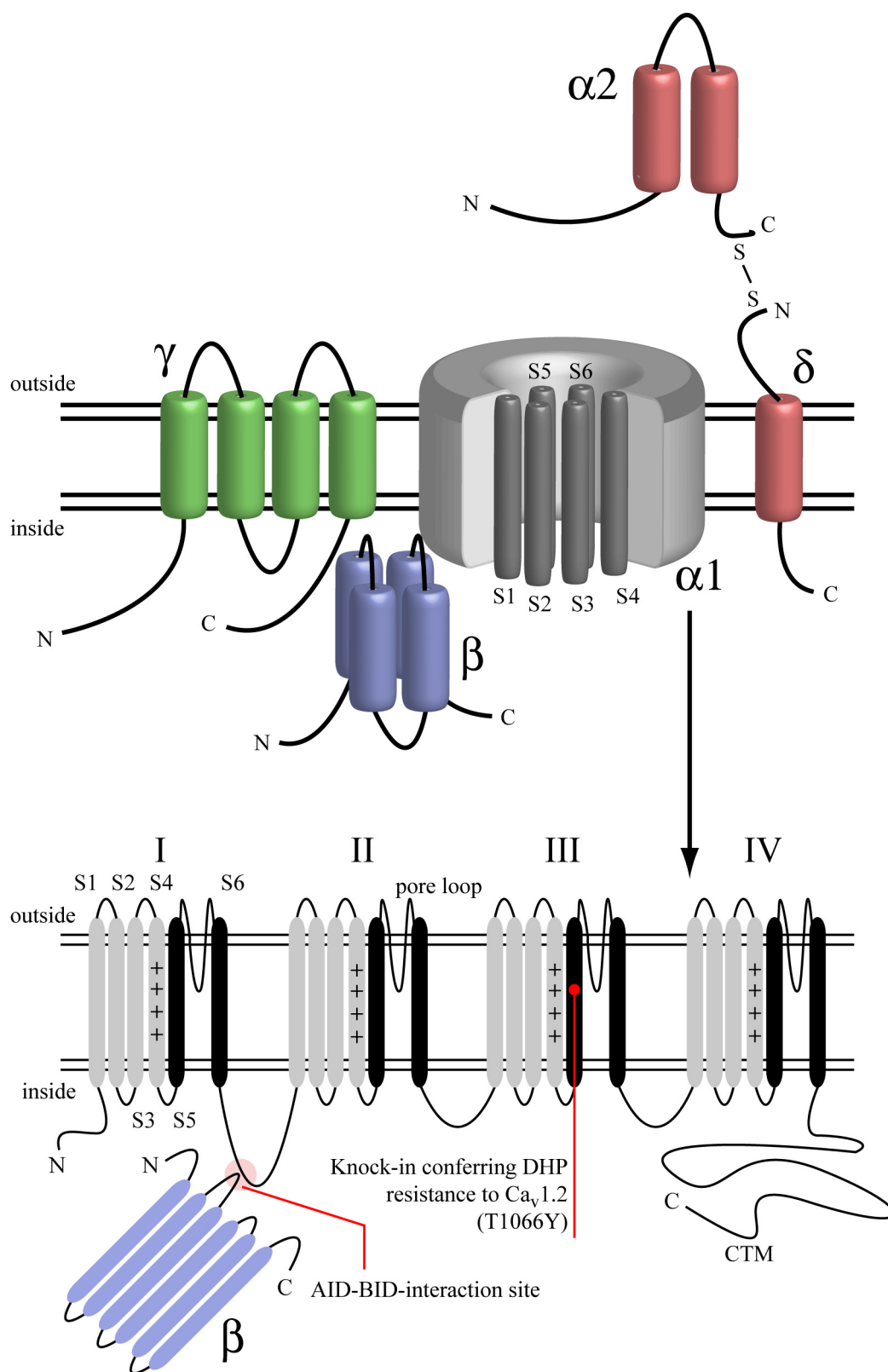
functions of β - on α 1-subunits a broad range of effects was described, especially for α 1 of $\text{Ca}_v1.2$ and β 3, including (I) enhanced peak currents and current densities, probably caused by a higher number of functional channels, improved targeting of expressed α 1 to the cell membrane and facilitated open-gating [Singer et al. 1991; Kamp et al. 1996], (II) accelerations of activation and inactivation kinetics, (III) a shift of the IV-curves to more hyperpolarized potentials as well as (IV) a more negative half-maximal inactivation constant [Singer et al. 1991; Wei et al. 1991; Hullin et al. 1992; Castellano et al. 1993a; Lacinova et al. 1995]. In addition the α 1- β -subunit interaction was reported to (V) affect the pharmacodynamics of VGCC-antagonists. In detail, the expression of β 3 in the presence of $\text{Ca}_v1.2$ increased the potencies of phenylalkylamines, such as verapamil and gallopamil, but did not significantly alter the IC_{50} s of DHPs, e.g. isradipine or mibefradil [Lacinova et al. 1995; Welling et al. 1995]. Finally it is important to mention that the implication of β -subunits for VGCCs is not limited to the modulation of electrophysiological and pharmacological properties via their α 1-subunits, but also (VI) extends to the regulation of gene silencing. β 4 interacting with CHCB2 in the nuclei of cochlear cells was reported to suppress transcription regionally, rather than promoter- or sequence-specifically [Hibino et al. 2003]. Whether the expression of proteins like VGCC-subunits is affected remains unknown.

The α 2 δ -subunit is a highly glycosylated protein complex consisting of a purely extracellular α 2-protein and a single membrane spanning α -helix of the δ -protein (fig. 1). The latter one is connected with the α 1-subunit and anchors the α 2-protein to the channel via a disulfide-link. Similarly to the β -subunit, four different α 2 δ -subunits have been described [Ellis et al. 1988; Klugbauer et al. 1999; Hobom et al. 2000; Qin et al. 2002]. Results about the modulatory role of α 2 δ -subunits are less abundant in the literature than for the β -subunits and also include some inconsistencies, namely the respective effects are described as being present or absent in different publications. However, this is not conclusively contradictory because different authors used different expression systems, different charge carriers as well as different α 1- and β -subunits. Reported effects of the α 2 δ -subunit modulating the electrophysiology of a voltage-gated Ca^{2+} channel, when additionally coexpressed to β in the presence of α 1, are generally comparable with that of the β -subunit, which are (I) increased current amplitudes, current densities [Lacinova and Hofmann 2005] and enhanced open probabilities without affecting open times of VGCCs in the presence of α 2 δ -1 [Shistik et al. 1995], (II) an acceleration of channel activation and inactivation, (III) a negative shift of the IV-relation and (IV) smaller V_{50} s for current inactivation [Singer et al. 1991; Felix et al. 1997]. Similar to β -subunits, α 2 δ -subunits (V) affect the pharmacodynamics of certain VGCC-antagonists. This was demonstrated for different types of ω -conotoxin on $\text{Ca}_v2.2$ -mediated currents, where the interaction of α 2 δ reduced the inhibitory effect of the agent [Mould et al. 2004]. Moreover, the antiepileptic drug gabapentin was shown to bind to α 2 δ with affinities between 9.4 and 59 nM depending on the expression system [Brown et al. 1998a; Brown et al. 1998b; Marais et al. 2001]. Thus, it was hypothesized that the anticonvulsant effect of gabapentin could be due to an indirect modulation of α 1 via direct interaction with α 2 δ , which causes a reduced Ca^{2+} influx [Gee et al. 1996]. As far as the tissue distribution of α 2 δ -expression is concerned, α 2 δ -1, 2 and 4 are

predominantly present in skeletal muscles, heart and except for $\alpha 2\delta$ -4 in the brain, whereas $\alpha 2\delta$ -3-gene expression was exclusively found in neuronal tissues [Klugbauer et al. 1999; Qin et al. 2002].

The third auxiliary subunit of VGCCs is the γ -subunit, which is in contrast to the other two regulatory subunits an integral membrane protein with 4 transmembrane helices and intracellular N- and C-terminus (fig. 1). Comparable to $\alpha 2\delta$ the γ -subunit has specific domains potentially glycosylated [Bosse et al. 1990]. γ -1 was the first described γ -subunit and is unique to skeletal muscle cells, whereas the γ -2-isoform is expressed in the brain with specific localizations in the olfactory bulbs, the cerebral cortex and the hippocampus including the CA3-region as well as the dentate gyrus [Letts et al. 1998]. The expression of 5 additional γ -subunits was shown by [Klugbauer et al. 2000] and [Burgess et al. 2001]. γ -3 and 4 were detected in mouse brains, in contrast to γ -5, which is abundant in skeletal muscles, the heart, liver and lung [Klugbauer et al. 2000]. Regarding the physiological effects of γ -subunits on electrophysiological properties of VGCCs, the coexpression of γ -1 in addition to $\beta 2a$ and $\alpha 2\delta$ -1 together with $Ca_v 1.2a$ caused (I) more transient inactivation kinetics and (II) a shift of the inactivation curve of about 30 mV in negative direction. Similar effects were obtained with γ -2, suggesting that both γ -1 and γ -2 are able to interact with $Ca_v 1.2$ [Lacinova and Hofmann 2005]. γ -2, 3 and 4 are suggested to be associated with all 3 neuronal non-L-type HVA Ca^{2+} channels, while γ -5 probably interacts with $Ca_v 3.x$ [Kang et al. 2001; Rousset et al. 2001; Lacinova and Hofmann 2005]. Moreover, (III) γ -subunits seem to have an opposing role to β - and $\alpha 2\delta$ -subunits in the regulation of VGCC-activity, namely γ downregulates Ca^{2+} currents, while β and $\alpha 2\delta$ have usually enhancing effects [Lacinova and Hofmann 2005]. Finally, as reported for β - and $\alpha 2\delta$ -subunits, (IV) γ -subunits affect protein targeting. In the particular case of γ , an association of γ -expression and AMPA-receptor-targeting to the synaptic space was also observed [Chen et al. 2000].

Fig. 1: (1) LTCCs are multimeric complexes formed by a conducting $\alpha 1$ -subunit and three auxiliary subunits ($\alpha 2\delta$, β , and γ). (2) The primary structure of the $\alpha 1$ -subunit consists of 4 domains each composed of 6 transmembrane segments. In III S5 the knock-in mutation of $Cav1.2DHP^{-/-}$ -mice is shown. AID = α -interaction domain, BID = β -interaction domain, CTM = C-terminal modulator (adapted from Bourinet et al. 2004 and Lacinova 2005, Singh et al. 2006, 2008).



1.5. L-type voltage-gated Ca^{2+} -channels (LTCCs, $\text{Ca}_v1.x$)

This diploma thesis focuses on LTCCs and their functional coupling to other ion channels. Therefore, this specific VGCC-subfamily will be discussed in more detail in the following chapters.

1.5.1. Expression and tissue distribution of LTCCs

The $\text{Ca}_v1.x$ subfamily of VGCCs consists of 4 members. While $\text{Ca}_v1.1$ ($\alpha1S$) and $\text{Ca}_v1.4$ ($\alpha1F$) are exclusively expressed in skeletal muscle and retinal cells, respectively, the two remaining subtypes $\text{Ca}_v1.2$ ($\alpha1C$) and $\text{Ca}_v1.3$ ($\alpha1D$) exhibit ubiquitously expression patterns in mammalian tissues and are amongst others abundantly expressed in the CNS [Sinnegger-Brauns et al. 2009]. However, there are controversially discussed findings showing the expression of $\text{Ca}_v1.1$ and $\text{Ca}_v1.4$ in the brain [Takahashi et al. 2003; Hayashida et al. 2005]. $\text{Ca}_v1.2$ is widely expressed in the cardiovascular system (cardiomyocytes and smooth muscle cells) and therefore called the cardiac isoform, but also found in the nervous and endocrine system [Striessnig et al. 2006]. $\text{Ca}_v1.3$ is present in many different excitable cells, such as neurons, sensory cells (e.g. cochlear inner and outer hair cells), neuroendocrine cells and cardiac pacemaker cells of the sinu-atrial and the AV-node, where APs are solely carried by $\text{Ca}_v1.3$ -currents [Clark et al. 2003]. On the contrary, in myocardial cells the AP-plateau phase is caused by $I_{\text{Cav}1.2}$ [Cavalie et al. 1983] (from [Hille 2001]). As far as the role of $\text{Ca}_v1.2$ and $\text{Ca}_v1.3$, in the pancreas is concerned, controversial data exist. Different mouse models and biochemical data indicate a contribution of $\text{Ca}_v1.3$ to pancreatic Ca^{2+} -currents [Namkung et al. 2001], whereas others conclude that there are no significant $\text{Ca}_v1.3$ -mediated effects in these endocrine cells [Barg et al. 2001; Schulla et al. 2003]. The latter opinion is in accordance with results presented by the group of Jörg Striessnig, which show that glucose induced insulin-secretion is DHP-insensitive in $\text{Ca}_v1.2\text{DHP}^{-/-}$ mice, suggesting that $\text{Ca}_v1.3$ is indeed not contributing to the LTCC-mediated Ca^{2+} -influx in pancreatic β -cells [Striessnig et al. 2006]. On the contrary, Hockerman and collaborators have reported that although both $\text{Ca}_v1.2$ - and $\text{Ca}_v1.3$ -DHP-insensitive-mutants couple to depolarization-stimulated insulin secretion, $\text{Ca}_v1.3\text{DHPi}^{-/-}$, but not $\text{Ca}_v1.2\text{DHPi}^{-/-}$ -mutants are involved in glucose-stimulated insulin secretion in INS-1 cells [Liu et al. 2003; Jacobo et al. 2009].

Besides its implication in neuroendocrine functions, $\text{Ca}_v1.2$ is responsible for LTCC-dependent and NMDA-receptor-independent LTP in hippocampal neurons, associated with MAP-kinase- and CREB-phosphorylation. However, both neuronal LTCC subtypes are able to induce CREB-activation. Generally, it has been reported that LTCCs play an important role in various brain functions and behaviour, as for example memory formation, anxiety, depression and drug taking [Striessnig et al. 2006]. If the expression levels of $\text{Ca}_v1.2$ and $\text{Ca}_v1.3$ in the rodent brain are compared, a surmounting $\text{Ca}_v1.2$ expression was demonstrated with a relation of 80 to 20 [Hell et al. 1993; Sinnegger-Brauns et al. 2004], which was additionally supported by studies

suggesting an even stronger divergence of about 90 to 10 [Sinnegger-Brauns et al. 2009]. Despite the fact that both $Ca_v1.2$ and $Ca_v1.3$ have a somatodendritic localization, they differ in their subcellular localization with respect to cluster formation and distribution in the distal dendrites [Hess et al. 1984; Obermair et al. 2004] (reviewed in [Vacher et al. 2008]).

1.5.2. Pharmacology of LTCCs

LTCC-agonists and -antagonists represent drugs with considerable experimental as well as clinical relevance, including three major substance classes: dihydropyridines (DHPs), phenylalkylamines (PAA) and benzothiazepines (BTZ, [Triggle 2003]). On account of the fact that VGCCs have no physiological ligands, such as a ligand-gated ion channel or GPCRs, it is difficult to term LTCC-modulating substances precisely. To simplify matters, a drug decreasing I_{Ca} is called antagonist (e.g. isradipine), whereas a compound increasing this current is named agonist (e.g. BayK 8644) in this diploma thesis. By blocking LTCCs, DHP-antagonists, such as nifedipine, nitrendipine, nimodipine, nisoldipine, amlodipine, isradipine ($IC_{50} = 40$ nM, [Sinnegger-Brauns et al. 2004]), lacidipine, lercenadipine and felodipine, were introduced as antihypertensive and antianginal agents [Triggle 2003]. However, in therapeutic concentrations DHPs have little effect on the myocardium and are therefore described as being vascular-selective in these concentrations, while different DHPs exhibit significant differences in their cardiovascular profile. Isradipine for example is about 10-times more vascular-selective than nifedipine with vascular-cardiac-selectivity-ratios of 100:1 and 10:1, respectively [Triggle 2003]. Nisoldipine is even more vascular-selective with a ratio of 1000:1 [Triggle 2003]. Regarding PAAs and BTZs, vascular and cardiac effects occur in a similar extend. In detail, cardiac actions of PAAs and BTZs can be separated in negatively chronotropic (at the sinu-atrial node), negatively dromotropic (at the AV-node) and negatively inotropic (at the myocardium) effects (overviewed in [Aktories 2009]).

Isradipine exhibits comparable affinities for $Ca_v1.2$ and $Ca_v1.3$ with subnanomolar dissociation constants. This suggests that the amino-acid sequence providing the DHP-binding site is homologues in these two LTCC-subtypes. However, isradipine displays an approximately 10-fold higher potency for $Ca_v1.2$ than for $Ca_v1.3$ [Striessnig et al. 2006]. Similar results were obtained for nimodipine [Xu et al. 2001]. This is primarily explained by differences in the state-dependent blocking mechanism of these substances [Striessnig et al. 2006]. The state-dependency is reflected by the dependence of the potencies on the holding potential. That means, the higher the holding potential and thus the more channels inactivate, the lower the IC_{50} -value of the respective DHP. On the contrary, hyperpolarizations, which favor recovery from inactivation, promote unbinding of DHPs and therefore decrease their potency (e.g. the IC_{50} of nitrendipine is 2000-fold lower, when the neuron is held at -15 mV instead of -80 mV). Conclusively, the pharmacological properties of DHPs rely on channel gating. This is

to some extent comparable to the use-dependency of the local anesthetic lidocaine acting on VGSCs or verapamil inhibiting VGCCs. However, the latter antagonists only block the open channel (overviewed in [Johnson et al. 1996; Hille 2001; Striessnig et al. 2006]). The molecular basis for the selectivity of DHPs for vasculature is provided by their specific state-dependency, namely DHPs are capable of effective blocking only under conditions of on-holding, tonic depolarizations as they occur in smooth muscles of blood vessels, but not in cardiomyocytes. It was suggested that the state-dependent block of mibefradil occurs because of slow recovery from open-channel-block during depolarized membrane potentials rather than of enhanced drug binding to the inactivated state [Aczel et al. 1998].

PAA (e.g. verapamil, gallopamil, devapamil) use-dependently act on LTCCs while blocking the open channel from the intracellular side [Hescheler et al. 1982], hence higher stimulation frequencies enhance their apparent affinity [Johnson et al. 1996]. In contrast to PAAs, BTZs (i.e. diltiazem, DTZ417) are known to bind from the outside at the linker sequence between IVS5 and IVS6 [Watanabe et al. 1993; Kurokawa et al. 1997]. However, in case of $Ca_v1.2$ it was shown that diltiazem also blocks in a use-dependent manner [Lacinova and Hofmann 2005]. The PAA-binding pocket is overlapping with that of DHPs and is located at position 1492 to 1535 (www.uniprot.org/uniprot/Q13936). The same three amino-acids (Y1485, A1489, I1492) seem to be necessary for the use-dependent block of LTCCs by both PAAs and BTZs [Lacinova and Hofmann 2005]. Furthermore, LTCC-blockade by PAAs depends on channel inactivation, which means that the more channels inactivate the higher the potency of PAAs [Hering 2002]. Moreover, both substance classes allosterically interact with binding DHPs [Glossmann et al. 1990] and exhibit a block potentiation on $Ca_v1.2$, which is independent of Ca^{2+} -mediated channel inactivation, but regulated by Ca^{2+} -ions interacting with glutamates in the pore region [Dilmac et al. 2003, 2004].

All three main classes of VGCC-antagonists (DHPs, PAAs and BTZs) interact with TM-regions of $\alpha 1$ -domain IV with additional sites for LTCCs in repeat I and III [Lacinova and Hofmann 2005]. Amino-acids involved in the high affinity block of $Ca_v1.2$ by DHPs are Q1065 in IIIS5 [He et al. 1997; Ito et al. 1997] and I1175, I1178, M1183 as well as Y1174 of IIIS6 [Bodi et al. 1997; Peterson et al. 1997] and D1494 in IVS6 [Peterson et al. 1997]. Especially important are T1061 and T1066, which are localized in segment 5 of the third domain. A mutation from T to Y causes in both cases a strong reduction of DHP-modulation. In case of T1066Y the DHP-binding to the $\alpha 1$ -subunit of $Ca_v1.2$ is almost completely abolished [He et al. 1997; Ito et al. 1997; Striessnig et al. 2006]. The DHP-binding pocket of the human $Ca_v1.2$ consists of two distinct regions: 1109-1199 (including the extracellular IIIS5-IIIS6-linker, the TM-IIIS6-region and the cytoplasmatic IIIS6-IVS1-linker), 1478-1546 (including the extracellular IVS5-IVS6-linker, the TM-IVS6-region and a moiety of the cytoplasmatic C-terminal region (www.uniprot.org/uniprot/Q13936)). The affinity of DHPs is also regulated by Ca^{2+} , which is coordinated by pore region glutamates. These glutamates in the narrow part of the pore form a region of very high negative charge density [Hille 2001]. Mutations of these glutamates to glycines in domain III and IV of $Ca_v1.1$ decreased the affinity of isradipine by 20- to 40-fold [Peterson et al. 1995].

Besides specific amino-acids in the $\alpha 1$ -subunit, the presence or absence of all known ancillary subunits affected the high affinity binding of DHPs to LTCCs [Mitterdorfer et al. 1994; Wei et al. 1995; Suh-Kim et al. 1996]. Receptor sites on VGCCs share general properties: (I) defined structure-activity-relationships of agonist- and antagonist-interactions with the binding site, (II) coupling of the binding site with the gating complex of the channel, (III) regulation by external and internal influences and (IV) changes in their function under pathological conditions, i.e. in channelopathies [Triggle 2003].

1.5.3. Electrophysiological properties of LTCCs

Differences between $\text{Ca}_v 1.2$ and $\text{Ca}_v 1.3$ are not restricted to their expression profile, subcellular localization and pharmacology, but also evident in their electrophysiological characteristics. Using Ba^{2+} 5 mM as charge carrier, $\text{Ca}_v 1.2$, heterologously expressed in *Xenopus* oocytes, produced currents that started to activate at approximately -35 mV and peaked at about 0 mV. This refers to an IV-pattern described as being prototypic HVA-like. In contrast, IV-curves for $\text{Ca}_v 1.3$, investigated in the same expression system, revealed thresholds of activation at \sim -55 mV and peak amplitudes at approximately -30 mV. Therefore, the two neuronal $\text{Ca}_v 1.x$ -isoforms have activation thresholds separated by \sim 20 mV [Xu and Lipscombe 2001]. Moreover, it was shown that the recordings obtained with Ba^{2+} 5mM as charge carrier were comparable with that measured using Ca^{2+} 2 mM (activation thresholds for $\text{Ca}_v 1.2$ and $\text{Ca}_v 1.3 = \sim$ -35 mV and \sim -50 mV, respectively [Lipscombe et al. 2004]). In [Koschak et al. 2001] the activation thresholds for $\text{Ca}_v 1.2$ and $\text{Ca}_v 1.3$ transfected into TS-A201 cells and measured at 15 - 20 mM Ba^{2+} lay at -31.5 and -45.7 mV, respectively. In this publication the activation threshold was defined as the voltage, where 5 % of I_{max} were elicited. However, in [Xu and Lipscombe 2001] and in [Lipscombe et al. 2004] such a definition was not given. To sum up, $\text{Ca}_v 1.2$ behaves as a classical HVA VGCC, which $\text{Ca}_v 1.3$ does not. In order to pay tribute to the comparably negative activation of some HVAs ($\text{Ca}_v 1.3$ and $\text{Ca}_v 2.3$) with V_{50} s higher than that of LVAs and lower than that of typical HVAs (i.e. $\text{Ca}_v 1.2$ and $\text{Ca}_v 2.2$) some authors use the description “medium voltage-activated” (MVA) to separate them functionally from the other two groups [Wicher et al. 1997]. However, LTCC activation parameters measured with different external Ca^{2+} or Ba^{2+} concentrations are not comparable due to charge surface screening effects. This effect describes the phenomenon that a reduced external concentration of divalent cations increases the number of uncovered negative charges of the membrane phospholipids. This leads to an ion flux independent and locally to the membrane restricted voltage deflection, which therefore does not affect the membrane resting potential, but acts as a positive offset potential for the voltage sensor of voltage dependent ion channels. Thus, the lower the covering of externally orientated negative charges of the membrane, the bigger the difference between the commanding voltage and the actual applied potential [Frankenhaeuser et al. 1957; Chad et al. 1986]. Due to the fact

that Ba^{2+} covers these negative charges with a lower efficiency than Ca^{2+} , Ba^{2+} -concentrations below 5 mM shift the LTCC-activation leftwards in relation to Ca^{2+} 2 mM. If Ba^{2+} -concentrations are enhanced to 10 or 20 mM the effect gets reversed and the channels will open at higher depolarizations than with Ca^{2+} 2 mM [Xu and Lipscombe 2001].

In [Koschak et al. 2001] IV-curves for $Ca_v1.2$ and $Ca_v1.3$ using Ba^{2+} 15 - 20 mM are published with peak currents lying at about 15 and 0 mV, respectively. This supports the postulated influence of the surface charge screening effect investigated by [Xu and Lipscombe 2001], where an increase of the external barium concentration from 5 to 20 mM caused an approximate right-shift of the current-voltage-relation of 20 mV. Furthermore, [Koschak et al. 2001] also point out that $Ca_v1.3$ opens at sub-threshold membrane potentials, whereas $Ca_v1.2$ starts to activate only at considerable depolarizations. Additionally, $Ca_v1.3$ exhibit little voltage-dependent inactivation and is suggested to produce large window currents at potentials around -50 mV [Xu and Lipscombe 2001].

If the specific LTCC-agonist BayK 8644 is applied, IV-curves of LTCCs shift to more hyperpolarized potentials in a range of about 10 mV [Xu and Lipscombe 2001]. In addition to that, LTCC-currents are increased during the administration of BayK by switching the channels to the so called mode-two-gating, where very long channel openings are favoured without altering the unitary current amplitude. Furthermore, in mode-two-gating the channel closing rate is about 100-times slower than in the mode-one-gating [Hess et al. 1984]. Interestingly, BayK displays both agonistic and antagonistic action on LTCCs depending on the respective optical enantiomer binding at the channel [Hille 2001; Xu and Lipscombe 2001].

If a certain depolarizing event, which causes the opening of VGCCs, is not quickly terminated by some outward rectifying conductances, a bipartite negative feedback mechanism transferring Ca^{2+} channels in the non conducting inactivated state is triggered, which therefore prevents the cell from a Ca^{2+} -overload. The two parts of this mechanism can be i.e. seen in current recordings of L-type voltage gated Ca^{2+} channels elicited via long-lasting voltage steps, where usually a two-phased time course of inactivation occurs. Whereas the fast time constant represents the Ca^{2+} -dependent fraction, the slow one corresponds to the voltage-dependent inactivation distinguished in experiments, where Ca^{2+} is exchanged with Ba^{2+} as charge carrier and thus Ca^{2+} -dependent inactivation is eliminated. This was demonstrated in both native cells [Cox et al. 1994] and heterologous expression studies [Shirokov 1999]. In primary cells the fast time constant lies between 7 [Richard et al. 1993] and 50 ms [Ganitkevich et al. 1986], while published values for the slow constant are in range of 65 [Masaki et al. 1997] to 400 ms [Johnson et al. 1994]. LTCCs heterologously expressed show generally higher τ s for the fast as well as for the slow fraction [Zong et al. 1996; Cens et al. 1999]. As there are only two well distinguishable inactivation mechanisms known until now, the variance in time constants for the fast as well as for the slow component in both primary and transfected cells is supposed to reflect the variability in the time-dependent concentration of Ca^{2+} in the locally neighbouring regions of VGCCs [Lacinova and Hofmann 2005].

Among all HVA channels the Ca^{2+} -mediated inactivation is most prominent in LTCCs [Lacinova and Hofmann 2005]. However, the effect is in a minor extent also present in $\text{Ca}_v2.1$ [Lee et al. 1999; Lee et al. 2000] and in $\text{Ca}_v2.2$ [Cox and Dunlap 1994; Shirokov 1999]. In $\text{Ca}_v2.3$ there is no significant difference between currents carried by Ba^{2+} and Ca^{2+} suggesting that R-type Ca^{2+} channels have no Ca^{2+} -dependent inactivation. Nevertheless, if monovalent ions are used as charge carrier for RTCCs, a fast component of inactivation is reduced, which hence slows the whole course of inactivation of these currents. Thus, the respective authors hypothesized that in $\text{Ca}_v2.3$ a voltage-independent inactivation mechanism exists, which is sensitive to divalent cations, but not selective for Ca^{2+} [Jouveneau et al. 2000]. This is in accordance with results from LTCC-currents, which refer to a small fraction of voltage-independent inactivation remaining, when Ca^{2+} is substituted by Ba^{2+} [Ferreira et al. 1997]. To sum up, Ca^{2+} -dependent inactivation was directly proven for $\text{Ca}_v1.y$, $\text{Ca}_v2.1$ and $\text{Ca}_v2.2$ and therefore appears not to be an universal property of VGCCs. A particularly fast form of Ca^{2+} -dependent inactivation was observed in cardiac myocytes, which is based on a Ca^{2+} -induced Ca^{2+} -release (CICR)-mediated amplification of the internal Ca^{2+} -rise after activating VGCCs leading to especially small time constants of 6 to 15 ms [Sham et al. 1995; Sham 1997]. The molecular mediator of internal Ca^{2+} to the induction of VGCC-inactivation is calmodulin (CaM), which has to bind Ca^{2+} before the process of inactivation can start [Zuhlke et al. 1999]. The so called EF-hand motif on the C-terminus is assumed to participate in the transduction of Ca^{2+} -CaM to channel inactivation [Peterson et al. 1999].

While R- and T-type voltage-gated Ca^{2+} channels exhibit no Ca^{2+} -dependent inactivation detectable by comparing Ca^{2+} - with Ba^{2+} -currents, all VGCCs inactivate in a voltage-dependent manner. Interestingly, if inactivation mediated by divalent cations is eliminated by completely replacing them with monovalent ions, the time course of inactivation has still two phases. In other words, the isolation of the voltage-dependent inactivation-component unveiled an additional ultra-slow component of voltage-dependent inactivation with time constants of several seconds [Mitarai et al. 2000; Lacinova and Hofmann 2005].

1.6. Ca²⁺-dependent ion channels

1.6.1. Classification and general properties of Ca²⁺-dependent

K⁺-channels (K_(Ca)s)

A specific type of ion channels, involving K⁺-, Cl⁻- and cation channels that are activated by certain rises of the local [Ca²⁺]_i, was already introduced in chapter 1.2. The respective currents mediated by these channels are usually termed I_{K(Ca)} or I_{AHP}, I_{Cl(Ca)} and I_{CAN}, respectively [Hille 2001].

K_(Ca)-channels come in two major subfamilies primarily distinguished by their single channel conductance, which is 100 - 400 pS [Vergara et al. 1998; Sah et al. 2002] in big conducting BK-, maxi-K_(Ca)- or K_(Ca)1.x-channels, also known as Slo-channels (Slo standing for the *Drosophila*-mutant Slowpoke), and at least 70 % lower in the small conducting SK- or K_(Ca)2.x-channel-group. In SK-channels the single channel conductance typically lies between 2 and 20 pS, which is about 4- to 5-fold lower than in a special SK-channel-subtype known as SK4 [Vergara et al. 1998; Sah and Faber 2002]. Hence, SK4- or IK-channels (K_(Ca)3.1) are intermediate conducting between classical SK-channels and BK-channels with a g_{SK4} of 20 to 100 pS [Vergara et al. 1998; Sah and Faber 2002]. Regarding the current classification of K_(Ca)-channels, three different subtypes have been cloned until now for both BK- and SK-channels (BK1-3 and SK1-3), while only one IK-channel has been described so far [Hille 2001].

Structural analysis revealed that SK- and IK-channels belong to a homogenous structural class with a 6TM-membrane topology, which is also typical for most voltage-gated ion channels, whereas BK-channels build a structurally different group forming 7TM- α -subunits (S0 - S6). The structural difference between 6TM- and 7TM-BK-channels is also manifested in the extracellular localization of the N-terminus and an additional α -helix preceding S1, called S0-segment [Hille 2001]. However, the voltage-sensing positive gating charges are in BK-channels localized in S4 like in other voltage-gated ion channels. Moreover, four additional intracellular hydrophobic segments (S7 - S10) have later been identified on the C-terminal side [Salkoff et al. 2006]. Maxi K_(Ca)-channels also build heteromeric assemblies with a supplementary 2TM- β -subunit, which occurs in three subtypes (β 1, 2/3 and 4). Hence, the native Slo-channel usually compromises either an α -subunit-tetramer alone, or an assembly of the α -subunit-tetramer with one of the three β -subunits [Sah and Faber 2002]. For SK-channels it was also proposed that they build α -subunit-tetramers either as homo-, or as heteromeres [Vergara et al. 1998; Sah and Faber 2002].

Auxiliary subunits have only been described for BK-channels while the association with a specific β -subunit was shown to shift the current-voltage-relation to more negative potentials and to enhance the channels Ca²⁺-sensitivity. Furthermore, β -subunits modulate BK-current inactivation, namely the coexpression of α with β 1 or β 4 in contrast to β 2/3 produces non-inactivating currents [Sah and Faber 2002].

Like all Ca²⁺-sensitive processes I_{K(Ca)}, I_{Cl(Ca)} and I_{CAN} are principally voltage-dependent by the

voltage-dependence of Ca^{2+} -entry. Besides that, SK- and IK-channels were shown to be inward rectifying [Kohler et al. 1996; Ishii et al. 1997]. This is in contrast to BK-channel-gating, which is thus sensitive for both $[\text{Ca}^{2+}]_i$ and alterations of the membrane potential. Supposing a constant $[\text{Ca}^{2+}]_i$, open probabilities, open times and amplitudes of maxi- $\text{K}_{(\text{Ca})}$ -single channel currents grow with increasing depolarization. Hence, on the assumption of a hypothetically static $[\text{Ca}^{2+}]_i$, Slo-channels behave like delayed rectifier K^+ -channels. Another difference between the 3 groups of $\text{K}_{(\text{Ca})}$ -channels is their Ca^{2+} -sensitivity. While SK- and IK-channels half maximally activate within rises from resting 30 - 200 nM to 400 - 600 nM $[\text{Ca}^{2+}]_i$, BK-channels need about 10-fold stronger Ca^{2+} -increases [Vergara et al. 1998]. Additionally, the Ca^{2+} -sensitivity of BK-channels is steeply voltage-dependent (half maximal activation with $[\text{Ca}^{2+}]_i$ of 1 - 10 μM at -50 mV, [Vergara et al. 1998]. From a structural point of view, the Ca^{2+} -sensitivity of $\text{K}_{(\text{Ca})}$ -channels is related to the C-terminal regions of every of their four pore-forming subunits. Furthermore, these domains are suggested to serve as inhibitors of channel-opening in the non-activated state, if Ca^{2+} is not bound [Hille 2001]. In BK-channels Ca^{2+} is directly bound via a domain in the S10-segment, which contains a series of negatively charged side residues and is known as the Ca^{2+} -bowl, while the Ca^{2+} -sensitivity of SK- and IK-channels is thought to be provided by the covalently association of one calmodulin-protein each with a certain cytoplasmatic C-terminal domain of the four SK-/IK-channel- α -subunits. The binding of Ca^{2+} to calmodulin is suggested to cause a series of conformational changes, which finally result in open-gating of the SK-channel [Schreiber et al. 1997; Keen et al. 1999; Shah et al. 2001; Sah and Faber 2002].

The kinetics of $\text{K}_{(\text{Ca})}$ -currents and their direct as well as indirect consequence to the discharge activity of an excitable cell are not easy to interpret, because one thing has to be kept in mind: These currents represent the response to a complex fusion of various cellular Ca^{2+} -specific processes including (I) Ca^{2+} -influx through the surface membrane, (II) Ca^{2+} -diffusion from the centre of accumulation to differently distant cell compartments, (III) Ca^{2+} -buffering via Ca^{2+} -reuptake in intracellular stores, via Ca^{2+} -binding proteins or via Ca^{2+} -extrusion and (IV) Ca^{2+} -binding to the respective channels as well as dissociation from them. Especially the spatial distribution of $\text{K}_{(\text{Ca})}$ -channels in relation to channels serving as their Ca^{2+} -source are important factors regulating $\text{K}_{(\text{Ca})}$ -currents [Hille 2001]. $\text{K}_{(\text{Ca})}1.x$ has been shown to be coassembled with its Ca^{2+} -sources in nanodomains, which are found within 20 - 50 nm of the respective Ca^{2+} -source. On the contrary, $\text{K}_{(\text{Ca})}2.x$ are located within microdomains at distances of a few hundred nm away from the Ca^{2+} -source [Fakler et al. 2008].

Additionally, both $\text{K}_{(\text{Ca})}1.x$ - and $\text{K}_{(\text{Ca})}2.x$ -currents are activated by Ca^{2+} -influx via VGCCs. Thus, different physiological roles of these channels are likely due to different co-localizations of $\text{K}_{(\text{Ca})}$ - with certain voltage-gated Ca^{2+} -channels [Sah and Faber 2002]. This aspect will be discussed in greater detail in chapter 4.8. when I will focus on different LTCC-couplings.

1.6.2. Tissue distribution and different roles of $K_{(Ca)}$ -channels in the neuronal discharge activity

BK- and SK-channels were both initially described in skeletal muscle cells but in the meantime their expression has been shown in many tissues including neuronal cells [Sah and Faber 2002]. Regarding the subcellular localization of SK-channels, immunohistochemical data have revealed that SK1, SK2 and SK3 are expressed in the CNS as well as in the PNS [Pedarzani et al. 2008]. Additionally, SK3 was shown to have a presynaptic localization in hippocampal neurons [Obermair et al. 2003]. Moreover, immunohistochemistry provided weak SK3 signals for pyramidal and granule cells. SK1 and SK2 are commonly found in the same neurons, whereas SK3 displays a completely different expression pattern [Pedarzani and Stocker 2008]. So far IK-channels have been identified in a few non-neuronal cell types such as epithelial cells or erythrocytes [Gardos 1958; Ishii et al. 1997] as well as in peripheral sensory, sympathetic and enteric neurons, but not in the CNS [Pedarzani and Stocker 2008]. As far as the auxiliary β -subunits are concerned, $\beta 1$ is mainly found in smooth muscle cells, $\beta 2/3$ exhibits a wider expression profile including the heart, brain and kidneys and $\beta 4$ -expression was exclusively proven in neuronal tissues [Sah and Faber 2002].

The effect of $K_{(Ca)}$ -currents on the membrane potential is generally known as an afterhyperpolarization (AHP) following either a single spike, a train of APs, or a burst. AHPs are divided into three types referring to their length and their time constant of decay, respectively. These types have been termed fast AHP (fAHP), medium AHP (mAHP) and slow AHP (sAHP). In the hippocampus 50 to 60 % of the cells exhibit sAHPs, about 20 % mAHPs and in only a small number of neurons both afterpotentials were observed [Shah et al. 2000a].

The fAHP is immediately activated during a single spike and lasts not longer than tens of ms. The current underlying the fAHP (I_{fAHP}) is voltage-dependent and exhibits a pharmacological profile (see the following chapter) fitting to the properties of BK-currents, suggesting that I_{fAHP} corresponds to I_{BK} . Furthermore, I_{fAHP} significantly contributes to AP-repolarizations [Sah and Faber 2002], electrical tuning of non-spiking properties of cochlear hair cells and presynaptic regulation of neurotransmitter release [Lancaster et al. 1987].

The mAHP is also relatively fast, activating within 5 ms, but lasts for 50 to several 100 ms. I_{mAHP} is voltage-independent and insensitive to BK-channel blockers as well as micromolar concentrations of tetraethylammonium (TEA), but inhibited by SK-antagonists (see following chapter) indicating that I_{SK} underlies the mAHP [Sah and Faber 2002]. However, this is in contrast to a publication of [Gu et al. 2005], which reports that KCNQ- (at -60 mV) and HCN-currents (at -80 mV), but not SK-channels are involved in the formation of the mAHP in CA1 pyramidal neurons. A role of I_{mAHP} in AP-repolarization has not been reported so far [Sah and Faber 2002].

In opposition to the two fast activating AHP-components, the sAHP activates comparably slow while reaching its peak only after hundreds of ms and decays even slower with time constants up to 5 s [Sah and Faber 2002]. Whereas fAHPs and mAHPs can be already activated via

a single spike, sAHPs are most commonly described to need a preceding spike train of at least 4 - 10 APs to be activated [Faber et al. 2001]. Although it is clear that I_{sAHP} is voltage-independent and activated by cytosolic Ca^{2+} -rises caused by VGCC-opening, its pharmacological profile is by far more complex than that of I_{fAHP} or I_{mAHP} including the modulation by various neurotransmitters, such as acetylcholine, glutamate, serotonin and noradrenaline. All of them showed an inhibiting effect on the sAHP [Nicoll 1988]. Hence, a consistent correlation between I_{sAHP} and a specific $\text{K}_{(\text{Ca})}$ -current on a molecular level has not been successfully obtained so far. The existing data about sAHPs are quite hard to overview and partly contradictory relating e.g. to the controversially answered question, if I_{sAHP} is apamin-sensitive and therefore SK-mediated or not (compare thus for instance [Grunnet et al. 2004; Kato et al. 2006] with [Shah et al. 2000b]). However, noise analyses would support SK-involvement by revealing a small single channel conductance for I_{sAHP} of 2 - 5 pS, which correlates well with reported SK-channel-conductances [Sah et al. 1995]. Because of the indubitable insensitivity of I_{sAHP} to BK-channel-blockers, the contribution of I_{BK} to the sAHP can be excluded [Shah and Haylett 2000a].

The state of investigation of $\text{K}_{(\text{Ca})}$ 3.1- or IK-channels is currently not as advanced as of the other $\text{K}_{(\text{Ca})}$ -channels, due to their generally sparse distribution, they did not receive such scientific attention as BK- or SK-channels in the past. However, with the exception that IK-channels have not been identified in any neuronal tissue, these channels could provide at least partly the missing link between the macroscopic I_{sAHP} -current and the molecular identity of the underlying channels. This assumption is supported by the relatively small single channel conductance of both IK-currents and I_{sAHP} and most promising by their pharmacology, namely that clotramizol is a widely described $\text{K}_{(\text{Ca})}$ 3.1-antagonist [Shah et al. 2006]. Unfortunately, this is just a speculation, because no heterologous expression studies of $\text{K}_{(\text{Ca})}$ 3.1 using UCL 2077 or substances with similar effects and comparative studies investigating a possible correlation between UCL 2077 (suppressing sAHPs in hippocampal pyramidal neurons) and TRAM-34 (a selective IK-antagonist), respectively have been performed up to now.

One principal function of $\text{K}_{(\text{Ca})}$ -channels, with respect to neuronal discharge activity, is their ability to act as a negative feed back mechanism in order to prevent the cell from extensive firing. Therefore, AHPs are enhanced for example with the growing duration of bursts or with the increasing frequency of spiking in an AP-train [Hille 2001]. This is in particular true for BK-channels, which play an important role in the negative feed back regulation of VGCCs [Sah and Faber 2002]). Moreover, AHPs are known to enable spike-frequency adaptation, where the firing frequency gradually slows down in response to a steady stimulus. This is due to the temporal and/or spatial summation of AHPs, which prolongs the time of subthreshold membrane potentials. Spike-frequency adaptation can be the basis for phasic firing and neurons, which exhibit this specific discharge behaviour, occur throughout the nervous system. In the sensory system it emphasizes the response to changes of inputs and represents one compensatory mechanism for slow transduction pathways in receptor cells. In the motor side of the nervous system, spike-frequency adaptation provides briskness to the induction of movement and helps compensating for delays in movement generation [Hille 2001].

1.6.3. Pharmacology of $K_{(Ca)}$ -channels

Among $K_{(Ca)}$ -channels the BK-group is the only one sensitive to TEA with potencies in the low micromolar range [Sah and Faber 2002]. Iberiotoxin ($IC_{50} = 1.7$ nM, [Galvez et al. 1990]), a toxin derived from scorpions, and paxilline ($IC_{50} = 1.9$ nM, [Sanchez et al. 1996]), a mycotoxine, are considered to be selective for BK-channels, while charybdotoxin ($IC_{50} = 2.9$ nM, [Galvez et al. 1990]) was also shown to block a number of other potassium channels [Shaw et al. 1995]. By blocking IK-channels charybdotoxin lacks selectivity within the $K_{(Ca)}$ -channel family [Pedarzani and Stocker 2008]. Besides blocking agents, different maxi $K_{(Ca)}$ -activators have been described in the literature. One of them is for example dehydrosoysaponin-1 (DHS-1, $K_i = 120$ nM), an herbal compound [McManus et al. 1993]. The already mentioned β -subunit of $K_{(Ca)}$ -channels is also of pharmacological interest, because the co-expression of the principal subunit with the $\beta 2/3$ -subunit significantly lowers the potency of charybdotoxin and DHS-1 compared to the exclusive expression of the α -subunit. Even more impressive is the effect of the expression of $\beta 4$ in addition to α , which confers the BK-channel insensitivity to both scorpion toxins charybdotoxin and iberiotoxin, which usually block these channels with low nanomolar potencies [Sah and Faber 2002]. Most recently the small NeuroSearch molecule 11021 was shown to act as an especially potent activator for BK-channels by shifting the IV-curve to more hyperpolarized potentials. Moreover, this substance increases the macroscopic maxi $K_{(Ca)}$ -current by enhancing the open probability of the channels. NS 11021 neither affects the single channel conductance, nor the Ca^{2+} -sensitivity of $K_{(Ca)}$ 1.1. Additionally, NS 11021 was shown to be far more selective than the most broadly applied BK-opener NS 1619. The potency of NS 11021 was determined as 0.4 μ M at half-maximal current inhibition using $K_{(Ca)}$ 1.1 heterologously expressed in *Xenopus* oocytes [Bentzen et al. 2007].

SK-channels are generally blocked by the bee venom toxin apamin, quaternary salts of bicuculline ($IC_{50} = 1.1 - 25$ μ M) and different synthesized organic substances named UCL 1684 and UCL 1848 ($IC_{50} = 0.11 - 2.1$ nM). IC_{50} -values for apamin and UCL 1684 differ a lot between the different SK-subtypes and also depend on the experimental system (IC_{50} for apamin = $0.027 - 12$ nM, IC_{50} for UCL 1684 = $0.28 - 9.5$ nM [Shah et al. 2001; Pedarzani and Stocker 2008]). In the case of the bee venom toxin apamin the human SK1 (hSK1) is the least sensitive ($IC_{50} = 0.7 - 12$ nM) and the different SK2s are species-independently the most sensitive ones ($IC_{50} = 27 - 140$ pM), whereas the SK3 represents intermediate sensitivity to apamin ($IC_{50} = 0.6 - 4$ nM). Contrary to the pharmacology of apamin the organic compound UCL 1684 has its highest potency on SK2 ($IC_{50} = 0.28 - 0.36$ nM), its lowest on SK3 ($IC_{50} = 5.8 - 9.5$ nM). The IC_{50} values of UCL 1684 for SK1 channels lie in between ($IC_{50} = 0.76$ nM). The variations in IC_{50} s are due to the use of human and rat SK channel clones as well as to different expression systems [Pedarzani and Stocker 2008].

Beside apamin, different scorpion toxins also specifically block $K_{(Ca)2.x}$ -channels including scyllatoxin or leiurotoxin I ($IC_{50} = 0.29 - 325$ nM) from *Leiurus quinquestriatus*, P05 ($IC_{50} = 25$ nM) from *Androctonus mauretanicus* and tamapin ($IC_{50} = 0.024 - 42$ nM) from *Mesobuthus tamulus* [Pedarzani and Stocker 2008].

$K_{(Ca)3.1}$ -channel do not only display a characteristic single channel conductance, but also a distinct pharmacology, clearly separating them from BK- and SK-channels. IK-channels are neither sensitive to micromolar concentrations of TEA, nor to apamin in commonly used mid-nanomolarity. However, these channels can be potently inhibited with the two scorpion toxins charbdoxin ($IC_{50} = 2 - 28$ nM) and maurotoxin ($IC_{50} = 0.8 - 1.4$ nM) as well as with organic compounds such as TRAM-34 ($IC_{50} = 20 - 310$ nM). Considering that both charybdotoxin and maurotoxin block BK-channels with high potencies too, TRAM-34 is certainly the most interesting substance from an experimental point of view [Pedarzani and Stocker 2008].

Comparable with DHS-1, current-enhancers are also known for SK-channels. The prototypic SK-channel-enhancer is 1-ethyl-2-benzimidazolinone (1-EBIO, $IC_{50} = 87 - 1040$ μ M), which was the first drug identified to act on SK-channels as a positive gating modulator by increasing the channel-sensitivity to Ca^{2+} . However, the effect of 1-EBIO is not selective within the $K_{(Ca)}$ -channel-group, because it affects IK-channels quite potently ($IC_{50} = 28.4 - 136$ μ M) too. Indeed, at the present time there is no drug available, neither an organic compound, nor a toxin, available, which significantly blocks one channel while being ineffective at the other. At least for IK-channels that is not entirely true, because the novel substance NS 309 provides an approximately 10-fold higher potency for $K_{(Ca)3.1}$ ($IC_{50} = 10 - 90$ nM) than for $K_{(Ca)2.y}$ ($IC_{50} = 0.12 - 1.2$ μ M). Therefore, at low nanomolar concentrations this drug activates IK- without enhancing SK-currents. Interestingly, most SK-/IK-channel-modulators display a higher potency for $K_{(Ca)3.1}$. However, this is not the case for a novel organic compound called NS 8593, which is due to two important features of particularly interest. On the one hand it was proposed to block SK-channels ($IC_{50} = 598 - 726$ μ M) by provoking the opposite effect of positive gating modulators, namely a shift of the $[Ca^{2+}]$ -activation-curve towards higher concentrations without affecting their maximal activation. This blocking mechanism was termed negative gating modulation and is a completely new principle of SK-channel-blockade, which is incomparable with the mechanisms of all other commonly applied SK-antagonists. On the other hand it is the only modulator acting on either SK-, or IK-channels being selective for one of them. Thus, NS 8593 has no effect on $K_{(Ca)3.1}$. [Pedarzani and Stocker 2008].

Additionally interesting is a new group of organic compounds derived from clotrimazole, which have been demonstrated to block I_{sAHP} without significantly affecting $K_{(Ca)1.x}$ - and $K_{(Ca)2.x}$ -currents indicating that neither BK-, nor SK-channels serve as mediators for the sAHP. The novel clotrimazole-analogue UCL 2077 for example was shown to suppress I_{sAHP} in cultured hippocampal neurons with an IC_{50} of 0.5 μ M, which is the highest potency of all known I_{sAHP} -inhibitors at the moment. UCL 2077 is reported to be the first clotrimazole-derivative, which is highly selective on I_{sAHP} while having minimal effects on input resistances, VGCCs and mAHPs as well as heterologously expressed SK-channels [Shah et al. 2006].

1.6.4. Other Ca²⁺-dependent ion channels

1.6.4.1. Ca²⁺-dependent non-selective cation channels (CANs)

The Ca²⁺-influx via VGCCs directly varies various Ca²⁺-dependent conductances, including not only K_(Ca)- (see chapter 1.6.1.), but also CAN- and Ca²⁺-dependent Cl⁻-channels (see chapter 1.6.4.3.). The current underlying depolarizing afterpotentials or afterdepolarizations (I_{ADP}) following a physiologically induced spike train or an experimentally elicited depolarizing current stimulus has been shown to be on the one hand activated via increased cytosolic Ca²⁺-concentrations and on the other hand to be non-selectively carried by cations as it displays a reversal potential near to 0 mV. Channels exhibiting such electrophysiological properties are CAN-channels, which have been shown to be permeable for Na⁺ and K⁺ to a similar extent, but impermeable for both Ca²⁺ and Cl⁻. Remarkably, I_{CAN} undergoes neither voltage-, nor Ca²⁺-dependent inactivation providing the capability for maintaining long-lasting membrane depolarizations [Partridge et al. 2000; Launay et al. 2002]. CAN-channels are widely expressed in excitable as well as non-excitable cells including regulation of discharge activity, cardiac rhythmicity, osmotic regulation in kidney cells and pancreatic fluid secretion. Particularly in neurons, they have been demonstrated to form ADPs as well as plateau potentials in order to mediate sustained membrane depolarizations and to support important cellular responses such as bursting, motor control and the formation of working memory [Launay et al. 2002; Schiller 2004].

As far as ADPs are concerned, a fast component (fADP) decaying below 10 % in a time range of 100 - 200 ms has been distinguished from a slower part (sADP), which usually lasts for several seconds [Haj-Dahmane et al. 1997]. VGCCs, NMDA-receptors and Ca²⁺-channels of intracellular Ca²⁺-stores have been suggested as possible sources for internal Ca²⁺-rises inducing CAN-activation [Partridge et al. 1999; Schiller 2004]. Furthermore, certain GPCRs such as metabotropic glutamate-receptors (mGluR) and muscarinic receptors have been reported to activate I_{CAN} and modulate sADPs, respectively [Congar et al. 1997]. However, the role of these GPCRs in evoking ADPs via direct or Ca²⁺-mediated CAN-activation is still under discussion [Karnup et al. 2001; Schiller 2004].

Pyramidal cells of layer V of the rodent medial prefrontal cortex show a tonic-phasic firing activity, which is characterized by a doublet or triplet of spikes and a slow adaptation of firing frequency in response to a constant depolarizing stimulation. This firing behaviour, especially the initial tonic response, is suggested to require two electrophysiological properties, that are low-threshold activating VGCCs on the one hand and CAN-channels mediating I_{fADP}s on the other hand. In this model both VGCCs and the resulting I_{fADP}s are postulated to mediate the initial fast firing of these cortical cells. In detail, the third and/or second spike(s) are/is supposed to be triggered by the summation of fADPs. This very first part of the neuronal response represents its tonic portion, which is terminated by the slower activation of K_(Ca)-channels inducing the phasic response. Therefore, in neurons exhibiting discharge patterns similar to the described one, fADPs display an important mechanism for delaying spike-frequency adaptation [Haj-Dahmane and Andrade 1997]. Moreover, I_{CAN} underlying plateau potentials

was shown to play an important role in the regulation of the excitability of nigral GABAergic neurons. In these cells, the Ca^{2+} -inward movement required for CAN-activation is provided by LTCC- and NMDA-receptor-activation. Additionally, it was suggested that enhanced CAN-currents shift these nigral neurons away from more regular firing patterns to irregular, bursty firing characteristically for pathological activities observable in Parkinson's disease or under conditions of dopaminergic denervation [Lee et al. 2007].

Although various publications have demonstrated that CAN-channels can be blocked by flufenamic acid [Shaw et al. 1995; Haj-Dahmane and Andrade 1997; Partridge and Valenzuela 2000; Schiller 2004; Lee and Tepper 2007], data about its potency on physiologically measured I_{CAN} , in contrast to heterologously expressed TRPM-currents (see following chapter) are rather rare in literature. For rodent supraoptic neurons an IC_{50} of $13.8 \mu\text{M}$ was determined [Ghamari-Langroudi et al. 2002]. CAN-inhibition by flufenamate has a comparably slow time course and needs up to 10 min to reach steady state [Ghamari-Langroudi and Bourque 2002]. However, if the drug is directly delivered into the cytosol, I_{CAN} is rapidly blocked within 20 s [Guinamard et al. 2002]. This suggests that flufenamic acid needs access to the internal side of the CAN-channel in order to block it, while transmembrane diffusion, when externally applied, slows down the inhibitory effect. Interestingly, it was reported that the application of flufenamate caused a biphasic effect consisting of a transient increase in I_{CAN} followed by its inhibition. The preceding I_{CAN} -enhancing effect lasted only for several tens of seconds and was determined to be due to a flufenamic acid-induced Ca^{2+} -release from intracellular stores [Partridge and Valenzuela 1999, 2000]. Because of additional effects on certain subtypes of K^{+} - and Ca^{2+} -activated Cl-channels as well as gap junctions, the pharmacological action of flufenamate has been proven to be largely unspecific [Schiller 2004].

Besides I_{CAN} , different other ionic mechanisms have been discussed to generate ADPs including Ca^{2+} -activated Cl-currents [Higashi et al. 1993] and an electrogenic $\text{Na}^{+}/\text{Ca}^{2+}$ -exchanger as well as the Ca^{2+} -dependent inactivation of resting K^{+} -currents [Haj-Dahmane and Andrade 1997; Schiller 2004]. However, data about I_{ADP} s that are still measurable at the Cl-equilibrium as well as their demonstrated voltage-dependence make the involvement of Ca^{2+} -activated Cl-channels and $\text{Na}^{+}/\text{Ca}^{2+}$ -antiporter in depolarizing afterpotentials quite unlikely. The model, implying the ionic exchanger as a contribution to I_{ADP} , would predict its complete voltage-independence, which is not the case [Haj-Dahmane and Andrade 1997].

1.6.4.2. Transient receptor potential (TRP)M4-channels are Ca^{2+} -activated monovalent cation channels

Regarding the molecular identity of channels underlying currents described as I_{CAN} or I_{ADP} , an overall scheme is by far less established than in the $\text{K}_{(\text{Ca})}$ -family with their associated currents. Although a broad range of TRP-channels displays a certain sensitivity to Ca^{2+} , predominantly by their Ca^{2+} -mediated modulation, only a small subset of TRP-channels has been identified to be directly gated by internal Ca^{2+} -rises (e.g. TRPM4 with M standing for melastatin). Especially TRPM4b was shown to provide the distinct electrophysiological property of a CAN-channel, which is a (I) slowly inactivating, (II) Ca^{2+} -dependent (III) inward current (directly induced after binding of Ca^{2+} with a $K_D \sim 0.4$ [Launay et al. 2002] almost (IV) exclusively carried by monovalent cations, (V) without any discrimination of K^+ over Na^+ and (VI) reversal potential at ~ 0 mV. Therefore, TRPM4b-channels complexly shape $[\text{Ca}^{2+}]_i$ by regulating the driving force for Ca^{2+} in a Ca^{2+} -dependent manner. Hence, TRPM4b-activation exhibits a negative feed-back control for Ca^{2+} -influx through the surface membrane (i.e. receptor-mediated) as a membrane depolarization decreases the driving force for Ca^{2+} . Furthermore, TRPM4b-currents are voltage-dependent by displaying enhanced single channel open probabilities and open times at depolarized membrane potentials, which are suggested to be responsible for the slight inward and outward rectification of these channels. Their single channel conductance lies at about 25 pS, which gave these channels the alternative description of 25 pS-NSC_{Ca}. The dose-response curve for Ca^{2+} and the inducing TRPM4b-current amplitude revealed an EC_{50} of 420 nM $[\text{Ca}^{2+}]_i$ and hill coefficients between 4 and 6 indicating a strong cooperativity between different Ca^{2+} -binding sites. On account of the fact that global cytosolic Ca^{2+} -transients induced by Gq-protein-activation are less effective in activating TRPM4b-currents than localized oscillatory changes in $[\text{Ca}^{2+}]_i$, at least some of the TRPM4b-channels are assumed to co-localize with store-operating Ca^{2+} -channels causing the spatially restricted Ca^{2+} -rises [Launay et al. 2002; Guinamard et al. 2006]. The activation of Gq-protein coupled receptors was also shown to modulate the Ca^{2+} -sensitivity of TRPM4b-channels via PKC-mediated phosphorylation [Nilius et al. 2005].

As far as the pharmacology of TRPM4b-channels is concerned, they can be blocked by the nonsteroidal anti-inflammatory drug flufenamic acid ($\text{IC}_{50} = 2.8 - 5.5 \mu\text{M}$) and by the hypoglycemic agent glibenclamide ($\text{IC}_{50} \sim 10 \mu\text{M}$), as well as by cytosolic ATP in mM concentrations [Nilius et al. 2004; Guinamard et al. 2006].

Recently, in the TRPM-protein family another channel with CAN-like properties was described as TRPM5. Its main differences in comparison to TRPM4b are missing ATP-binding cassettes and thus a failing inhibition with $[\text{ATP}]_i$ and a 10-fold lower potency of flufenamic acid with an IC_{50} of 24.5 μM [Hofmann et al. 2003; Ullrich et al. 2005].

1.6.4.3. Ca^{2+} -dependent Cl^- -channels ($\text{Cl}_{(\text{Ca})\text{s}}$)

To date Cl^- -channels can be divided into four different classes distinguished by the stimulus of gating, which is either a de- or hyperpolarization of the membrane potential, cell swelling, cAMP-dependent phosphorylation, or an elevation of $[\text{Ca}^{2+}]_i$. Channels responding to the latter stimulus modality are called $\text{Cl}_{(\text{Ca})}$ -channels, which have been ubiquitously observed. Their gating-properties are similar to that of BK-channels displaying both voltage- and Ca^{2+} -dependency. In detail, single channel openings are increased by $[\text{Ca}^{2+}]_i$ -rises as well as by membrane depolarizations. As with BK-channels, the depolarization needed to open $\text{Cl}_{(\text{Ca})}$ -channels decreases with enhanced cytosolic Ca^{2+} -concentrations [Hille 2001].

In certain epithelial cells, $\text{Cl}_{(\text{Ca})}$ -channels to mediate Ca^{2+} -dependent (i.e. hormonally induced) net fluxes of salt and fluid across the cell sheets. Referring to their role in the neuronal activity, $\text{Cl}_{(\text{Ca})}$ -channels are supposed to have comparable functions to SK-channels except their differences in reversal potentials. Whereas SK-channels usually mediate Ca^{2+} -dependent AHPs, $\text{Cl}_{(\text{Ca})}$ -channels display a reversal potential near the voltage at resting conditions and thus primarily stabilize this. That means, dependent on the respective driving force for Cl^- , $\text{Cl}_{(\text{Ca})}$ -channel-activation causes either AHPs, or ADPs [Hille 2001].

1.6.5. Functional coupling of LTCC-mediated Ca^{2+} -influx to different Ca^{2+} -dependent ion channels

$[\text{Ca}^{2+}]_i$ necessary for activation of Ca^{2+} -dependent ion channels can be obtained from various sources, providing Ca^{2+} from both the inter- and intracellular space. As this diploma thesis focuses on the role of LTCCs in neuronal activities, the last part of chapter 1.6. deals with the connection of local $[\text{Ca}^{2+}]_i$ -elevations caused by LTCC-opening with the following changes in ionic conductances as well as with their resulting effects on the membrane potential. The Ca^{2+} -influx via LTCCs has many different coupling-targets and within the group of Ca^{2+} -activated ion channels, $\text{K}_{(\text{Ca})1.x}$, $\text{K}_{(\text{Ca})2.x}$ and CAN-channels in the surface membrane and ryanodin-receptors (RyR) in the membrane of intracellular Ca^{2+} -stores are among the most extensively investigated ([Hille 2001], fig. 2).

1.6.5.1. Functional coupling of LTCC to $K_{(Ca)}1.x$

LTCCs were shown to couple directly (I) as well as indirectly (II) to BK-channels. (I) As far as the direct coupling is concerned, a co-assembly of $Ca_v1.2$ and $Ca_v1.3$ with $K_{(Ca)}1.x$ was proven for various neuronal tissues throughout the rat brain including e.g. the hippocampus [Grunnet and Kaufmann 2004]. From a functional point of view, a coupling between LTCCs and BK-channels was published for rat superior cervical ganglia (SCG)-neurons [Davies et al. 1996] and for neocortical pyramidal neurons [Sun et al. 2003]. Co-immunoprecipitation in the rat brain revealed that among the HVA VGCCs $Ca_v2.2$ is the subtype most abundantly associated with BK-channels. However, in a minor extend $Ca_v1.2$ was also shown to form such associations. Moreover, in contrast to the co-expression of $Ca_v2.2$ $\alpha1$ and Ca_v $\beta3$ together with $K_{(Ca)}1.y$ (Slo_{27}), only few examples of rapid functional coupling were observed, if $Ca_v1.2$ $\alpha1$, Ca_v $\beta3$ and $K_{(Ca)}1.x$ (Slo_{27}) were co-expressed [Loane et al. 2007]. Furthermore, BK-channels were shown to build macromolecular complexes with $Ca_v1.2$, $Ca_v2.1$ and $Ca_v2.2$, which reconstituted after heterologous co-expression in *Xenopus* oocytes into a functional “ Ca^{2+} -nanodomain”, where VGCC-mediated Ca^{2+} -inward currents activated BK-channels at physiological voltage ranges within ms [Berkefeld et al. 2006]. K^+ -outward currents measured from $Ca_v2.1/K_{(Ca)}1.x$ -complexes exhibited shorter rise time constants and more negative IV-relations than complexes consisting of $Ca_v1.2$ and $K_{(Ca)}1.x$ irrespective of the differences between the two Ca_v -subtypes. If AP-shaped pulse protocols were used, I_{BK} from $Ca_v2.1/K_{(Ca)}1.x$ -complexes activated with shorter AP-amplitudes and lasted longer than $Ca_v1.2/K_{(Ca)}1.x$ -mediated BK-currents suggesting that I_{BK} -properties are differently shaped by the specific associated VGCC-subtype (fig. 2, [Berkefeld et al. 2008]).

(II) Indirect LTCC-coupling to $K_{(Ca)}1.x$. In cerebellar granule cells stimulation of mGluR type I (mGluR1) provides two different pathways of $[Ca^{2+}]_i$ -elevation coupling to $K_{(Ca)}1.x$ -activation. Internal Ca^{2+} -rises after activation of mGluR1 are induced on the one hand by LTCC-mediated Ca^{2+} -induced Ca^{2+} -release (CICR) via Ryanodin receptors (RyR) and on the other hand by Ca^{2+} -release via IP_3 -receptors (IP_3R). The fact that mGluR1-induced I_{BK} -facilitation was abolished in the absence of Ca^{2+} in the pipette solution in cell-attached recordings gives reason to hypothesize that BK-channels are co-localized with the LTCC-RyR-interaction system. Furthermore, such co-localizations have already been reported for frog neuromuscular junctions and neurons of *Helix sp.* [Chavis et al. 1998]. The hint that LTCCs are functionally coupling to RyRs is further supported by the physical association of $Ca_v1.3$ $\alpha1$ with RyR type 2 (RyR2) shown with co-immunoprecipitation assays in the rodent hippocampus. However, in this case LTCC-mediated CICR during membrane depolarization was even measured in the absence of Ca^{2+} in the bath solution. Hence, LTCC-induced RyR2-activation does not actually require Ca^{2+} -influx via LTCCs indicating that BK-activation via the LTCC-RyR2-interaction system does not necessarily imply actual LTCC-mediated Ca^{2+} -influx [Kim et al. 2007]. Possible physiological functions of this coupling system are glutamatergic modulation of AP-repolarization via I_{BK} -facilitation, a BK-mediated protecting function against Ca^{2+} -overload during intense glutamatergic transmission,

fine tuning of fast excitatory synaptic transmission and the translation of synaptic activity into changes in the expression profile of proteins involved in learning and memory [Chavis et al. 1998; Kim et al. 2007]. Moreover, a contribution of RyRs to $[Ca^{2+}]_i$ activating I_{sAHP} was observed in rat hippocampal pyramidal neurons [Tanabe et al. 1998; Shah and Haylett 2000a]. This probably refers to an interaction of LTCC-induced CICR with the channels underlying I_{sAHP} (fig. 2).

1.6.5.2. Functional coupling of LTCC to $K_{(Ca)2.x}$, I_{mAHP} and I_{sAHP}

(I) LTCC-coupling to I_{sAHP} Besides indirectly activating I_{sAHP} via LTCC-induced CICR (see chapter 1.6.5.2.), a direct relation of LTCC-mediated Ca^{2+} -entry and I_{sAHP} has been shown in slices of the hippocampus [Tanabe et al. 1998; Lima et al. 2007] as well as in isolated hippocampal cells [Shah and Haylett 2000a]. Moreover, a specific $Cav1.3$ - I_{sAHP} -interaction was shown for the amygdala and the CA1 region of the hippocampus. As far as the $Ca_v1.3^{-/-}$ -mice are concerned they exhibited significantly reduced sAHPs, while a faster component of the AHP remained [McKinney et al. 2009].

(II) LTCC-coupling to I_{mAHP} In addition to that a functional relation between $Ca_v1.x$ and I_{mAHP} which is in contrast to I_{sAHP} widely accepted to be caused by SK-activation (see chapter 1.6.2.), has been demonstrated in hippocampal slices cultures. However, the reducing effect of LTCC-inhibition on I_{mAHP} was significantly smaller than on I_{sAHP} [Lima and Marrion 2007]. On the assumption that I_{SK1} at least partly corresponds to I_{mAHP} data from [Bowden et al. 2001] support the notion of a coupling between LTCCs and I_{mAHP} in hippocampal cells, by proving both physical and functional interaction of $Ca_v1.3$ and SK1. In order to compare $Ca_v1.x$ -couplings to $K_{(Ca)1.x}$ and $K_{(Ca)2.x}$, respectively [Marrion et al. 1998] have reported for hippocampal neurons that LTCCs only activate SK-channels, when BK-channels are not activated in the same cell-attached patch. Due to their measurements of SK-activation kinetics they conclude a distance between LTCCs and SKs of 50 - 150 nM. This is in contrast to NTCCs, which are supposed to be closely associated with BK-channels [Marrion and Tavalin 1998].

1.6.5.3. Functional coupling of LTCC to CAN

Although investigations are certainly more advanced in the field of inhibitory LTCC-couplings, at least a few data can be found demonstrating a coupling of LTCCs to CAN-channels, for example in nigral GABAergic neurons. In detail, these neurons exhibited plateau potentials when depolarized from hyperpolarized membrane potentials, which were shown to be caused by I_{CAN} activated via LTCC-mediated Ca^{2+} -influx [Lee and Tepper 2007].

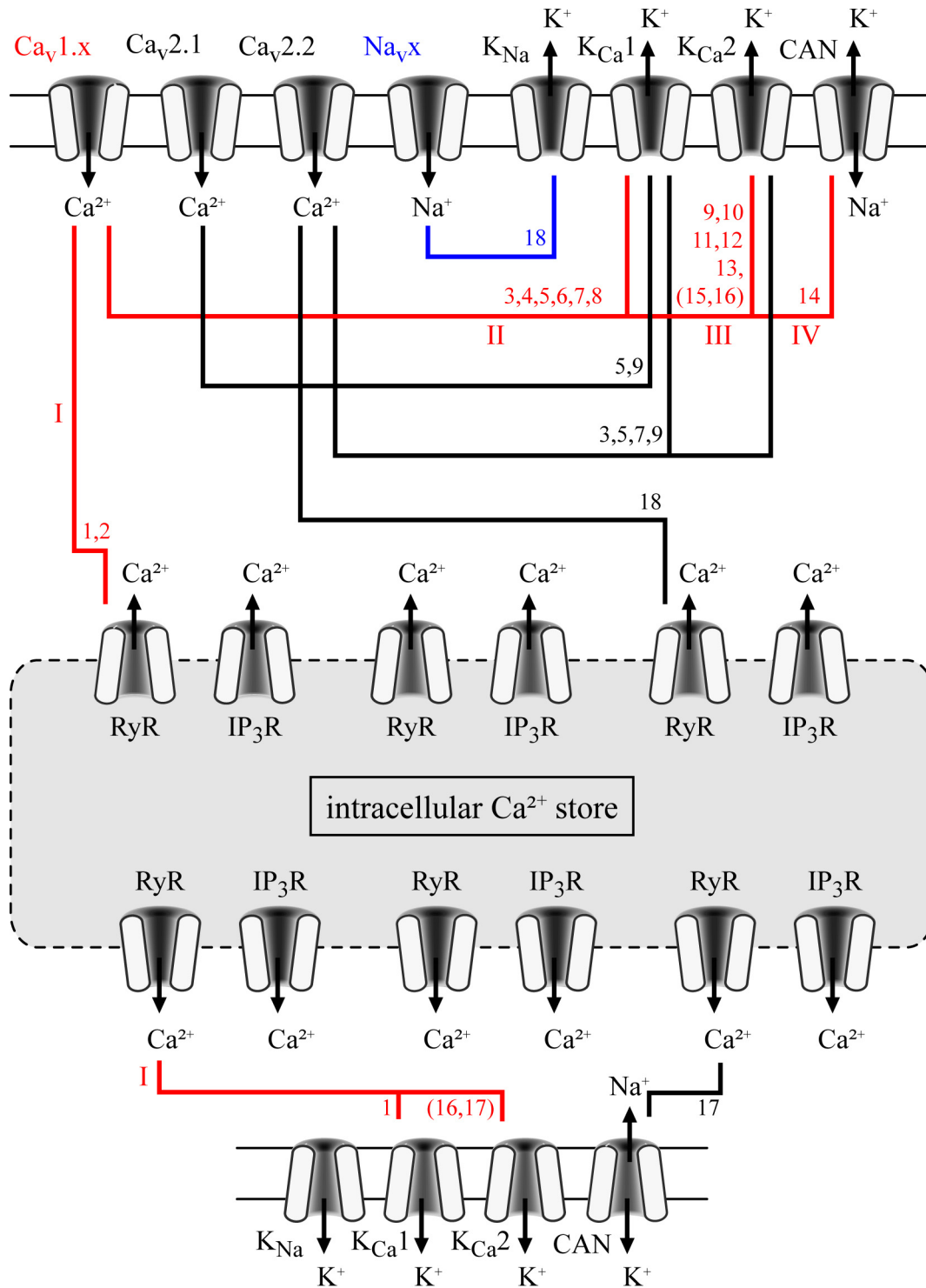


Fig. 2: Simplified scheme of voltage-gated Ca^{2+} - and Na^+ -channels functionally coupling to different Ca^{2+} - and Na^+ -dependent ion channels. Note that the numbers in brackets refer to an interaction with the current underlying sAHPs. The roman numerals label the four main pathways of LTCC-coupling (red). The numbers 1 - 19 stand for the respective publications (1...Chavis et al. 1998, 2...Kim et al. 2007, 3...Loane et al. 2007, 4...Grunet and Kaufmann 2004, 5...Berkefeld and Fakler 2008, 6...Davies et al. 1996, 7...Sun et al. 2003, 8...Berkefeld et al. 2006, 9...Lima and Marion 2007, 10...Bowden et al. 2001, 11...Marrion and Tavolin 1998, 12...Moyer et al. 1992, 13...Rascal et al. 1991, 14...Lee and Tepper 2007, 15...Shah and Haylett 2000, 16...Tanabe et al. 1998, 17...Vogalis et al. 2002, 18...Bhattacharjee and Kaczmarek 2005).

1.7. Specific question of this diploma thesis

Recent publications show that, $Ca_v1.3$ compared to $Ca_v1.2$ seems to have a minor contribution in regulating the activity of hippocampal neurons [Moosmang et al. 2005; Lacinova et al. 2008]. These findings are supported by the lack of neurological phenotypes in $Ca_v1.3^{-/-}$ -mice [Clark et al. 2003]. Furthermore, there is a greater versatility in $Ca_v1.2$ -splice variants including anomalously gating LTCCs [Kavalali et al. 1994; Koschak et al. 2007]. However in contradiction to the data obtained from the knock out mice, immunocytochemical studies as well as in situ hybridization revealed the presence of both neuronal L-type-isoforms in the rodent hippocampus [Hell et al. 1993; Ludwig et al. 1997].

Furthermore, the role of LTCCs in epileptiform/epileptogenic activity has remained unclear. In both, clinical investigations and animal experiments pro- and antiepileptic action of LTCCs were observed [Fragoso-Veloz et al. 1990; de Falco et al. 1992; Shitak et al. 2007].

Thus, the aim of this diploma thesis was to investigate how LTCCs contribute to neuronal firing activity in cultures of primary hippocampal neurons on level of single cells as well as the in vitro network. In order to address this issue, electrophysiological experiments using the patch clamp technique were performed. Moreover, these experiments should provide the basis for further comparative studies using $Ca_v1.2^{-/-}$ - and $Ca_v1.3^{-/-}$ -mice.

2. MATERIAL AND METHODS

2.1. Preparation of primary hippocampus culture from rats

Rats of at most one day of age were decapitated. After opening the calvaria the brain was put in a PUCK KYN filled culture dish. The autoclaved and sterile filtered puck solution contained NaCl 137 mM, KCl 4.5 mM, Na₂HPO₄ x 2 H₂O 1.1 mM, KH₂PO₄ 1.1 mM and glucose 6.1 mM and was adjusted to pH 7.3 with NaOH. The concentration of kynurenic acid, a NMDA receptor antagonist [Vamos et al. 2009] in the PUCK KYN solution was 1 mM. Then the two hemispheres were detached from each other and the meninges were removed. After turning the hemisphere's inside out, the hippocampus appears in the middle of each brain half. The hippocampi were removed by using small scissors and a scalpel and collected in a fresh PUCK KYN filled culture dish. Subsequently, the isolated hippocampal tissue was freed from parts of connective tissue and blood vessels, perforated with the tip of a scalpel and transferred in papain solution (25 units/mL). The incubation in the enzyme lasted for approximately 20 - 30 min at 37 °C (5 % CO₂). Then the hippocampus pieces were pipetted into ice-cold stop solution (PUCK KYN with 33 % FCS) in order to end the ongoing digestion of connective tissue. Afterwards the hippocampi were transferred into in DMEM medium + PS (for 50 mL: 45 mL DMEM high glucose +/- 25000 IU/L penicillin and 25 mg/L streptomycin PS, 5 mL FCS heat inactivated, 100 µL MgCl₂ 1M, 125 µL NUTS (NUTS contained 50 mg/10 mL ITS (insulin:transferrin:Na-selenite = 25:25:0.025), 0.015 mg/ 10 mL progesterone, 72.5 mg/ 10 mL putrescine)) and titrated with fire polished Pasteur pipettes of different diameter. This process was repeated until the tissue was fully disintegrated and the cell suspension became cloudy. NUTS contained 50 mg/10 mL ITS (insulin:transferrin:Na-selenite = 25:25:0.025), 0.015 mg/ 10 mL progesterone, 72.5 mg/ 10 mL putrescine. The next step was to determine the cell density by using a cell counting chamber. The required volume of cell suspension for a certain cell concentration was then pipetted in the glass ring, which was positioned in a PDL-coated 35 mm culture dish filled

with 2 mL medium. After a certain time allowed for adhesion of the neurons at the dish bottom (one to two hours), the glass rings were removed. On the next day, the medium was replaced by antibiotic free DMEM. 4 days after preparation, ARA C (Cytosine-beta-D-arabinofuranoside hydrochloride) was added to stop growth of glia cells. ARA-C is a cytostatic agent especially affecting fast proliferating cells, while damaging DNA-synthesis, when cell cycle holds in S-phase [Aktories 2009]. In order to level out the evaporation of medium at 37 °C out, 150 µL autoclaved and sterile filtered MQ water was added once a week.

2.2. Transformation, DNA purification and transient transfection of HEK-_{TS}A201 cells

Transfection designates the incorporation of DNA in form of plasmids in living eukaryote cells, which can be either cell lines (i.e. HEK-_{TS}A201, HeLa, KB-3-1), or primary cells (e.g. neurons). This results in the heterologous expression of certain genes, such as receptor- or ion channel-subunits and fluorescing molecules like GFP, respectively. In contrast to stable transfections, in transient ones the plasmid stays outside the genome and is slowly lost by degradation or dilution through cell division. Moreover, transient transfections have a by far higher efficiency than their stable complement. In stable transfections the respective gene can be either expressed constitutively, or by induction of a promoter [Numberger 1996; Brown 1999; Alberts 2002].

On the first day of the whole procedure, liquid LB medium (Tryptone 10 g/L, yeast extract 5 g/L, NaCl 10 g/L) and LB agar plates (+ 15 agar g/L) were prepared, adjusted to pH 7.3 with NaOH and autoclaved. Before plating the agar and adding the appropriate amount of antibiotics (ampicilin 50 µg/mL), the plates had to cool down to about 50 °C. This had to be done next to the flame of a Bunsen burner. Concerning the liquid LB medium, antibiotics were added to the selection medium for the pre and main culture, whereas the medium for the freshly transformed *E. coli* was left without. Alternatively to LB medium (for Cav1.2 constructs) circle grow bio101 medium (40 g circle grow powder/L) was used for Cav1.3 constructs. On the second day, the respective DNA-constructs had to be amplified. This was done by using a procedure called transformation, where the DNA-receiving cell (i.e. a bacterium such as *E. coli*) incorporates “naked” DNA-molecules and recombines them [Alberts 2002]. For the sake of improving the transformation efficiency competent bacteria (stored at -80 °C) were used. After taking them out of the freezer, the 50 µL aliquots were immediately put on ice. To each vial 10 µL of the plasmid (0.01 µg/µL) or the equal amount of MQ water as a negative control were pipetted and carefully dispersed in the solution. Afterwards, the bacteria were incubated on ice for 30 min. Before the bacteria were cooled down on ice again, they were put in the preheated thermomixer at 42 °C for exactly 45 s. The following incubation on ice lasted for about 2 min. Subsequently, 1 mL of antibiotic-free circle grow bio101 medium was added to the vials, which were then mixed at 37 °C for 30 to 60 min (1000 rpm). Afterwards, 50 µL of

the *E. coli* culture were spread out on circle grow bio101 agar plates with antibiotics by using a fire polished spatula Drigalsky. The plates with the transformed *E. coli* were then incubated upside down at 37 °C for 12 h. On the following day it was first checked, if there was absolutely no growth of the negative control and single colonies of the positive control. 5 mL of antibiotic containing circle grow bio101 medium were put in a sterile 12 mL tube with cap, in which a single colony of the positive control picked up using a toothpick was transferred (preculture). For negative control an unloaded tooth pick was incubated. Afterwards, the tubes were shaken (150 rpm) at 37 °C. About six hours later the negative control was checked and 100 µL of the preculture were transferred to about 200 mL circle grow bio101 medium (with antibiotics) for the main culture. These cultures were now shaken (200 - 250 rpm) overnight at 37 °C. On the fourth day the overnight culture was centrifuged at 5000 rpm for 25 min, the supernatant was discarded and the resulting cell pellet was further used. Afterwards, DNA was purified using an EndoFree Plasmid Purification Maxi Kit by Quiagen according to the manufacturers instructions. Subsequently, the DNA concentration as well as its purity was measured via the ratio of the absorption at 260 and 280 nm (UV spectrophotometry).

For splitting _{TS}A201-HEK cells in a 10 cm culture dish, they were washed twice with 6 mL PBS and incubated with 6 mL EDTA at room temperature for 3 min. The resulting cell suspension was then centrifuged for 5 min at 800 rpm. The supernatant was removed, whereas the cell pellet was resuspended with 1 mL medium (DMEM low glucose + PS, 10 % FCS). After determining the cell density, 150 000 cells were seeded in a 35 mm PDL-coated culture dish filled with 2 mL medium. For the purpose of transfection certain amounts of the plasmids with the respective genes (i.e. 3 µg α 1, 2 µg β 3, 2.5 µg α 2 δ , 0.75 µg GFP per 3 mL medium) were mixed together and diluted in 250 µL serum free medium without antibiotics (DMEM low glucose). In the meantime 15 µL of Lipofectamine 2000 (Invitrogen) were diluted in 250 µL SFM (-ABS) and incubated for 5 min at room temperature. After this, the latter solution was transferred to the DNA containing solution. This was gently mixed and incubated at room temperature for at least 20 min. Before the transfection reagents were added to the HEK-_{TS}A201 cells, they had to be washed once with SFM (-ABS). After four to six hours of incubation (37 °C, 5 % CO₂) the serum free medium was exchanged with the medium containing PS and 10 % FCS. In order to ensure no further activity of Lipofectamin, the cells were once washed with medium. On the following day the transfected cells were split and seed at lower density (50 000). From this point on these cells were incubated at 30 °C instead of 37 °C.

One α 1-subunit each for Ca_v1.2 α 1C77 [Liao et al. 2004], Ca_v1.2 α 1C77^{DHPi} (T1036Y) and for Ca_v1.3long [Koschak et al. 2001] or Ca_v1.3long^{DHPi} (T1022Y) was electrophysiologically investigated after heterologously expressing it in HEK-_{TS}A201 cells together with the auxiliary subunits β 3 and α 2 δ .

2.3. Solutions and drugs

Both in whole cell and perforated patch recording mode, the inner (pipette) solution always corresponded to the cytosol, whereas the outer one corresponded to the extracellular fluid. In the whole cell mode the cytoplasmic solution will become replaced by the pipette electrolyte (chapter 2.7.), whereas in the perforated patch mode the cytosolic composition is kept unaltered. The most frequently used inner solution was based on potassium gluconate with a relatively low $[Cl^-]_i$ of 7 mM, which is described as being physiological for mature hippocampal neurons [Ben-Ari 2002, 2006]. A major disadvantage of inner solutions containing low concentrations of Cl^- is the comparatively high resulting liquid junction potential, caused by the slow diffusion velocity of gluconate (chapter 2.5.). The composition of the potassium gluconate pipette solution was as follows: potassium gluconate 120 mM, Nagluconate 1.5 mM, NaCl 3.5 mM, $CaCl_2$ 1.5 mM, $MgCl_2$ 0.25 mM, HEPES 10 mM (buffer), EGTA 5 mM (Ca^{2+} -chelator). Additionally, KOH was added to adjust pH to 7.3. An alternative inner solution was used in if Ca^{2+} -currents were measured. Hence, potassium gluconate was replaced by CsCl, in order to block delayed rectifier K^+ -channels [Hille 2001]. The complete composition of this solution was: CsCl 130 mM, TEACl 20 mM, $CaCl_2$ 0.24 mM, HEPES 10 mM, glucose 10 mM, EGTA 5 mM. The adjustment of pH to 7.2 was done with CsOH.

In order to allow adaptation of the outer solution to diverse experimental situations, a constant stock of NaCl 120 mM, KCl 3 mM, HEPES 10 mM and glucose 20 mM (for balancing osmolarity) was used (NaOH for adjusting pH to 7.35). In most cases, apart from the following exceptions, NaCl 20 mM, $CaCl_2$ 2 mM and $MgCl_2$ 2 mM were added. If K^+ channels should be unselectively blocked, the supplementation with NaCl 20 mM was replaced by TEACl 20 mM (i.e. recordings of $GABA_A$ - and LTCC-currents, chapter 2.5., 3.1.).

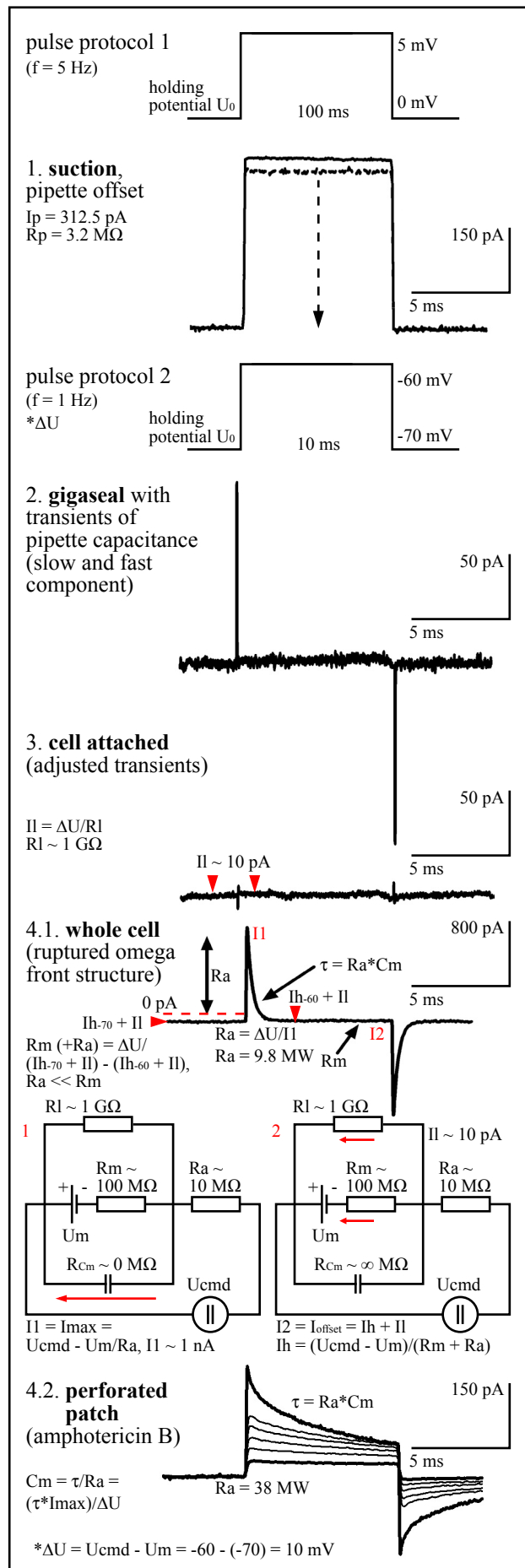
Moreover, for measuring LTCC-currents in transfected $T_{TS}A201$ cells under conditions of enhanced driving forces, the external $[Ca]$ or $[Ba]$ was enhanced from 2 to 10 mM. Besides the standard stock, a completely different solution was employed, if only a substantially reduced Na-influx should be permitted. Thus, the $[Na^+]$ was reduced to 1.5 mM by replacing it with choline 140 mM. The concentrations of K^+ , Ca^{2+} , Mg^{2+} , HEPES and glucose stayed the same. The Cl^- -concentration was slightly decreased from 151 to 148 mM. As bases KOH 3 mM and NaOH 1.6 mM were used. Voltage-gated Na^+ channels, except of TTX-insensitive channels, were blocked by TTX 500 nM [Hille 2001].

Drugs were dissolved in either dimethyl sulfoxide DMSO (lipophilic solvent), or recording buffer (e.g. proteins as apamin or ATXII and hydrophilic substances like XE991 or muscimol). If DMSO was used as solvent, the respective amount was added to buffer, which then served as control solution. Thus, final concentrations of DMSO were constantly kept at 0.3 %. ATXII, BayK, DMSO, flufenamic acid, isradipine, muscimol and TEA were purchased from Sigma-Aldrich (Vienna, Austria), Apamin, UCL 1684, UCL 2077 and XE991 from Tocris Bioscience (Ellisville, Missouri 63021, USA).

2.4. Patch clamp set up and preparations for measurements

Patch electrodes P were formed of borosilicate capillaries (Science Products GB150-8P, dimension 0,86 x 1.50 x 80mm) with a Sutter P97 horizontal puller. Pipette resistances R_p lay between 1.5 and 2.5 with CsCl⁻ (whole cell) and 2 and 4 M Ω with potassium gluconate inner solution IS, respectively. After dipping the pipettes into inner solution (tip filling) and back filling them by using a thin quartz glass pipette (microfill), they were conductively connected via a Ag/AgCl electrode ME with the headstage HS (Axon Instruments CV-7B) by fixing them with a pipette holder. In order to minimize R_p and possible noise, air bubbles were removed and the pipette was filled with inner solution to an extent that the solution just reaches the electrode [Numberger 1996]. For the purpose of avoiding offset potentials (chapter 2.4.) or at least to keep them constant, the silver wires had to be chlorinated, i.e. by putting them into Na⁺-hypochlorite according to: $2 \text{Ag} + 2 \text{HOCl} + 2 \text{H}^+ \rightarrow 2 \text{AgCl} + 2 \text{H}_2\text{O}$ [Sherman-Gold 1993]. A significant drift of the pipette offset potential (chapter 2.4.) is a conceivable indication of a damaged AgCl-coat [Numberger 1996]. The reference electrode RE consisted of Ag/AgCl, too. From the headstage, signals were transmitted to a Multiclamp 700B amplifier AMP (Axon Instruments) controlled by the software Multiclamp 700B commander 2.1.0.13 (Axon Instruments). A Digidata 1440A (Axon Instruments) digitizer DIGI converted the received analogous A signals in a digital D form, which then could be recorded by a personal computer PC using Clampex 10.2 (Axon Instruments). Substances were applied to the cells by a superfusion S device (DAD 12, ALA Scientific Instruments). All parts of the set up were grounded via a Faraday cage FC or the grounding jack of the headstage (reference electrode) and the amplifier, respectively. Cells were selected for electrophysiological recordings by visually observing them under 100- and 400-fold magnification using an inverse microscope (Nikon Eclipse TE3000) with phase contrast, transmitted light and optionally with a super high pressure mercury lamp (excitation filter with $\lambda = 475 \text{ nm}$) and a broadband fluorescence filter for GFP (λ of peak emission = 509 nm). The microscope as well as the superfusion reservoirs and the micromanipulators (Luigs und Neumann SMI/Mini 25) for the superfusion tip (ALA Scientific Instruments, Micromanifold, 12 @ 100 μM tips, 1 @ 200 μM flush) holder, the headstage and the cell dish holder were protected from vibration and electrical disturbance while standing on a compressed air damped desk DE (TMC, Micro-g 63-564) and surrounded by a Faraday cage, respectively. By positioning the superfusion tip on the edge of the visual field a small neuronal network including the patched neuron was exposed to the applied drug (fig. 3).

Shortly before electrophysiological recordings culture dishes were taken out of the incubator, twice washed with outer solution and filled with 2.25 mL of the same solution. For perforated patch recordings an amphotericin B stock solution (50 mg/mL) was 1:100 diluted in inner solution.



of Cl^- from the electrode into the bath and thus to a change in the pipette offset potential [Numberger 1996]. Pipette offset potentials were approximated and compensated by Multiclamp 700B commander 2.1.0.13 as the voltage, where no current flows (fig. 5). If this adjustment would not be made, the commanding potential U_{cmd} would not correctly be applied to the membrane (fig. 3, [Numberger 1996]).

The second source for offset potentials, beside the one at the electrodes (pipette offset potential), is a potential between differently composed electrolytes (liquid junction potential, LJP). At their interface, ions diffuse from one solution into the other along their chemical gradients. If ions, such as Cl^- in comparison to gluconate, have different diffusion velocities, which are e.g. dependent on the size of the ion, electrical potentials will result. That means, the larger the difference in the mobility of the respective ions, the higher the liquid junction potential will be (i.e. the LJP is smaller, if sulfonate instead of

Fig. 4: The four preparing stages preceding every voltage-clamp experiment. Two representative equivalent circuits are shown for the currents I_1 and I_2 measured under whole-cell conditions (4) before adjusting the capacitive transients of the cell. I_1 is just given by the access resistance R_a and therefore large, whereas I_2 is additionally limited by the membrane resistance R_m . At I_2 the membrane can be interpreted as a resistance, while inbetween it corresponds to a capacitor. For current-clamp measurements other adjustments had to be done (for further details see text (Bretschneider and De Weille 2006, Neher and Sakmann 1995, Numberger and Draguhn 1996)).

gluconate is used for substituting Cl⁻ in the pipette solution). Glutamate for example is known to have an especially low diffusion velocity leading to a high LJP of about 10 mV [Numberger 1996]. When the offset potential is adjusted to the pipette offset potential, one component of the correction also compensates for the liquid junction potential. This starts to become crucial in the cell attached configuration, where a tight contact between the cell membrane and the pipette prevents the further occurrence of LJPs. Hence, the voltage, where no current flows, was wrongly set by the value of the liquid junction potential, which can be calculated or looked up in literature [Neher 1992]. In different literary sources advices to correct LJPs can be found by subtracting the offset compensation with the calculated value for the LJP (fig. 5, [Neher 1995; Numberger 1996; Hille 2001]).

An attempt to determine the actually existing LJP for the experimental settings used here was made by measuring the reversal (equilibrium, E) potential for Cl⁻, according to the assumption that the LJP = measured E_{Cl⁻} - theoretically predicted E_{Cl⁻}. This was achieved by activating GABA_A-receptors with the specific agonist muscimol 3 μM in the presence of TTX 500 nM and TEA 20 mM. TTX was applied to inhibit synaptic transmission and TEA to block delayed rectifier K⁺-channels. If for whole cell measurements a complete ionic exchange between the pipette solution and the cytosol is presumed after waiting for a period of at least 10 min, the cytoplasmatic Cl⁻-concentration should be defined by the one of the pipette solution (here 7 mM for the potassium gluconate inner solution). Therefore, the Cl⁻ reversal potential was calculated as -78.6 mV at T = 298 K and [Cl⁻]_o = 151 mM using the Nernst equation. F = Faraday's constant = 9.6485*10⁴ C/mol, R = gas constant = 8.3145 J/mol*K [Hille 2001] according to:

Calculation of the liquid junction potential using Clampex 10.2 junction potential calculator

$$E_{Cl} = \frac{RT}{zF} \ln \frac{[Cl^-]_o}{[Cl^-]_i}$$

revealed a value of 17.6 mV, the ionic gradient 151 (outside) to 7 mM (inside), an Ag/AgCl-wire and a temperature of 25 °C. Under whole cell conditions the single cell results for the Cl⁻-reversal were: -75.5 mV (cell 1), -70.6 mV (2), -70.4 mV (3), -66.4 mV (4) and -65.7 (5). For experiments with perforated patch the interpolated Cl⁻-equilibrium potentials revealed values of -93.7 mV (cell 1), -89.7 mV (2) and -54.4 mV (3). The median and interquartile ranges for whole cell (-70.5 and 7.1 mV) and perforated patch (-89.7, 39.2 mV) experiments were significantly different (p < 0.05). Note that the variance of values was strongly enhanced by using the perforated patch (fig. 6).

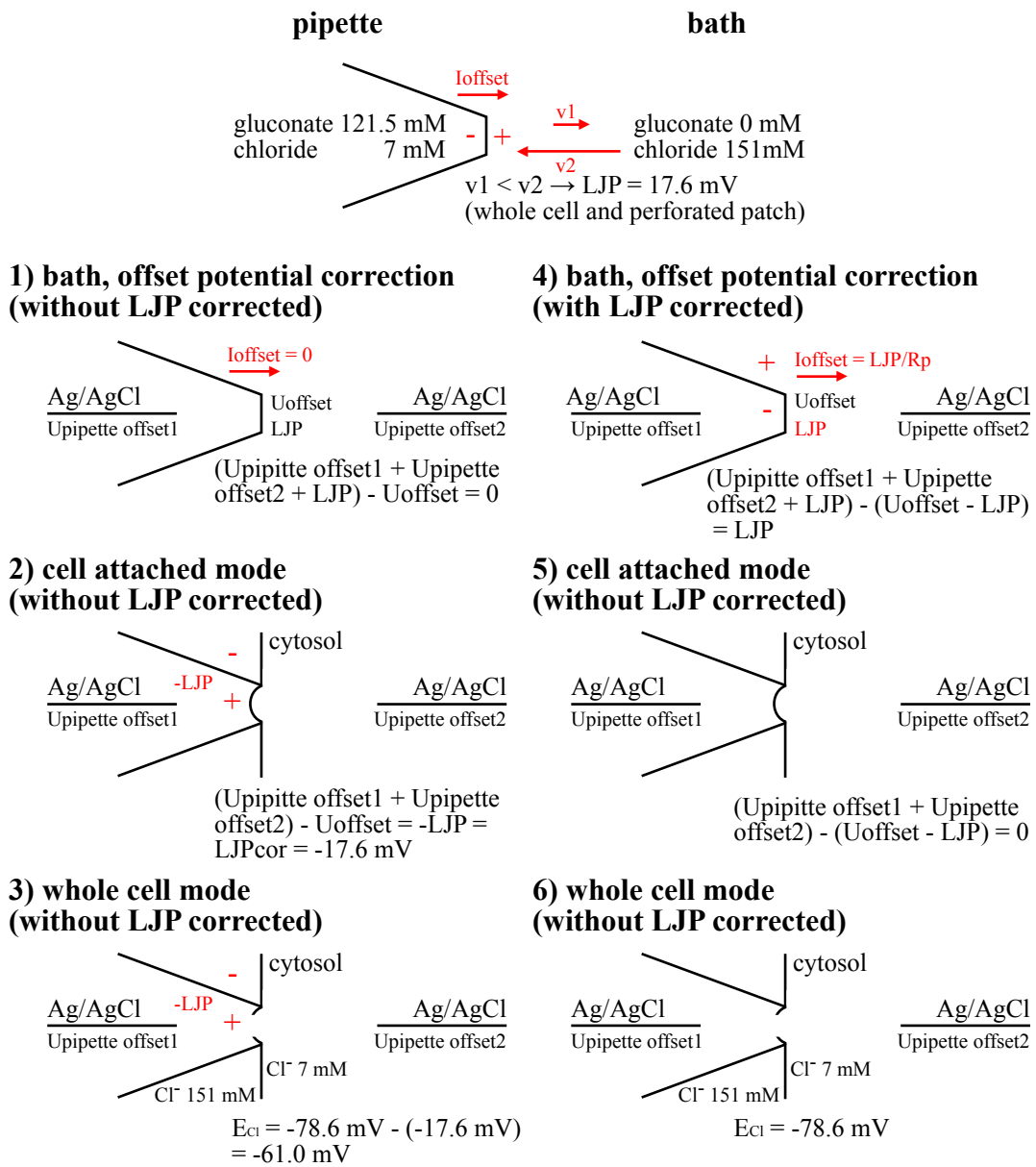


Fig. 5: The liquid junction potential (adapted from Multiclamp 700B manual 2006).

2.5.1. The liquid junction potential in whole cell experiments

As the difference between the measured E_{Cl} (-70.5 mV) and the theoretically predicted E_{Cl} (-78.6 mV) reflects the LJP, it was determined as 8.1 mV under these conditions. This corresponds to the values published by [Podlogar et al. 2006]. However, the deflection between the experimentally determined (8.1 mV) and theoretically calculated LJP (17.6 mV) was 9.5 mV.

Concerning these results, 3 alternative conclusions can be drawn. (I) I have a different LJP in my experimental setting then it was calculated by Clampex 10.2, (II) there was another unidentified potential underlying, which compensated the LJP by 9.5 mV, or (III) the Cl^- -diffusion from the pipette into the cytosol, especially into the long and complex shaped processes of a differentiated

hippocampal neuron, was insufficient (chapter 2.7., [Neher 1995]. Taking the latter possibility into account, this would indicate that the $[Cl^-]_i$ of the cells was lower than published in literature for mature hippocampal neurons lying at approximately 7 mM [Ben-Ari 2002]. The estimated $[Cl^-]_i$ of 4.9 mM corresponds to a theoretical E_{Cl} of -88.1 mV predicted by the measured E_{Cl} (-70.5 mV) and the correction for the calculated LJP of 17.6 mV (fig. 5.1 - 5.6). A detailed calculation can be found in the appendix (chapter 6.3.).

Due to the fact that theoretically calculated LJP was not experimentally confirmed, I made the decision not to correct for the LJP in any of my further experiments.

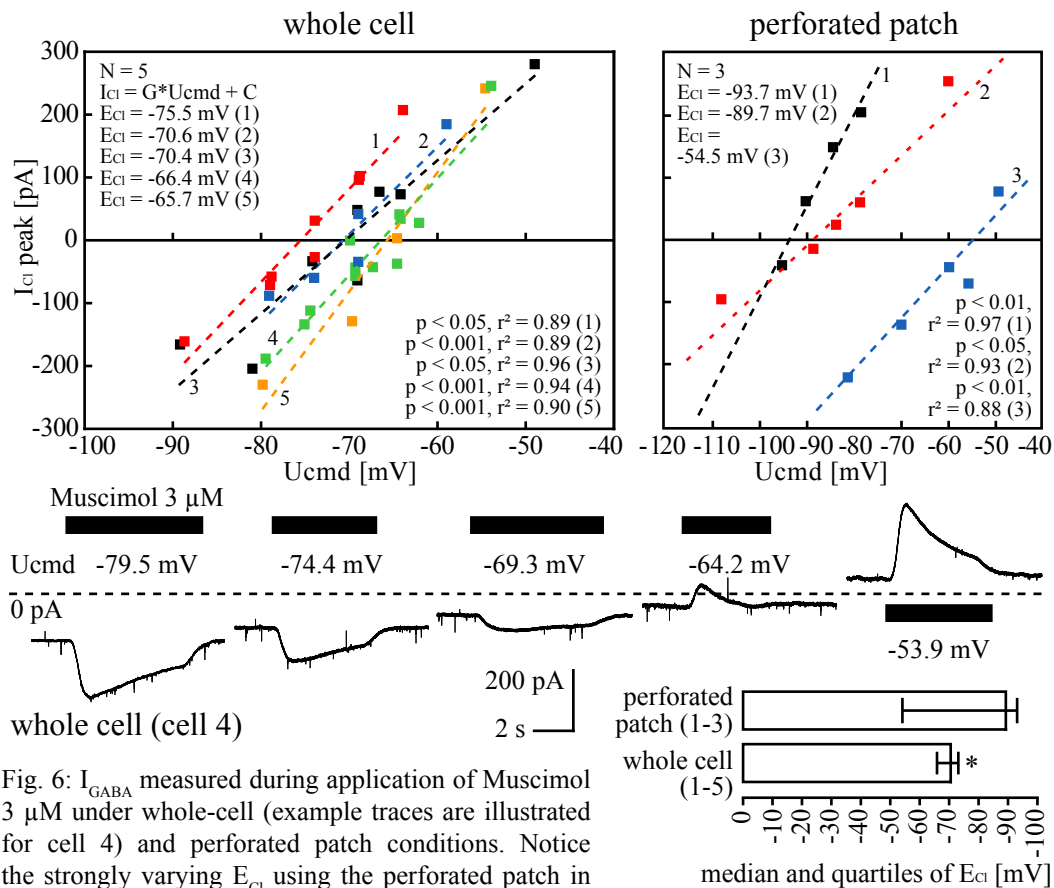


Fig. 6: I_{GABA} measured during application of Muscimol 3 μ M under whole-cell (example traces are illustrated for cell 4) and perforated patch conditions. Notice the strongly varying E_{Cl} using the perforated patch in contrast to the whole-cell recordings (for interpretations of this divergence see text).

2.5.2. The liquid junction potential in perforated patch experiments

Using the perforated patch configuration the E_{Cl} was determined at -89.7 mV leading to a predicted LJP of -11.1 mV. Moreover, the variance in E_{Cl} was more than 5-fold higher in the perforated patch than in the whole cell experiments. Since pores made by amphotericin B are known to conduct monovalent cations approximately 10-times better than anions [Numberger 1996], it is likely that the control of the cytosolic $[Cl^-]_i$ is worse in the perforated patch mode than under whole cell conditions. If the $[Cl^-]_i$ is indeed more or less kept unaltered in the perforated

patch configuration even after an equilibrium period of more than 10 min, I would assume that cultured hippocampal neurons exhibit variability in their $[Cl^-]_i$, ranging from 2 mM (cell 1) to 9.2 mM (cell 3), when the LJP was assumed as 17.6 mV. A detailed calculation can be found in the appendix (chapter 6.1.).

Conclusively, due to the lack of controlling the cytosolic $[Cl^-]$ in the perforated patch mode, it is not possible to determine the LJP in this configuration properly by measuring E_{Cl} .

2.6. Cell attached mode (gigaseal) and compensation of capacitive artifacts

After correcting the offset potential, the pipette tip was carefully lowered in order to touch the cell membrane, which is usually accompanied by a reduction of R_p of about 0.2 M Ω (fig. 4.1, dotted line). Subsequently, a small membrane patch was sucked in the pipette tip. This led to a considerable decrease of the current I_l flowing from the electrode in the bath if a certain voltage was applied (fig. 4.3). Generally, it is assumed that the edges of the sucked membrane patch tightly press against the glass wall of the pipette tip and therefore build an isolating layer between inner and outer solution. The respective resistance is now called leak resistance R_l and should typically reach values near to 1 G Ω . The recording now achieves the condition of a so called “Gigaseal” (fig. 4.2, 4.3). The deformed membrane patch sucked in the pipette is on account of its shape described as omega front structure, whereas the recording configuration is termed cell attached (fig. 4.3) and e.g. used for single channel measurements [Numberger 1996].

A capacitor consists of two conductors, which are insulated against each other. If the conductors are differently charged, a potential appears between them. The number of separated charges Q and the resulting voltage U are proportional, while the capacitance C is the corresponding factor $Q = C \cdot U$ [Horvath 1999]. Regarding the patch clamp experiment at the time of being cell attached, it is the pipette with its internal and surrounding solution, the pipette holder and the sucked-in membrane patch, which all act as capacitors. The further used term “pipette capacitance” includes all three mentioned capacitances. The capacitance is defined by the conductor’s areas A and their distance d ($C = \epsilon \epsilon_0 \cdot A/d$, of ϵ_0 = dielectric constant of an air filled capacitor, ϵ = dielectric constant of a phospholipid filled capacitor).

Therefore, the pipette capacitance correlates with the amount of glass surface submerged in the bath solution and is e.g. enhanced, when the fluid level in the culture dish or in the pipette increases [Numberger 1996; Horvath 1999]. As it is seen in figure 5.2 transient currents occur at the time of making a voltage step ΔU (i.e. 10 mV) and stepping back to holding potential U_0 (i.e. -70 mV), respectively (fig. 4, pulse protocol 2). These transients represent the loading and unloading of the pipette capacitor and are therefore called capacitive artifacts [Hille 2001]. That means, every change of U_{cmd} will cause a charging process of the pipette, or later,

if under whole cell conditions, of the cell capacitance until a certain amount of charges is separated. A compensation of the pipette capacitance prevents the amplifier from saturation, if big voltage steps are made, and makes the interpretation of the measured signals easier, but does not affect the speed and accuracy of patch clamp recordings in general. Accordingly, charging processes are the same with or without capacitance compensation. The principle of capacitance compensations, both for the pipette and the cell, are additional circuitries, which feed the electrode independent from the operational amplifier OA (chapter 2.4.). At this point four different inputs for the commanding potential are important: at the differential amplifier DA, at the operational amplifier and at the RC-elements of the pipette and the cell capacitance compensation.

The properties of the two RC-elements (R_{var} , C_{var}) can be adjusted in a way that the resulting capacitive transients are more or less similar to that of the pipette and the cell, respectively. Thus, the time course of voltage, after the respective RC-element and before being amplified and stabilized by the operational amplifier 2 (OA2) and differentiated by the injection capacitor (C_i) is equivalent to that at the pipette and the cell. The important thing now is that C_i injects the loading current independently from OA and DA into the electrode without affecting the measuring circuit. The pipette capacitance compensator is usually characterized by a small amplitude and a fast time constant (~ 10 pF), in comparison to that of the cell (~ 100 pF). Moreover, it is important to mention that complex shaped cells, as neurons are, do not act as a single RC-element. The passive loading processes (chapter 2.7.) of such cells are only approximately describable with as sum of exponential functions. Consequently, cell size measurements have to be carefully interpreted, because it is not unlikely that the compensation only covers the soma. Besides, alteration of the relative amplitude of certain parts of the loading process of the cell capacitor can be characteristic for certain cell geometry (e.g. the relative amplitude of the slower loading component rises with an increasing growth of the dendritic arbor (fig. 3, [Numberger 1996]).

2.7. Whole cell configuration, series resistance compensation and space clamp problem

In contrast to the cell attached mode, in whole cell configuration signals are not only generated by a few channels, but from a certain population. Consequently, the basic noise level is increased, which limits the resolution to 5 to 20 pA, depending on the specific measuring conditions. Hence, whole cell recordings are comparable with intracellular ones, though the electrical principles are completely different (chapter 2.9.). In order to achieve whole cell conditions, which means to get access to the cytosol, the omega front structure of the cell attached patch has to be ruptured (fig. 4.4). This was always done by suction.

An alternative possibility is the application of frequent and high alternating current (buzzing,

zap). Sometimes it was necessary to maintain a certain sub pressure. If this was not done or the sub pressure was too strong, the access resistance increased, either by resealing of the membrane patch, or plugging the rupture with sucked in organelles, such as the nucleus [Numberger 1996].

In the whole cell mode, the pipette solution directly diffuses into the cytoplasm and will eventually fully replace it. Accordingly, the internal solution should be designed to largely mimic the cytosol. However, the larger the volume of the patched neuron (the more molecules (here represented by the charge Q) need to reach a certain concentration), the smaller the diffusion constant D (mainly dependent on the molecular weight of the diffusing substances), the smaller the diffusion area A (given by the tightness of the pipette tip and the processes of the cell) and the lower the concentration gradient $\Delta c/\Delta x$, the longer it will take to establish an equilibrium [Pusch 1988; Neher 1995; Eckert 2002]. These considerations are summarized in the first law of Fick [Eckert 2002]:

$$\frac{\Delta Q}{\Delta t} = D * A * \frac{\Delta c}{\Delta x} \rightarrow \Delta t = \Delta Q * \frac{1}{D * A} * \frac{\Delta x}{\Delta c}$$

If a constant time required to obtain the equilibrium is assumed, the control of the intracellular composition decreases rapidly in particular with increasing distance from the pipette tip, because the time a molecule needs to diffuse from a certain place to another grows with the square of the diffusion path [Campbell 2003]. Consequently, there is much more control of the electrolyte filling the soma than that filling the distal dendrites [Neher 1995]. In whole cell configuration a neuron can lose molecules with up to 20 kD molecular weight. Thus, functional important substances like ATP or IP3 are diluted out, which can lead to a progressive decrease of certain currents - a process termed “rundown” (chapter 2.8., [Numberger 1996; Keplinger et al. 2000; Zhen et al. 2006].

During or after sealing pulse protocol 1 was exchanged by pulse protocol 2, where the holding potential ($U_0 = -70$ mV) was set to the expected resting potential ($U_m =$ membrane potential). Otherwise the cell, if the membrane patch suddenly ruptured, would be clamped to 0 mV. This would cause a strong depolarization eventually leading to excitotoxicity. Moreover the sealing process is known to improve, when negative potentials are applied. After getting a proper access (optimally resistances should reach the 2-fold of R_p , but at least it should not exceed ~ 10 M Ω), once more capacitive artifacts appear, which are now due to the loading of the cell capacitor during the voltage step (i.e. $\Delta U = 10$ mV). At the start of the loading process (if the gigaseal remained unaffected), there is a short circuit ($I_1 = (U_{cmd} - U_m)/R_a = \sim 1$ nA) through the unloaded cell capacitor R_{cm} (~ 0 M Ω) and nearly no voltage drop appears at the membrane resistance R_m . Therefore, the occurring loading currents are the greater, the smaller R_a , whereas the loading time constant τ depends on the capacitance and the series resistance ($\tau = R_a * C_m$). Accordingly, the smaller both the access resistant and the cell size, the faster a neuron reaches or is clamped to a certain potential. Consequently, the greater the value for τ , the longer differs the compensatory current I_c (chapter 2.9.) from the actual conductive changes of

the membrane. As a result, the actual voltage clamp varied from the commanding voltage U_{cmd} during the loading of the cell capacitor. In an extreme case, a high series resistance can lead to a strongly distorted representation of the cellular currents. If there are no active alterations of the membrane resistance R_m , the cell membrane was exponentially loaded: $U(t) = U_0 * (1 - e^{-t/\tau}) + C$, while $U(\tau) = U_0 * (1 - (1/e)) + C$, $U(\tau) = 0.63 * U_0 + C$ and the area under the curve represents the number of separated charges. Accordingly, the smaller R_a (the higher the transients), the smaller is τ (the faster the loading process), if the measured cell capacitance remains constant [Hille 2001]. The more the capacitor is loaded, the more increases R_{Cm} , until it gets infinite, when the cell membrane is fully charged. At this point the current $I_2 (= I_{offset})$ is assembled by I_l through the leak resistance and the holding current I_h , which depends on R_m and R_a ($I_h = (U_{cmd} - U_m)/(R_m + R_a)$). When the current I_1 flows the cell membrane acts as a capacitor, whereas when I_2 flows it has the property of a resistance. As it is shown in figure 5.4 the applied voltage drops at the sum of R_a and R_m , which are connected in series. Hence, together they are described as a voltage divider. Thus, for proper measuring conditions, it is necessary to have a by far greater membrane than series resistance. Otherwise, with an inadequate R_m - R_a -relationship, the difference between U_{cmd} and the actually applied voltage increases. This is known in electrophysiology as the so called “Rs-problem”, which is not only enhanced with growing series resistances, but also with decreasing membrane resistances, as it can happen, when especially large conductances are activated or the cell membrane is damaged (fig. 3, 4.4, [Numberger 1996; Büttner 2004]).

In order to minimize the “Rs-problem” common patch clamp amplifier have a Rs-compensation-mechanism, which in contrast to the one of the pipette capacitance intervenes actively and not just “cosmetically”. Comparably with the former described relationship between the access resistance and the loading of the cell capacitor, a properly adjusted Ra-compensation leads to a smaller time loading constant and therefore to a faster and more accurate application of the commanding potential. The general principle of the series resistance compensation is to correct any difference between U_{cmd} and the voltage U_m , which is left after the drop at R_a , by adding an additional potential $U_m' = U_m - U_{cmd} = R_a * I_c$. Hence, the commanding voltage is changed into $U_{cmd}' = U_{cmd} + U_m'$. Disadvantages of this positive feed backing control circuit are the enhanced noise and the tendency to oscillations and instabilities, if the compensation is set too high. The majority of the tested neurons tolerated the standard setting of 70 % Rs-correction and 2 kHz bandwidth. The percentage of correction corresponds to U_m' relatively to U_{cmd} (i.e. if $R_a = 10 \text{ M}\Omega$ and Rs-correction = 90 %, 9 $\text{M}\Omega$ of the series resistance is compensated), whereas the bandwidth defines the -3 dB cutoff frequency of the feed backed signal. Thus, the more transient the recorded signal is, the higher the bandwidth has to be. The prediction control, which is comparable with the principle of “supercharging” [Armstrong 1987], enhances the commanding voltage by adding a certain potential to reduce the time needed for loading the membrane capacitor ($\tau * U_{cmd}' \sim U_{cmd}$). However, the prediction, as well as the cross link between it and the bandwidth were never activated in the experiments presented here, in order to avoid oscillations (fig. 3, [Numberger 1996], Multiclamp 700B manual 2006, <http://support>).

axon.com).

Similar to the previously described situation, there are several electrical bottlenecks within a differentiated neuron, such as the proximal axon and proximal dendrites. These structures act as series resistances, on each of which a part of the applied voltage drops. Thus, for the peripheral parts of the membrane less voltage is left to drop there. Furthermore, the worse accessible a certain cell compartment is (i.e. dendrites in comparison to the well reachable soma), the slower will be the loading of its membrane. This phenomenon is also known as “space-clamp-problem” [Armstrong 1992; Numberger 1996].

2.8. The perforated patch configuration

As mentioned in the previous chapter, one of the most important limitations of the whole cell mode is the loss of the physiological cytoplasmatic composition (in particular of ATP and other second messengers) and the resulting rundown of certain currents, for example of L-type- and M-currents [Boehm 1998; Kepplinger et al. 2000; Zhen et al. 2006]. Consequently, in the majority of my experiments I got an electrical access to the cell by perforating instead of rupturing the sucked-in membrane patch with the bacterial antibiotic amphotericin B [Rae 1991]. The only two exceptions were the voltage-clamp experiments for measuring GABA_A-currents (chapter 2.5.) and currents of different LTCC-constructs after transiently expressing them in *tsA201*-cells (chapter 3.1.). This was due to the increased R_s -problem under perforated patch conditions, where access resistances usually did not fall below $\sim 35 \text{ M}\Omega$ (chapter 2.7.). Amphotericin B, as well as nystatin and gramicidin A, makes pores in cholesterol containing membranes, which have a diameter of about 0.8 nm and are therefore not permeable for molecules with a size at least comparable to the one of glucose [Horn 1988; Rae 1991; Ebihara 1995; Kyrozis 1995]. However, the pores unselectively conduct monovalent cations, better than anions, and are fully impermeable for divalent cations. Since amphotericin B is highly hydrophobic, it had to be solved in Dimethyl-sulfoxid (DMSO). Because of its instability, the amphotericin B stock (50 mg/mL) was freshly diluted in inner solution (1:100) just before every measurement and was then kept under light protection. Not only its stability, but also that it was well diluted (vortexing \rightarrow sonicating \rightarrow vortexing) determined the pore-forming ability and hence the acquisition of a proper access resistance. In view of the fact that the addition of such pore forming substances impairs sealing, filling of the tip with antibiotic-free solution up to a few mm and backfilling with the amphotericin-containing solution is important (chapter 2.4.). Already during the establishment of the gigaseal the first pores start to form, which can be seen by small whole cell artifacts. Thus, under the perforated patch mode it is difficult to check the quality of the seal exactly, because there is no real cell attached configuration. However, it takes about 30 min to get a constant R_a and cell capacitance, respectively, which then remained for up to 2 h in my experiments (fig. 4.4, [Numberger 1996]).

2.9. Principles of voltage and current clamp

If a cell is clamped to a certain voltage U_{cmd} (commanding voltage) different from the detected one $U_p = U_m$ (in reference to the grounded bath), the operational amplifier OA of the headstage converts the voltage difference $U_{cmd} - U_p$ into a compensatory current I_c , which then flows through the feedback resistor R_f and the measuring electrode ME into the cell. Accordingly, ME has the function of measuring and injecting current at the same time [Bretschneider 2006]. The high internal resistance of OA causes that I_c can only flow through ME, but not back into the amplifier leading to theoretically lossless current injections. Additionally, the two entrances of OA can measure their applied voltage without any passing current [Numberger 1996]. Thus, every change of the membrane potential due to altered channel permeabilities is adjusted to the commanding voltage by adapting the compensatory current until there is no difference between U_m and U_{cmd} . That implies the capability to control the membrane voltage and is known as a negative feedback mechanism (Cole 1949, [Numberger 1996]). The differential amplifier DA, like OA a part of the headstage HS, compares U_{cmd} with U_p once more and transmits U_m to the amplifier, where the signal is transformed into the measured current $I_m = (U_{cmd} - U_m) \cdot G_m$, where G is the conductance of the whole membrane at a certain steady state [Bretschneider 2006]. Hence, the whole unit of OA, R_f and DA is called current-voltage-converter with a typical loading time constant of $\tau = 1$ ms [Numberger 1996]. I_m corresponds to I_c and is just the opposite of the physiological appearing currents of the cell [Kandel 1996]. If an in- or outflux of positive ions, such as Ca^{2+} and Na^{2+} or K^+ occurs, it is called in- or outward current and is represented by a negative or positive value. Concerning negative charged ions (Cl^-), an actually appearing influx causes an enrichment of cations on the outside and is consequently termed as an outward current. This is the convention for the whole cell configuration, whereas the signs have to be inverted in the cell attached mode and for the inside out patch, respectively. The altering of the feedback resistor is a possibility of adjusting the resolution and dynamic range of recordings. The higher R_f is, the lower the noise and the lower the current of saturation will be. This is comparable with different gain-settings of the amplifier (Multiclamp 700B manual 2006, <http://support.axon.com>, [Numberger 1996]).

Besides controlling the membrane voltage, common patch clamp amplifier, such as the Multiclamp 700B and the Axopatch 200B for instance, also offer the possibility to inject a certain current and to record the membrane potential (current clamp). Hence, it is possible to record and elicit action potentials or to investigate the contribution of specific ion channels to the membrane potential, when de- or hyperpolarizing it. Moreover, observations of the excitation patterns (e.g. irregular spiking, bursting, plateau potentials, phasic/tonic behavior) can be done. In the current clamp mode a different headstage circuit than in the voltage clamp is used. If a certain current I_{in} should be injected, it is converted into the proportional voltage U_{in} . Like U_p (= voltage coming from the cell membrane and registered at the electrode) U_i lies at one of the 2 inputs of a summing amplifier SA, which integrates the 2 signals into $U_p + U_{in}$. $U_p + U_{in}$ is then converted in a proportional current by dropping at the feedback resistor R_f .

Consequently, the current flowing through R_f and therefore into the measuring electrode ME and into the cell is given by $I_{in} = U_{in}/R_f$, as long stray capacitances are ignored (fig. 3).

As it is in the voltage clamp the dynamic range of current that can be injected depends on the feedback resistor. At the steady state of this situation, the injected current (e.g. positive) causes a depolarization U_p , which is again recorded by ME. OA is an operative amplifier with an effectively infinite internal resistance. Under current clamp settings the series resistance is compensated by the bridge balance, where a repetitive hyperpolarizing current is injected into the cell (tuning, e.g.: -100 pA at 2 Hz). If current flows through the pipette, a voltage drop at R_a occurs, which is added to the recorded membrane potential. Therefore, the bridge balance is adjusted in a way that the overlying potential is corrected. In detail, a differential amplifier DA subtracts the voltage drop at R_a ($U_{drop} = R_a \cdot I$) from the potential recorded at the electrode U_p , whereas the true membrane potential U_m is the result ($U_m = U_p - U_{drop}$). Furthermore, during tuning the pipette capacitance neutralization is adjusted in such a manner that no transient artifacts at the beginning and end of every pulse are visible. Otherwise the stray electrode capacitance would act as a filter for the membrane potential signal. Thus, in contrast to the situation in the voltage clamp the capacitance compensation has a direct impact on the recording in the current clamp, meaning that it is not only “cosmetic”. Additionally, the “disable if oscillation detected”-function was activated, as increased values of the pipette capacitance neutralization can cause oscillations. This function also protects the cell from oscillating during measurements, if electrode properties change for example and is similar to the disabling mode of the R_s -compensation in the voltage clamp. Apart from the tuning function, with a Multiclamp 700B amplifier a slow current to maintain the membrane potential at a certain value can be injected. Another recording mode is the voltage follower setting ($I = 0$), where all command inputs are disconnected and the recorded signal represents the intrinsic potential of the neuron. If no voltage-gated ion channels are activated, a current injection leads to the passive loading of the membrane, while the membrane resistance can be calculated by $R_m = U_{max}/I_{in}$. In contrast to the voltage clamp, in the voltage follower mode the time loading constant is given by $\tau = R_m \cdot C_m$. Thus, the loading of the cell capacitor generally needs longer than in the voltage clamp, where the time loading constant is given by $\tau = R_a \cdot C_m$ (fig. 3, Multiclamp 700B manual 2006, <http://support.axon.com>, [Numberger 1996]).

2.10. Filtering and digitization of signals

All signals were digitally recorded. For that reason it is important that every digitization requires a preceding analogous low-pass filtering of the signal with a known cut off frequency. The explanation for that is the Nyquist-criterion, which states that signals with a specific natural frequency have to be digitized with an at least 2-fold higher frequency than its natural one (Nyquist-frequency). Otherwise the high frequency fractions are recoded into retarded and

entirely artificial apparent signals (aliasing). In order to avoid the aliasing effect, only oscillations with a natural frequency below the Nyquist-frequency should remain for digitization. This is achieved by using a low-pass filter with an appropriate cut off frequency, above which all fractions are eliminated. In literature it is recommended to use a 2- to 5-fold higher digitization than low-pass filtering frequency. As I decided to keep the filtering frequency above 10 kHz (in order to record APs properly), the sampling frequency of 20 kHz just fulfilled the minimal demand of the Nyquist-criterion.

The cut off frequency of a filter is defined by the frequency, where the amplitude of the signal is reduced by $1/\sqrt{2}$ ($I_{out} = I_{in} * 1/\sqrt{2}$). The Multiclamp 700B amplifier uses as a standard setting a Bessel low-pass filter. The advantages of such a filter are the lack of a strong phase displacement of fast signal fractions, the avoidance of oscillations, if transient signal onsets appear and a low signal distortion. However, the disadvantage is a certain amplitude weakening below the cut off frequency. The number n of serial arranged filter elements (poles) determines how accurate signals above the cut off frequency are erased (filter of n^{th} order). The Multiclamp 700B amplifier uses a 4- or 8-pole Bessel filter.

The cell capacitor itself also represents a filter (RC-element), which limits the frequency of recorded current- or voltage-alterations. The cut off frequency of a cell is given by $f = 1/2 * \pi * \tau$. Thus, the higher the access resistance is, the lower the cut off frequency will be. On account of the fact that τ is given by the product of R_m and C_m in the current clamp, the cut-off frequency is generally higher in the current than in the voltage clamp. Especially, in reference to the following chapter it is essential to state the second advantage of low-pass filtering the recordings, which is the augmentation of the signal-noise-ratio - a parameter, which is exceedingly important for automatic event detection (chapter 2.11., chapter results physiological activity, Multiclamp 700B manual 2006, <http://support.axon.com>, [Numberger 1996]).

2.11. Leak subtraction, data analysis and statistics

In the voltage clamp experiments, apart from the IV-curve measurements, an option called leak subtraction was activated. This was done by Clampex 10.2., simultaneously to the actual recording. Since every voltage step ΔU causes in dependence on the membrane resistance R_m an offset current $I_{off} = \Delta U/R_m$, which is completely unrelated to voltage-gated conductances and therefore entirely due to the passively electrical response of the membrane, this current can be subtracted as leak. Due to the fact that voltage steps are frequently used in pulse protocols for investigating voltage-dependent ion channels, the occurring offset currents become substantial and thus can disturb further analysis of the signals. One possibility of subtracting I_{off} is to make a certain number of subsweeps, which are in sum equivalent to the respective voltage step of the measuring protocol. A common used form is the p/4-protocol, where 4 subpulses are made, the resulting offset currents averaged, their mean multiplied by the factor 4 and this value finally

added (negative) to or subtracted (positive) from the signal of interest. Whether a negative or a positive voltage step is made, depends on the measuring conditions. However, one has to insure that the leak subtraction protocol has as little as possible effect on voltage-gated conductances. In addition, it is important to point out that the leak subtraction, similar to the capacitance compensation (chapter 2.6.), is a purely cosmetic mechanism, which makes the signals easier to analyze and protects the circuit from saturation, but which does not counteract retarded or incomplete clamping of the membrane potential, as the Rs-correction and -prediction do (chapter 2.7., [Numberger 1996]).

In the analysis of the Cl⁻-equilibrium to measure the liquid junction potential the respective muscimol 3 μM induced peak currents were plotted against the commanding voltage. The resulting data points were linearly fitted by GraphPad Prism 4.03 and Statistica 6.1, respectively. E_{Cl} was calculated as $I_{Cl} = G_{Cl} * U_{cmd} + C$, where $I_{Cl} = 0$ and $E_{Cl} = U_{cmd} = -C/G_{Cl}$ (fig. 6).

For analyzing the firing activity of hippocampal neurons, event times [ms], as well as afterhyperpolarization AHP areas [mV*ms] and spiking frequencies [Hz] were determined for every cell by a software-based event detection mode (threshold search) using Clampfit 10.2. (Axon Instruments). The baseline was positioned at the resting potential under control conditions, whereas the trigger and the re-arm were set at Δ10 and Δ5 mV, respectively. Thus, if the membrane potential lay below the re-arm and then reached the trigger an event was registered until the voltage fell below the trigger again. Signals with a duration below 1 ms were rejected as “noise”. Regarding the event times and the AHP areas the respective median was used for further analysis, because of the mostly non parametric situation of the data set. After that three major classes were formed, defined by their principle discharge behavior: (I) spiker and burster (II) with and (III) without substantial afterhyperpolarizations. To test whether the three groups can be differentiated into further subclasses, cluster analyses were performed using Statistica 6.1. As a measure of distance the “City-block (Manhattan) distance” was used. It is computed as the sum of all absolute differences between two points across dimensions ($distance(x,y) = \sum_i |x_i - y_i|$). Since for each cluster analysis only one dimension was taken into account, the Manhattan distance was simply calculated as $distance(x,y) = x - y$. In most cases, this distance measure yields results similar to the more commonly used Euclidian distance ($distance(x,y) = \{\sum_i (x_i - y_i)^2\}^{1/2}$) with the exception that outlying values are damped because they are not squared. The distance for dividing the respective clusters was at least set to 25 % of the maximum distance. The chosen amalgamation rule was that of a complete linkage, which is described by the distance of the furthest neighbours of two different clusters. It is suitable for datasets, where lump- rather than chain-like structures are assumed (fig. 21 - 23, [Lammel 2008] supplemental data, [Sachs 2002]).

For analyzing the voltage of LTCC-activation, when increasing depolarizing current was injected (current clamp ramps), the crossings of the isradipine traces with the DMSO and BayK ones, respectively, were determined and plotted against their frequency. For the resulting frequency distributions a unimodal (single Gaussian distribution) fit was compared with a bimodal (sum of two Gaussian distributions) one using a F-test performed by Graphpad Prism

4.03. The less complex unimodal model for each data set corresponds to the null hypothesis, which was rejected, if the bimodal fit was significantly better than the unimodal, depending on the respective goodness of fit R^2 and the degrees of freedom df of particular distribution. If the sum of two Gaussian distributions was the preferred model, the two peaks (mean1 and 2) were tested for significant difference by a two-tailed t-test, while $p < 0.001$ was indicated by ***. Possible variance homogeneities were tested by F-test. (fig. 9).

For the purpose of exploring the different LTCC couplings, in every experiment 5 current pulses of increasing amplitude were injected for 8 s. This specific pulse duration should provide comparability with previously done experiments. The amount of current injected was adapted to the respective recording conditions (bridge resistance, cell capacitance) in such a way that at least -30 mV were reached with the last (strongest) pulse. The maximum ampacities lay between 75 and 500 pA. The AHP/ADP amplitude [mV] and the AHP/ADP [mV*ms] area, respectively, after stepping back to the intrinsic membrane potential by setting $I = 0$, were exclusively evaluated in relation to the prepulse baseline (fig. 10). The results were tested with a Kruskal-Wallis H-test with Dunn's multiple comparison post hoc test (fig. 13, 15, 16, 19, 20). In order to characterize the observed control AHPs and ADPs (after events), their durations were evaluated by fitting the decay starting at the peak amplitude with a single exponential function and extracting the respective τ s. When $t = 4*\tau$, the peak amplitude is reduced by approximately 98 %. Thus, I set the start point of the after event, where the extension of the post pulse baseline crossed the recording signal, and the end point at $t_{\text{peak}} + 4*\tau$. The resulting durations were plotted by their medians (quartiles) and tested with a Kruskal-Wallis H-test (with Dunn's multiple comparison post hoc test) for significant differences. *** indicates for $p < 0.001$, ** for $p < 0.01$ and * for $p < 0.05$ (fig. 11).

Currents measured from heterologously expressing LTCC-constructs, were normalized to the peak currents at 0 mV for $Ca_v1.3$ long and 15 mV for $Ca_v1.2\alpha1C77$, respectively. IV-curves were fitted according to the equation $Y = G_{\text{max}} * ((X - U_r) / (1 + \exp((V_{50} - X) / K)))$, where Y is the current, X is the applied voltage, U_r is the reversal potential, V_{50} is the voltage of half-maximal activation and K is the slope-factor of the Boltzmann-term. V_5 stands for the activation threshold determined as 5 % of the peak current [Koschak et al. 2001].

3. RESULTS

3.1. Comparison of different Ca_v1.2- and Ca_v1.3-constructs heterologously expressed in HEK-_{TS}A201 cells

This diploma work was part of a FWF project (P19710) devoted to the study of LTCCs in normal and abnormal electrical activity. In the framework of this study DHP-insensitive LTCC-constructs were generated from the respective wild type constructs (Ca_v1.2 α 1C77 and Ca_v1.3long) by Nina Krako (PhD student, Scuola Normale Superiore, European Brain Research Institute, Roma, Italy). All constructs were transfected in HEK-cells together with the α 2 δ 1- and the β 3-subunit. Only HEK-cells expressing GFP were selected for measurements. I_{Ca2+} or I_{Ba2+} were elicited by stepping from -80 mV to 0 (for evoking peak currents of Ca_v1.3long) or 10 mV (Ca_v1.2 α 1C77) for 150 ms. This was all done in the presence of TTX 500 nM and TEA 20 mM in the bath solution and Cs⁺ 130 mM in the pipette solution to block the majority of Na⁺- and K⁺-channels. All recordings were performed using Ca²⁺ 10 mM or Ba²⁺ 10 mM. Both BayK and isradipine were applied at a concentration of 3 μ M. I tested the constructs for general VGCC-functionality (Ca²⁺ and voltage dependent inactivation, tail current) and the mutants for DHP-insensitivity (DHPi). Ca²⁺-dependent inactivation can only be seen for I_{Ca2+}, whereas in I_{Ba2+} the pure voltage dependent inactivation is isolated (fig. 7).

In order to analyze the activation of Ca_v1.2 with that of Ca_v1.3 and especially to compare activation thresholds obtained from current clamp experiments with activation thresholds from the voltage clamp, I measured activation curves of Ca_v1.2 and Ca_v1.3. If the activation properties of Ca_v1.3long and Ca_v1.2 α 1C77 were compared, the well known fact that Ca_v1.3-constructs activate at more hyperpolarized potentials could be reproduced in my experiments. This applied for the V₅₀-values (V₅₀-value for I_{Ba2+} under DMSO: Ca_v1.3long and Ca_v1.2 α 1C77 = -18.9 mV (N = 5) and -1.0 +/- 1.3 mV (N = 7)) as well as for the peak voltage Vmax (-6 and 12 mV). As far as the reversal potentials are concerned, the potential for Ca_v1.2 α 1C77 was approximately

10 mV shifted to the right in relation to that of $\text{Ca}_v1.3\text{long}$ ($U_{r_{\text{Ba}^{2+}}}$ for $\text{Ca}_v1.3\text{long} = 55.3$ ($N = 5$), for $\text{Ca}_v1.2\alpha1\text{C77} = -60.8$ ($N = 7$), fig. 8). As I was especially interested in comparing activation thresholds determined under current and voltage clamp conditions, respectively, I calculated them for the heterologously expressed constructs (V_5 for $\text{Ca}_v1.3\text{long}$ and $\text{Ca}_v1.2\alpha1\text{C77} = -40$ and -30 mV, fig. 8). All values were calculated from the equation $Y = G_{\text{max}} * ((X - U_r) / (1 + \exp((V_{50} - X) / K)))$.

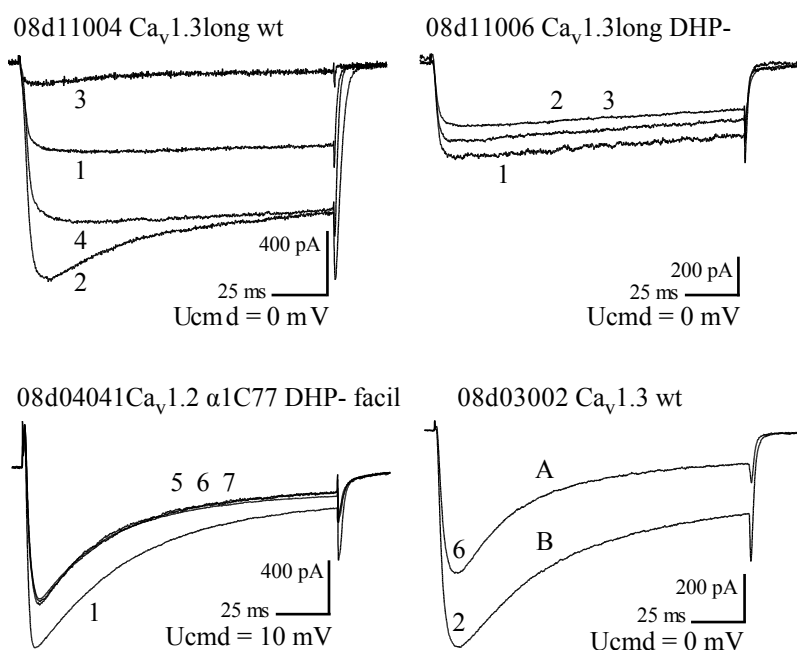


Fig. 7: Example traces shown for $\text{Ca}_v1.3\text{long}$ as wild type and DHP-insensitive mutant as well as for the $\text{Ca}_v1.2\alpha1\text{C77}$ DHP-insensitive mutant. In 08d03002 the pure voltage-dependent inactivation ($I_{\text{Ba}^{2+}}$) is shown in B, whereas A includes both the voltage- and Ca^{2+} -dependent inactivation ($I_{\text{Ca}^{2+}}$). The DHP-insensitivity of the mutants was tested for both constructs (1 = I_{Ba} DMSO, 2 = I_{Ba} BayK 3 μM , 3 = I_{Ba} isradipine 3 μM , 4 = I_{Ba} BayK 3 μM wash out, 5 = I_{Ca} DMSO, 6 = I_{Ca} BayK 3 μM , 7 = I_{Ca} isradipine 3 μM , external $[\text{Ba}^{2+}] = 10$ mM, external $[\text{Ca}^{2+}] = 10$ mM).

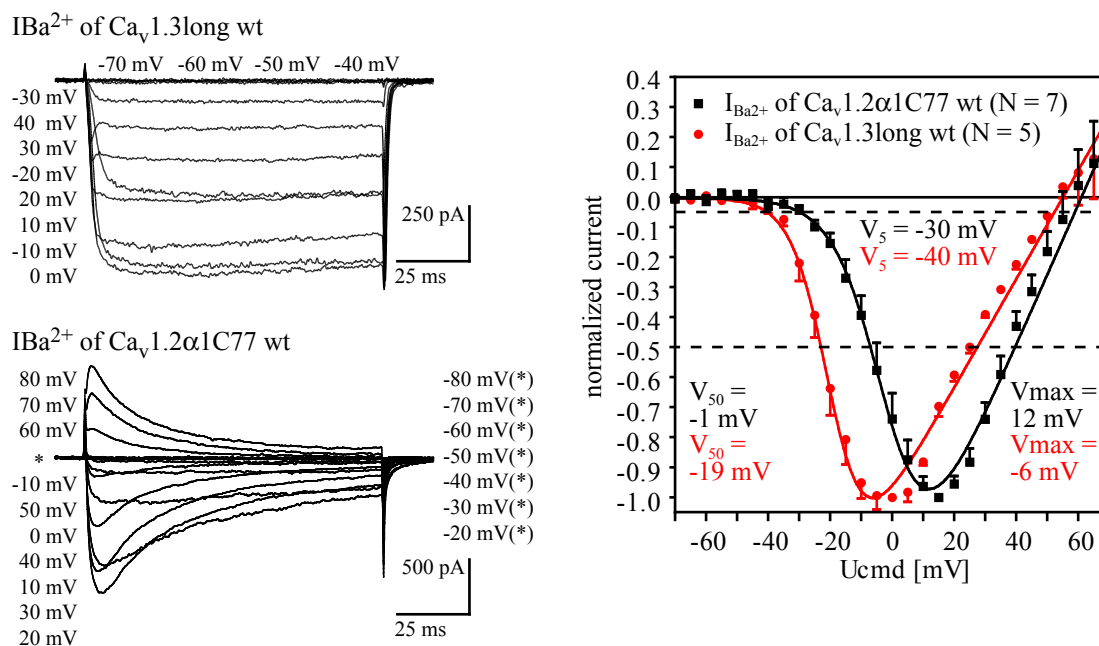


Fig. 8: IV-curves for $\text{Ca}_v1.2\alpha1\text{C77}$ wt and $\text{Ca}_v1.3\text{long}$ wt. The current was normalized to the peak current at 0 mV ($\text{Ca}_v1.3$) and 15 mV ($\text{Ca}_v1.2$), respectively. Note the left shift in channel activation and the reversal potential U_r of the $\text{Ca}_v1.3\text{long}$. V_5 = voltage of 5 % peak current (= activation threshold), V_{50} = half-maximal voltage for activation, V_{max} = peak voltage, all values were calculated from the equation: $Y = G_{\text{max}} * ((X - U_r) / (1 + \exp((V_{50} - X) / K)))$. $U_r(\text{Cav}1.3\text{long}) = -55.3$ mV; $U_r(\text{Cav}1.2\alpha1\text{C77}) = -60.8$ mV.

3.2. The role of Ca_v1.3 in hippocampal neurons

The next set of experiments of my diploma thesis dealt with the question, at which potential the contribution of LTCC-mediated Ca²⁺-entry starts to affect the further depolarization of the membrane (voltage of LTCC activation). By analyzing this, I wanted to test the postulate that Ca_v1.3 plays a negligible role in the overall LTCC-effect in hippocampal neurons (see chapter 1.7.).

3.2.1. Determination of LTCC activation voltage

Since 20 - 30 day old hippocampal neurons have extensive arborization, the voltage clamp was not considered as an appropriate method to answer the question in our *in vitro* model. Thus, an analysis was performed based on the current clamp technique. In detail, current ramps of 1200 pA peak amplitudes and durations of 250 ms were injected into the hippocampal neurons while constantly applying TTX 500 nM (slope = 4.8 pA/ms, fig. 9.3, chapter 2.11).

The LTCC-activation voltage was determined as the crossing between the isradipine response and the response under control and the response obtained by the application of BayK, respectively. The plotting of the LTCC-activation voltage against its frequency revealed a bimodal shape. This was particularly evident in the case of BayK. Here, the comparison of the single normal distribution with the sum of two Gaussians proved the latter model as preferred (F-test: $F = 60.91$, $p < 0.01$, $R^2 = 0.99$). Furthermore, the two peaks mean1 = -53.5 mV (termed “medium voltage activated” or MVA) and mean2 = -42.4 mV (termed “high voltage activated” or HVA) were significantly different (t-test (2-tailed): $t = 8.7$, $df = 16$, $p < 0.001$, F-test: $F = 3.289$, $p > 0.05$). In the case of DMSO, though there was the tendency of a bimodal shape ($R^2 = 0.67$) and thus the goodness of fit for a single Gaussian was relatively low ($R^2 = 0.19$), the null hypothesis, which was the single Gaussian distribution, could not be rejected (F-test: $F = 1.57$, $p > 0.05$). However, the approximated peaks for the LTCC activation thresholds under control conditions were at mean1 = -44.2 mV (“MVA”) and mean2 > -35 mV (“HVA”). Taken together, this data indicate that at least two populations of LTCCs with differing voltage-dependent activation ranges operate in these neurons (fig. 9.1, 9.2).

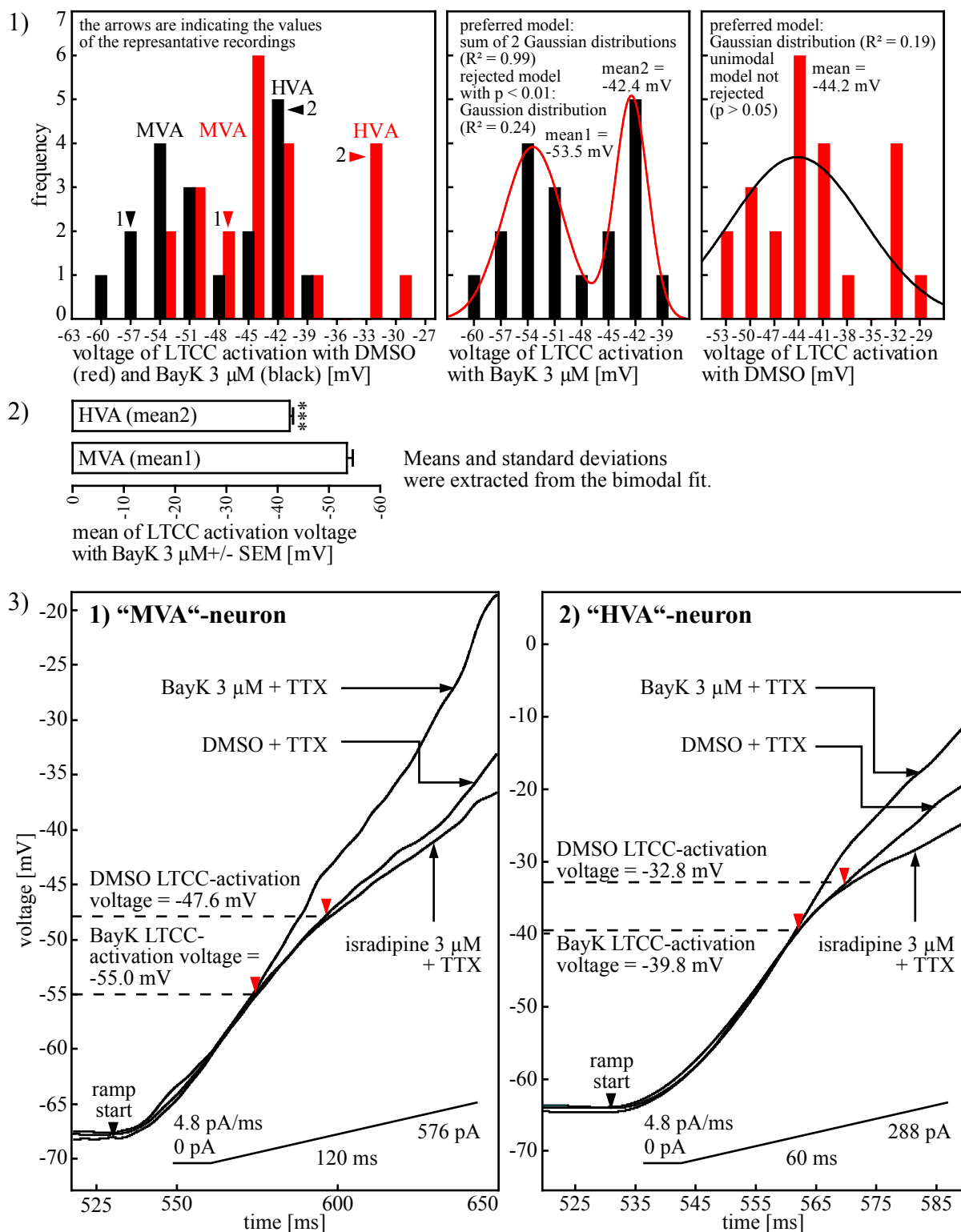


Fig. 9: Voltage of LTCC-activation evaluated by comparing the isradipine-trace with the traces for DMSO and BayK 3 μ M, respectively. The whole distribution of all LTCC-activation potentials determined for both DMSO (red) and BayK 3 μ M (black) are given in (1, left). For each distribution a simple Gaussian-fit was compared with a sum of two Gaussian-fit for significant difference in the goodness of fit (R^2). For BayK 3 μ M the sum of two Gaussian-distribution was preferred (1, middle), whereas for DMSO the single Gaussian model was not rejected (1, right). Due to the statistical support for the BayK-recordings that the distribution of LTCC-activation voltage is bimodal, the two parameters of the sum of two Gaussian model were compared for statistical difference (2) using a 2-tailed student t-test ($t = 8.7$, $df = 16$, $p < 0.001$, variances were not significantly different proven by Fisher's F-test ($F = 3.3$, $dfn = 8$, $dfd = 8$, $p > 0.05$)).

3.3. The regulation of hippocampal firing activity by LTCCs

3.3.1. LTCC-couplings in hippocampal neurons

Next I focused on the regulation of hippocampal discharge activities by the LTCC-mediated coupling to Ca^{2+} -dependent ion channels. In sum 46 hippocampal neurons were tested using the current clamp method with three to five incremental pulse-shaped current injections lasting for 8 s in order to impose increasing depolarizations on the membrane. This was performed to investigate the functional coupling of LTCC-mediated Ca^{2+} -influx to Ca^{2+} -dependent ion channels. VGSCs were blocked by TTX 500 nM. 35 of the tested 46 cells responded with an AHP, whereas 11 responded with an ADP to the depolarization. 8 out of the 35 AHP-forming neurons were only counted and not further analyzed because they were part of a different set of pharmacological experiments leading to 27 pharmacologically investigated AHPs. 7 out of these 27 AHPs were DHP- as well as apamin-insensitive (100 nM), but inhibited with the KCNQ-channel blocker XE 991 10 μM . The median duration of these AHP was 1935 ms (interquartile range = 753 ms, fig. 10, tab. 1).

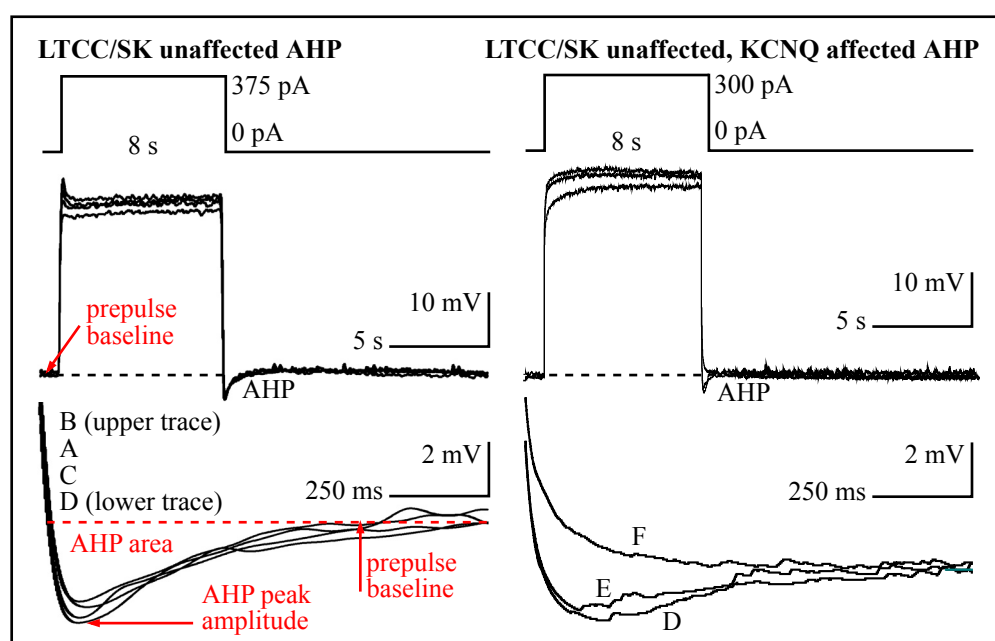


Fig. 10: Example traces for isradipine 3 μM and apamin 100 nM unaffected, but XE 991 10 μM affected AHP (A = DMSO, B = BayK 3 μM , C = BayK 3 μM + apamin 100 nM, D = isradipine 3 μM , E = isradipine 3 μM + apamin 100 nM, F = XE 991 10 μM).

The remaining 20 AHPs were affected by the application of DHPs. Additionally, these AHPs were either inhibited by apamin 100 nM, or UCL 1684 30 nM. In 15 out of these 20 cells the evoked AHP was enhanced by BayK, whereas in the remaining 5 LTCC-activation remained more or less without effect (non-significant reduction of the AHP). Independent of this BayK-induced effect, in 10 of these cells SK-blockade by apamin caused only a reduction of the AHP (“AHP \downarrow ”), whereas in the remaining 10 cells the application of apamin or UCL 1684 unmasked

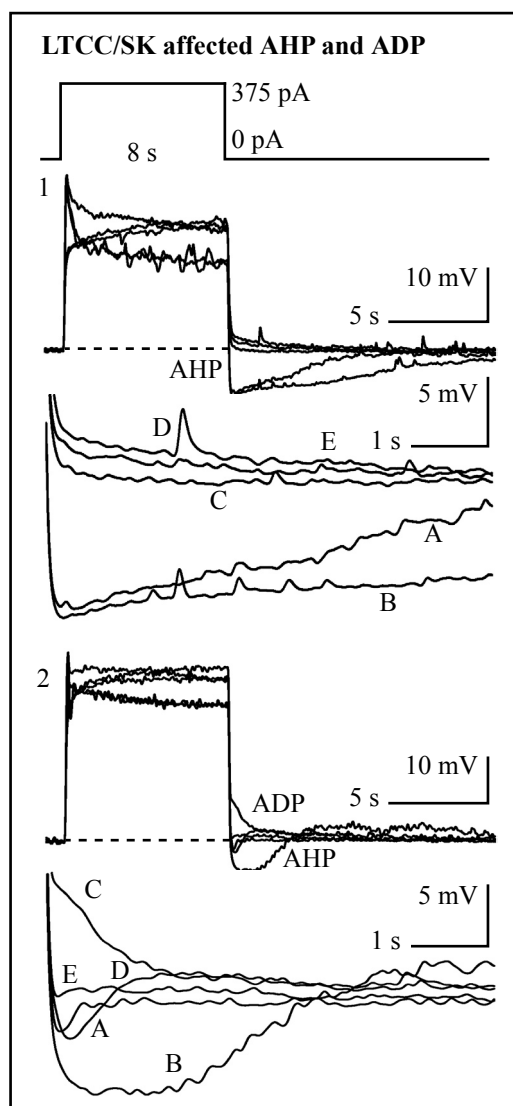


Fig. 12: Example traces for an AHP being either reduced (1), or unmasking an ADP (2) with apamin 100 nM. In both cases BayK 3 μ M led to an increase in relation to the control recording and isradipine 3 μ M to the full inhibition of the afterevent (A = DMSO, B = BayK 3 μ M, C = BayK 3 μ M + apamin 100 nM, D = isradipine 3 μ M, E = isradipine 3 μ M + apamin 100 nM).

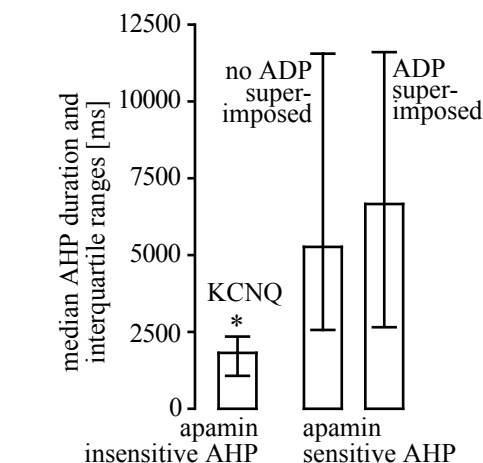


Fig. 11: Durations of different AHPs: The KCNQ-mediated AHP was significantly shorter than the apamin-sensitive AHPs.

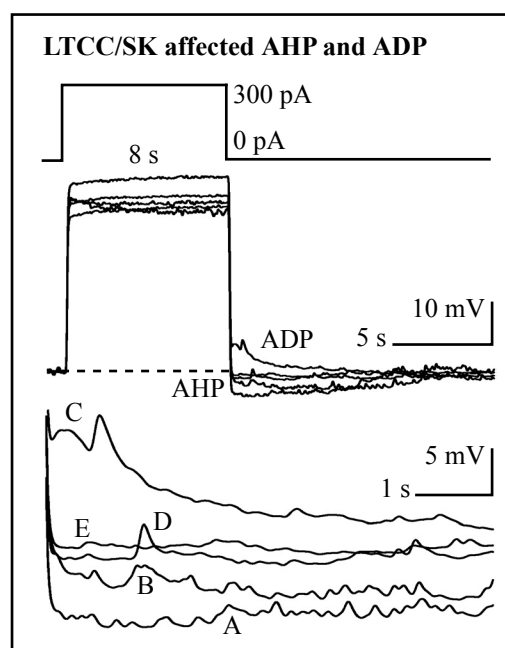


Fig. 14: Example traces of an experiment, which is mostly comparable with that in 15.2 except that LTCC-activation with BayK 3 μ M reduced the AHP measured with the solvent only (A = DMSO, B = BayK 3 μ M, C = BayK 3 μ M + UCL 1684 30 nM, D = isradipine 3 μ M, E = isradipine 3 μ M + UCL 1684 30 nM).

an ADP (“AHP→ADP”). This indicates that under these experimental conditions there were cells with SK-channels operating alone, or in parallel with a Ca^{2+} -activated excitatory conductance (fig. 12, 14, tab. 1). The duration of the “AHP↓”-AHPs was not significantly different from that of the “AHP→ADP”-AHPs with medians of 5585 ms (interquartile range = 7850) and 7065 ms (interquartile range = 8770), respectively. However, the durations of both of them were significantly higher than that of the KCNQ-mediated AHPs (KCNQ-mediated AHP (N = 6),

“AHP↓”-AHPs (N = 10), “AHP→ADP”-AHPs (N = 10), Kruskal-Wallis H-test: $H = 9.345$, $p < 0.05$, Dunn's multiple comparison test: KCNQ-mediated AHP vs. “AHP↓”-AHPs: $p < 0.05$; KCNQ-mediated AHP vs. “AHP→ADP”-AHPs: $p < 0.05$; “AHP↓”-AHPs vs. “AHP→ADP”-AHPs: $p > 0.05$; fig. 11, tab. 1).

In contrast to the AHP generating cells, a minor number of neurons (11/46) showed the opposite effect, namely that they responded with ADPs to the current pulse, when stepping back to resting potential. The augmenting effect of BayK on the ADP-area and -amplitude was smaller than on the respective AHP-parameters. Moreover, every neuron responding with an ADP was affected by SK-blockade, namely showing a further enhancement of the depolarizing afterevent (fig. 17, 18, tab. 1).

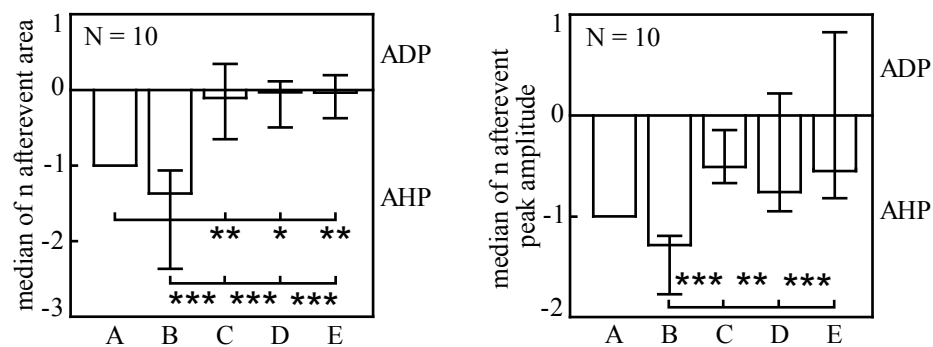


Fig. 13: Apamin-sensitive AHPs without ADPs. Values are represented by their normalized (n) medians and interquartile ranges (labeling as in fig. 15).

Tab. 1: Overview of all effects obtained from LTCC-coupling experiments (a = affected, ua = unaffected, AHP = afterhyperpolarization, ADP = afterdepolarization, n.d. = not done, x = fully inhibited, * marks AHPs, which were just counted, but not further investigated).

N	DMSO	BayK	BayK + apamin	BayK + UCL 1684	low [Na ⁺] BayK + apamin	isradipine	Cd ²⁺	XE-991	channel contribution
7	AHP	ua	ua	ua	ua	ua	ua	ua	KCNQ a, LTCC, SK ua
10	AHP	AHP	AHP ↓	n.d.	n.d.	x	n.d.	n.d.	LTCC, SK a
5	AHP	AHP ↑	ADP	n.d.	n.d.	x	n.d.	n.d.	LTCC, SK a
5	AHP	ua	n.d.	ADP	n.d.	x	n.d.	n.d.	LTCC, SK a
4	ADP	ADP ↑	ADP ↑↑	n.d.	n.d.	x	n.d.	n.d.	LTCC, SK a
7	ADP	ADP ↑	ADP ↑↑	n.d.	ADP ↓	x	n.d.	n.d.	LTCC, SK, CAN a
8*	AHP								

3.3.1.1. Inhibition of LTCC-mediated AHPs by blocking $K_{Ca}2.x$ -channels with apamin or UCL 1684

As already mentioned 35 out of 46 tested neurons showed hyperpolarizing afterevents with BayK (median/interquartile range of afterevent area and amplitude normalized to DMSO = -1.37/1.30 and -1.29/0.58). In the “AHP↓”-AHP-forming cells (10/35) the diminishing effect of the apamin application showed up as a reduction in the AHP area [mV*ms] as well as in the AHP amplitude [mV]. In both cases the BayK-augmented AHP was significantly decreased by the co-application of apamin 100 nM (-0.11/1.00 and -0.51/0.52) and was then indistinguishable from response obtained in isradipine with (-0.03/0.61 and -0.76/1.17) or without apamin (-0.01/0.57 and -0.55/1.65). This indicates that the AHPs were predominantly LTCC- and SK-mediated (Kruskal Wallis H test for the AHP area and amplitude (N = 10 and 10): H = 16.46 and 28.30, $p < 0.001$ and $p < 0.001$; Dunn’s multiple comparison test: BayK vs. BayK + apamin: $p < 0.001$ and $p < 0.001$, BayK + apamin vs. isradipine: $p > 0.05$ and $p > 0.05$, BayK + apamin vs. isradipine + apamin: $p > 0.05$ and $p > 0.05$, fig. 12.1, 13; tab. 2, 3). A complete assembly of the statistical analysis can be found in the appendix (chapter 6.4).

In neurons with “AHP→ADP”-AHPs (10/35), the co-application of BayK 3 μ M and apamin 100 nM (5/10) significantly reduced the BayK-augmented AHP (-3.25/8.05 and -1.22/1.32, prior to the application of the toxin) and even unmasked depolarizing afterpotentials (18.99/22.72 and 1.92/2.19). Comparable results were obtained, when UCL 1684 was used instead of apamin (-0.71/1.97 and -0.62/0.96, before the application of the UCL compound vs. 0.35/0.53 and 0.85/1.06). With the exception of the afterevent amplitude evaluated for the UCL-experiments, all comparisons revealed significant differences. The application of isradipine inhibited the ADPs obtained after SK-blockade. This shows that in these cells two different afterpotential modalities operate in parallel, which were both dependent on LTCC-activation (apamin-experiments: Kruskal Wallis H test for the AHP area and amplitude (N = 5 and 5): H = 16.46 and 24.14, $p < 0.01$ and $p < 0.001$, Dunn’s multiple comparison test: BayK vs. BayK + apamin: $p < 0.01$ and $p < 0.001$; UCL-experiment: Kruskal Wallis H test for the AHP area and amplitude (N = 5 and 5): H = 18.33 and 18.63, $p < 0.01$ and $p < 0.001$, Dunn’s multiple comparison test: BayK vs. BayK + UCL 1684: $p < 0.05$ and $p > 0.05$, fig. 12.2, 14, 15, 16, tab. 2, 3).

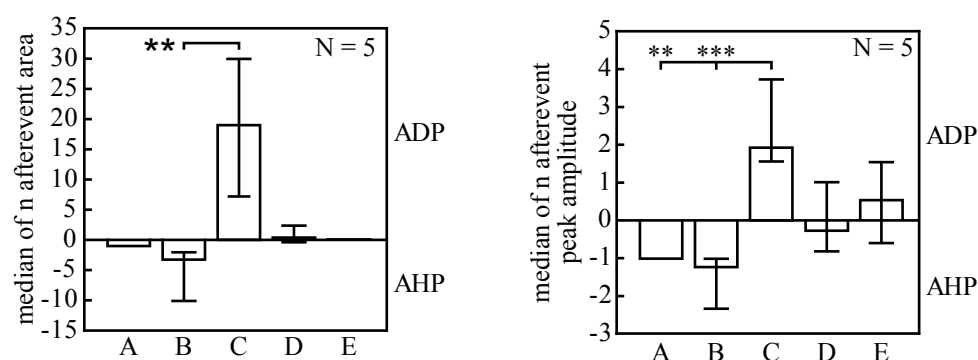


Fig. 15: Apamin-sensitive AHPs with ADPs underlying. Values are represented by their normalized (n) medians and interquartile ranges (labeling as in fig. 15).

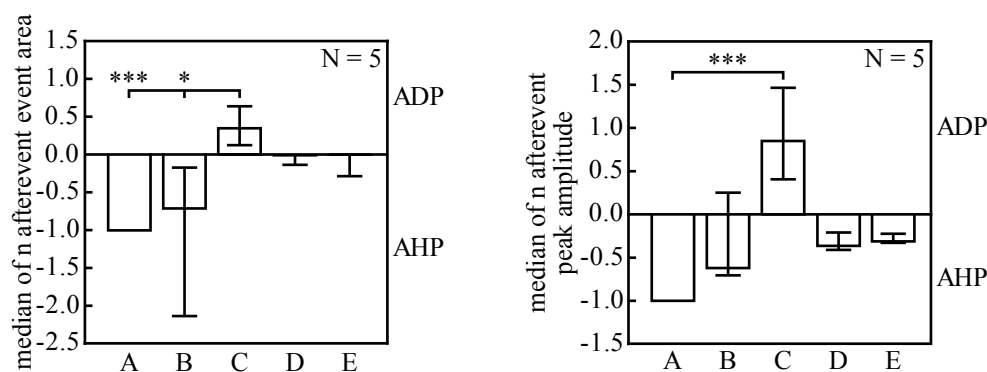


Fig. 16: AHPs sensitive to UCL 1684 30 nM. SK-channels blockade revealed underlying ADPs. Values are represented by their normalized (n) medians and interquartile ranges (labeling as in fig. 17).

3.3.1.2. LTCC-mediated ADPs were enhanced by blocking K_{Ca} 2.x-channels with apamin and inhibited by Na^+ substitution

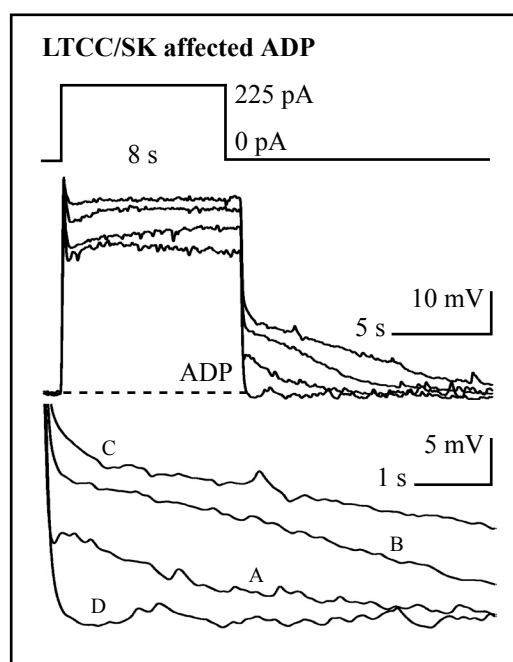


Fig. 17: Representative recording for a neuron showing a LTCC- and SK-mediated ADP (A = DMSO, B = BayK 3 μ M, C = B + apamin 100 nM, D = isradipine 3 μ M, E = D + apamin 100 nM (not shown)).

In contrast to the cells described in chapter 3.3.1 in 11 out of 46 cells ADPs were already present under DMSO (always set to 1, see above) and BayK 3 μ M (1.50/0.63 and 1.04/0.20), respectively. Moreover, the BayK-augmented ADPs were further enhanced by the additional application of apamin 100 nM (2.22/3.99 and 1.13/0.25) indicating that a SK-mediated AHP was superimposed and thereby partly reduced the ADP under BayK. If the external Na^+ -concentration was reduced from 140 to 1.5 mM (see chapter 2.3), the BayK-augmented ADPs was significantly reduced (0.34/0.68 and 0.62/0.29). This is the physiological profile of a CAN-channel. As shown for the hyperpolarizing afterevents LTCC-blockade with isradipine 3 μ M fully inhibited the ADP (0.02/0.13 and 0.18/0.50) showing that the Na^+ -conductance

underlying the BayK-augmented ADPs is dependent on LTCC-mediated Ca^{2+} -influx. To sum up, these experiments reveal that LTCCs functionally couple to ADP-forming CAN-channels. All values are given as median/interquartile ranges of afterevent area and amplitude normalized to DMSO (Kruskal Wallis H test for the AHP area and amplitude (N = 7 and 7): H = 47.64 and 40.14, $p < 0.001$ and $p < 0.001$, Dunn's multiple comparison test: BayK + apamin vs. low Na^+ - BayK + apamin: $p < 0.01$ and $p < 0.01$, low Na^+ - BayK + apamin vs. BayK + wash out: $p < 0.01$ and $p = 0.054$, fig. 17 - 20, tab. 2, 3).

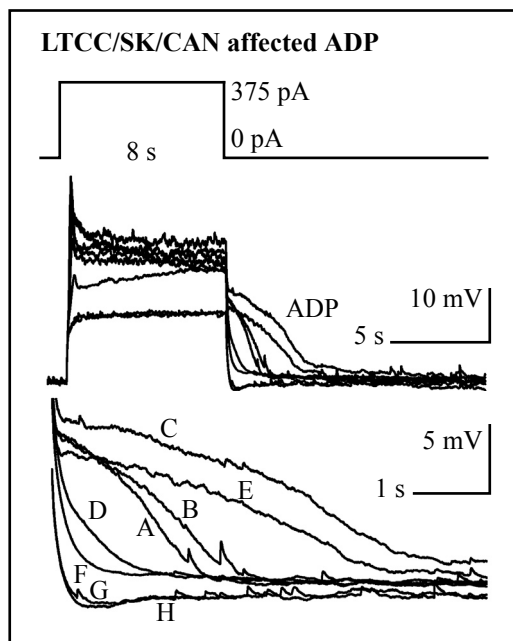


Fig. 18: Example traces for an ADP elicited under control conditions (DMSO) and enhanced with LTCC-activation using BayK 3 μ M. The ADP was almost fully eliminated when the low $[Na^+]$ -buffer was applied indicating that the ADP is carried by a CAN-channel. (A = DMSO, B = BayK 3 μ M, C = B + apamin 100 nM, D = C 100 nM low $[Na^+]$, E = C wash out, F = isradipine 3 μ M, G = F + apamin 100 nM, H = G 100 nM low $[Na^+]$).

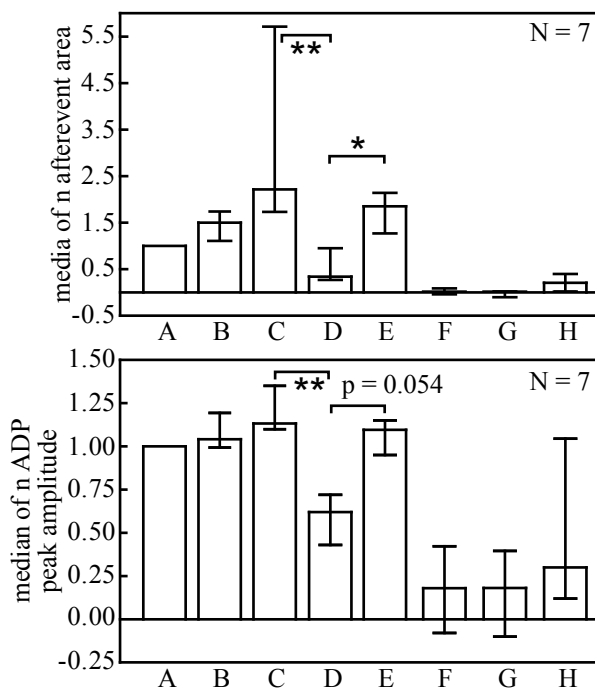
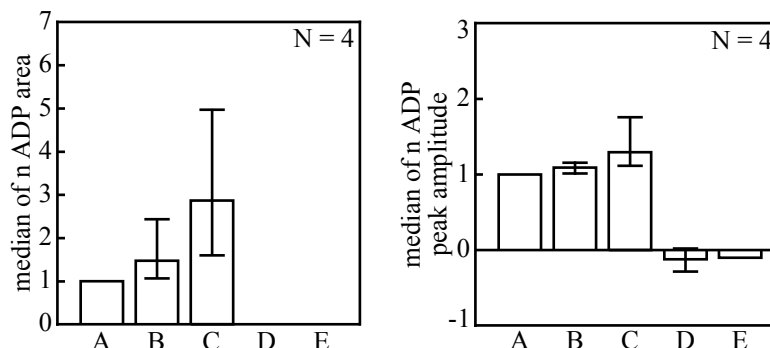


Fig. 20: ADPs evoked by LTCC-induced Ca^{2+} -influx were significantly inhibited via exchange of Na^+ with choline leading to an external $[Na^+]$ of 1.5 mM instead of 140 mM. At least for the afterevent area this effect was significantly reversible (labeling as in fig. 22).

Fig. 19: Normalized (n) medians and interquartile ranges of ADPs already observed in the control recording (DMSO), which were enhanced by BayK 3 μ M as well as by the additional application of apamin 100 nM (labeling as in fig. 21).



Tab. 2: Afterevent area (median and interquartile range) for tab. 3 without LTCC- and SK-affected cells. Negative values represent AHPs, while positive stand for ADPs (n.d. = not done).

N	BayK	BayK + apamin	BayK + UCL 1684	low $[Na^+]$ BayK + apamin	isradipine	isradipine + apamin	isradipine + UCL 1684	low $[Na^+]$ isradipine + apamin
10	-1.37, 1.30	0.11, 1.00	n.d.	n.d.	-0.03, 0.61	-0.01, 0.57	n.d.	n.d.
5	-3.25, 8.05	18.99, 22.72	n.d.	n.d.	0.38, 2.74	0.08	n.d.	n.d.
5	-0.71, 1.97	x	0.35, 0.53	n.d.	-0.03, 0.14	n.d.	-0.01, 0.29	n.d.
4	1.48, 1.37	2.87, 3.39	n.d.	n.d.	-0.03, 0.07	-0.08	n.d.	n.d.
7	1.50, 0.63	2.22, 3.99	n.d.	0.34, 0.68	0.02, 0.13	0.02, 0.12	n.d.	0.21, 0.42

Tab. 3: Afterevent peak amplitude (median and interquartile range) for tab. 3 without LTCC- and SK-unaffected cells. Negative values represent AHPs, while positive stand for ADPs (n.d. = not done).

N	BayK	BayK + apamin	BayK + UCL 1684	low [Na ⁺] BayK + apamin	isradipine	isradipine + apamin	isradipine + UCL 1684	low [Na ⁺] isradipine + apamin
10	-1.29, 0.58	-0.51, 0.52	n.d.	n.d.	-0.76, 1.17	-0.55, 1.65	n.d.	n.d.
5	-1.22, 1.32	1.92, 2.19	n.d.	n.d.	-0.26, 1.83	0.54, 2.14	n.d.	n.d.
5	-0.62, 0.96	n.d.	0.85, 1.06	n.d.	-0.36, 0.20	n.d.	-0.31, 0.11	n.d.
4	1.09, 0.14	1.30, 0.66	n.d.	n.d.	-0.12, 0.31	-0.10	n.d.	n.d.
7	1.04, 0.20	1.13, 0.25	n.d.	0.62, 0.29	0.18, 0.50	0.18, 0.50	n.d.	0.29, 0.92

3.3.1.3. De- and hyperpolarizing LTCC-couplings differ in their “coupling efficiency”

If the neurons were experimentally depolarized for 8 s, three-fourth responded with an AHP, whereas only one fourth responded with an ADP. By varying the pulse duration from 100 ms to 10 s in the presence of BayK 3 μ M and TTX 500 nM, I found out that, in cells where both couplings are present, positive afterpotentials dominate at very short pulse durations, but decrease very fast with increasing time of depolarization (N = 8). Pulse durations between 500 ms and 2 s led to rather small afterpotential areas owing to the turning point from ADPs to AHPs at pulse lengths of about 1 s. Longer depolarizations quickly strengthened the impact of the hyperpolarizing coupling, which was strongest at 10 s indicating that AHPs were not saturated after pulse durations of 8 s (fig. 21.1).

Comparable results were obtained from experiments using different strengths of the preceding depolarization instead of different pulse durations (pulse duration was kept at 8 s). In these experiments the BayK-augmented ADP area significantly correlated with the depolarization strength in a negative manner (N = 7, $p < 0.001$, $R^2 = 0.55$). Pulses 1 to 4 (fig. 21.2) indicated a negative linear relation between the preceding depolarization and the AHP-area. However, strong outward rectification limited a proportional further depolarization with the highest current injection (pulse 5, fig. 21.2, 21.4). Hence, this last data point was left out of the regression model (fig. 21.2).

In another series of experiments the BayK concentration was increased from 0.03 (-3445 mV*ms/2122 mV*ms) to 0.3 (-5205 mV*ms/3659 mV*ms) and 3 μ M (-9763 mV*ms/5806 mV*ms). From 0.03 to 3 μ M BayK the LTCC-mediated AHP was significantly reduced (Kruskal Wallis H test (N = 5): $H = 10.26$, $p < 0.01$, Dunn’s multiple comparison test: 0.03 μ M vs. 3 μ M: $p < 0.01$, fig. 21.3). All measurements of chapter 3.2.1.3. were done in close collaboration with Petra Geier (PhD student in FWF project P19710).

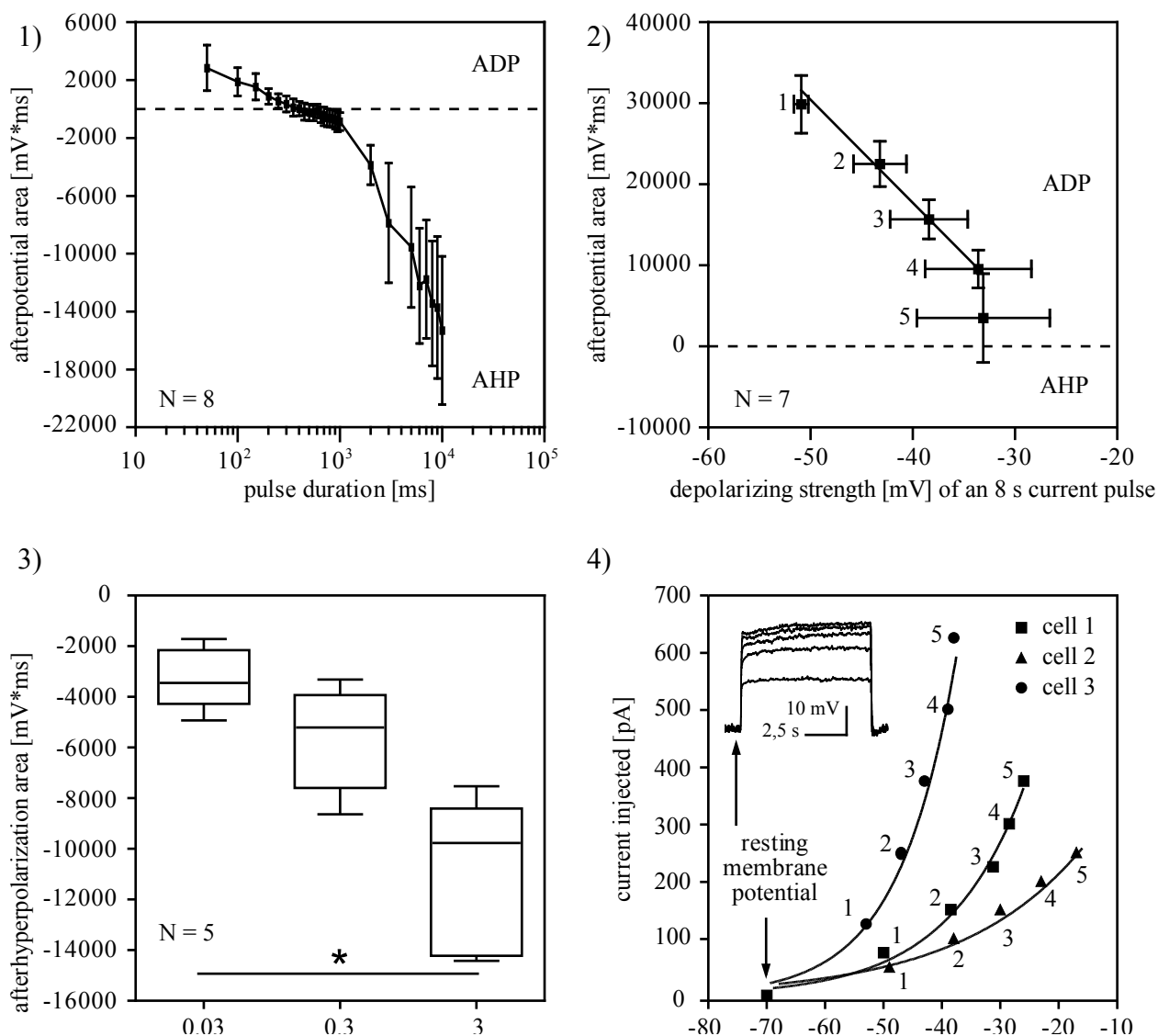


Fig. 21: By varying the pulse length (1), the pulse strength (2) and [BayK] (3), we obtained evidence that AHPs and ADPs differ in their efficiency of coupling to LTCC-mediated Ca²⁺-influx. (1) Note the time range (500 ms - 2 s), where the ADP starts to reverse into an AHP. (2) With the exception of the strongest depolarization 5 (the system is already saturated, for a detailed explanation see (4)), the AHP-area correlates with the strength of the preceding depolarization. (3) The AHP-area depends on the amount of LTCC-mediated Ca²⁺-influx. (4) Outward-rectification increases with the growing amount of current injected. Thereby, the strength of achievable depolarizations is limited. Cells exhibit different strengths of outward-rectification.

3.3.2. The contribution of LTCCs to normal electrical discharge activity

In a final set of experiments, I wanted to know, if my functional coupling model provides concrete physiological implications. Thus, the role of LTCCs in the electrical activity of hippocampal neurons was studied by recording their membrane potential without blocking synaptic transmission. The measurements were done in the voltage follower mode, where I was set to 0 and the signals were continuously recorded. Predefined criteria for taking a cell into statistical account were as follows: (I) a resting potential below -50 mV and (II) the ability of firing action potentials with an overshoot above 0 mV. This was verified before the experiment by applying a depolarizing current, if required.

In order to reveal functional patterns in the diversity of LTCC-mediated effects on hippocampal firing, cluster analyses for event durations and spike frequencies were performed. Before putting the data into cluster analyses, the neurons were qualitatively classified into three fundamentally different firing patterns measured under control conditions: spiking (N = 12), bursting (N = 11) and bursting with pronounced AHP-formation (N = 8, fig. 22.3 - 24.3; tab. 4, 5). The x-axis of the dendrograms indicates the relative difference between two data points or clusters, which is linkage distance divided through the respective maximal overall distance. Cluster sizes varied from one to five cells (fig. 22.2 - 24.2).

In about two thirds of all bursting neurons (including both cells with and without pronounced AHP-formation) LTCC activation with BayK enhanced the discharge activity by leading to burst prolongations BP and plateau potentials PP (mean of median event times normalized to DMSO +/- SEM for BP with BayK = 1.6 +/- 0.3 and with isradipine = 0.9 +/- 0.3, N = 5; mean of median event times normalized to DMSO +/- SEM for BP (AHP) with BayK = 2.3 +/- 0.4 and with isradipine = 1.1 +/- 0.2, N = 3; mean of median event times normalized to DMSO +/- SEM for PP with BayK = 113.4 +/- 92.0 and with isradipine = 0.9 +/- 0.4, N = 3; mean of median event times normalized to DMSO +/- SEM for PP (AHP) with BayK = 69.1 +/- 64.3 and with isradipine = 1.4 +/- 0.4, N = 2; fig. 22.1 - 23.1, tab. 4, 5).

In about one third of all bursting cells the opposite effect was observed, namely that isradipine augmented the electrical activity (mean of median event times normalized to DMSO +/- SEM for BP with isradipine = 2.1 +/- 0.6 and with BayK = 0.8 +/- 0.1, N = 3; mean of median event times normalized to DMSO +/- SEM for BP (AHP) with isradipine = 1.6 +/- 0.2 and with BayK = 0.6 +/- 0.2, N = 3; fig. 22.1 - 23.1, tab. 4, 5).

12 out of 31 neurons exhibited spiking-like firing patterns. This showed up either as enhanced spiking ES frequencies with BayK (as compared to DMSO) or decreased spiking DS frequencies with isradipine (as compared to DMSO and BayK (mean of AP frequency normalized to DMSO +/- SEM for ES with BayK = 1.7 +/- 0.2 and with isradipine = 1.2 +/- 0.1, N = 3; mean of AP frequency normalized to DMSO +/- SEM for DS with isradipine = 0.2 +/- 0.1 and with BayK = 1.0 +/- 0.1, N = 5)). The observation that spiking frequencies were enhanced with BayK and decreased by isradipine (both compared to DMSO) was also obtained (mean of AP frequency

normalized to DMSO +/- SEM for ES with BayK = 2.9 and DS with isradipine = 0, N = 1). In contrast to the bursting neurons no LTCC mediated diminishment of activity was observed among the spiking cells. Instead of that, 25 % of the spiking neurons exhibited no effect, if the dihydropyridines were applied (mean of AP frequency normalized to DMSO +/- SEM for ES with BayK = 0.7 +/- 0.1 and DS with isradipine = 0.9 +/- 0.2, N = 3 tab. 4, 5).

To sum up, in 68 % of the bursting neurons and in all of the spiking cells (totally 80 %), except the not affected ones, LTCC mediated enhanced electrical activity, whereas in 32 % of the burster LTCC mediated reduced electrical activity (totally 20 %).

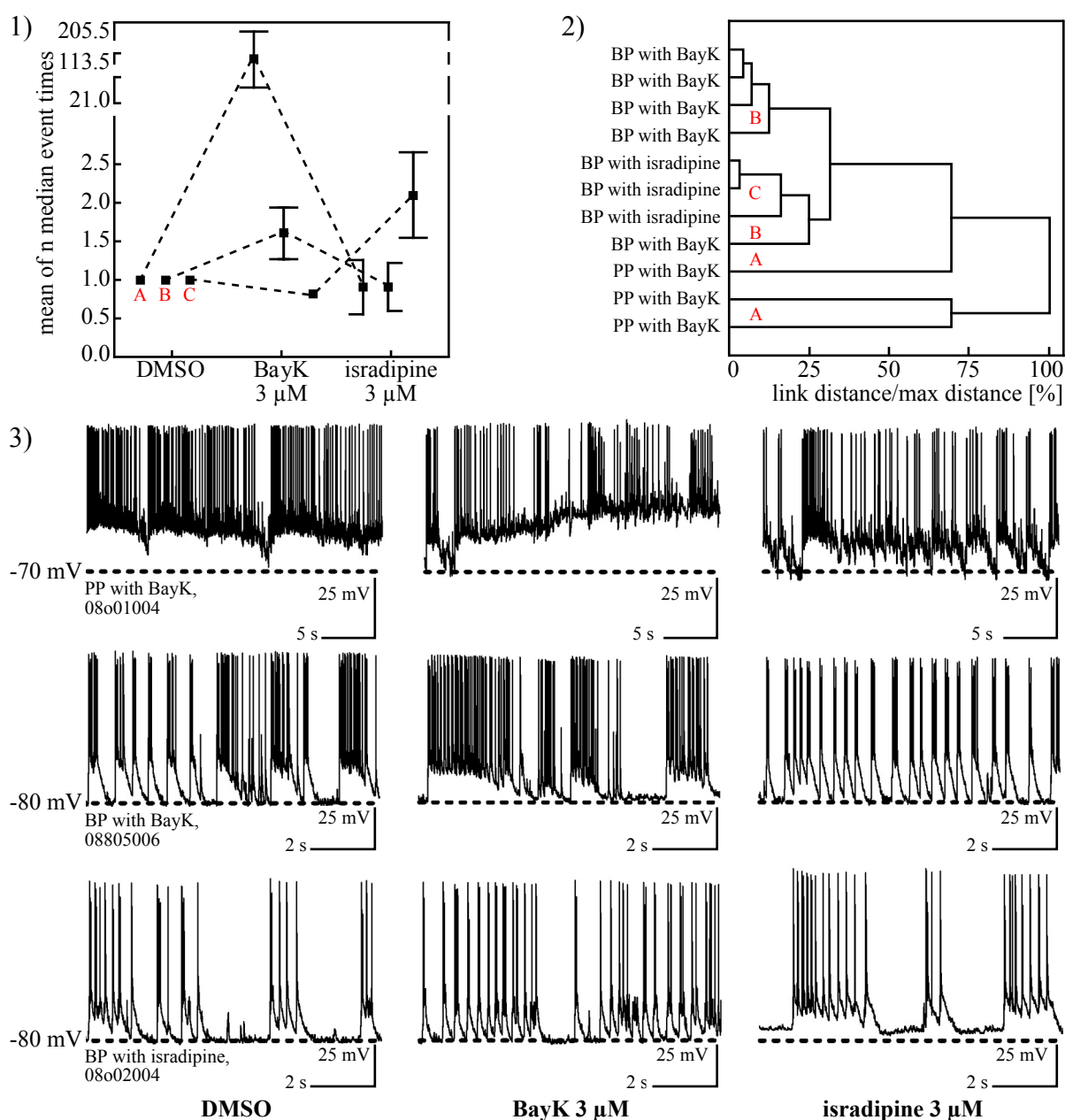


Fig. 22: Discharge activity of bursting neurons, which exhibited no apparent AHP, measured under control conditions (DMSO), LTCC-activation (BayK 3 μM) and -inhibition (isradipine 3 μM). (1) Mean +/- SEM of normalized (n) median event times evaluated for cells clustering in (2). (3) Example traces for cells displaying plateau potentials (PPs) with BayK 3 μM (A), burst prolongations (BPs) with BayK 3 μM (B) and burst prolongations with isradipine 3 μM (C).

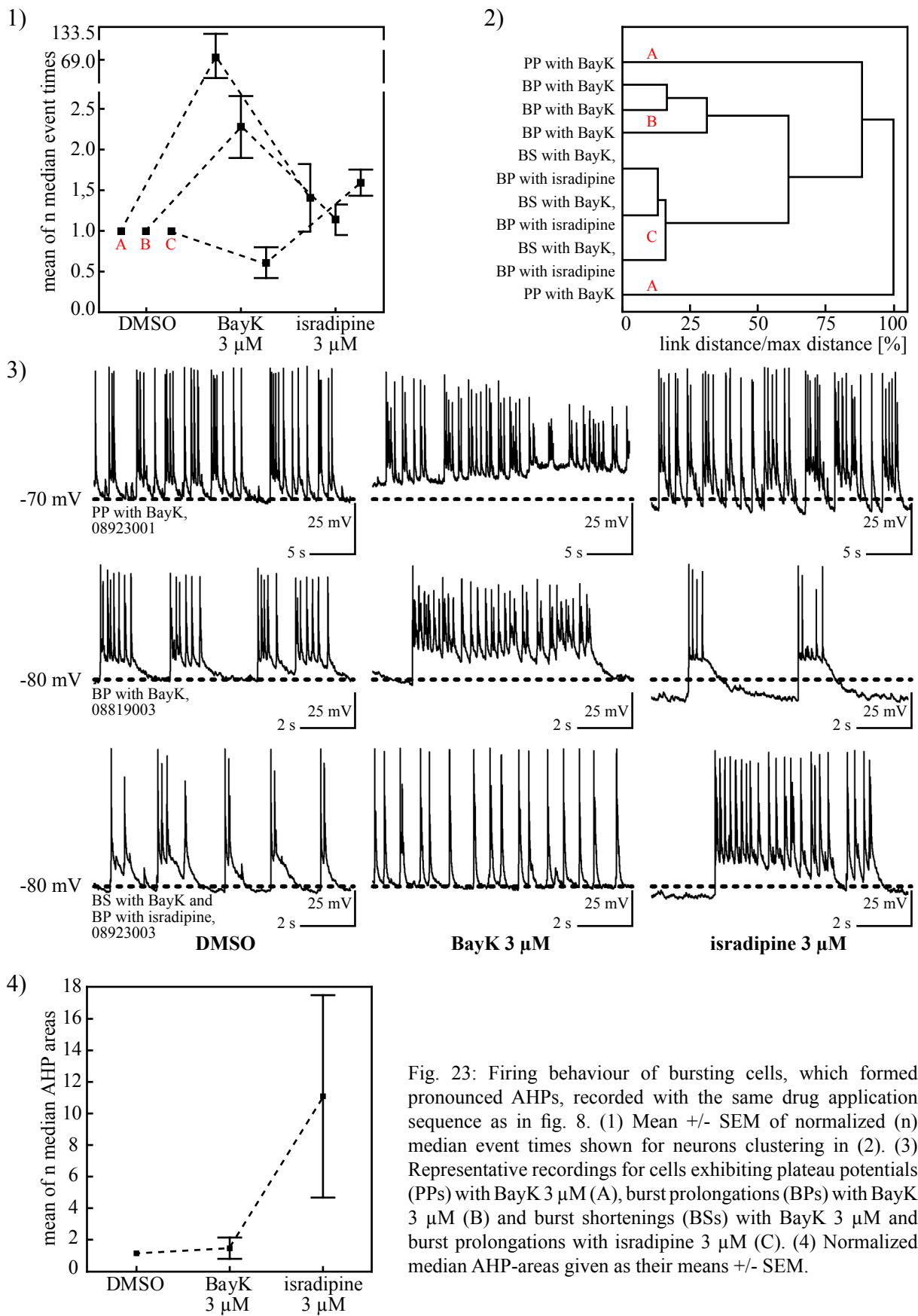


Fig. 23: Firing behaviour of bursting cells, which formed pronounced AHPs, recorded with the same drug application sequence as in fig. 8. (1) Mean +/- SEM of normalized (n) median event times shown for neurons clustering in (2). (3) Representative recordings for cells exhibiting plateau potentials (PPs) with BayK 3 μM (A), burst prolongations (BPs) with BayK 3 μM (B) and burst shortenings (BSs) with BayK 3 μM and burst prolongations with isradipine 3 μM (C). (4) Normalized median AHP-areas given as their means +/- SEM.

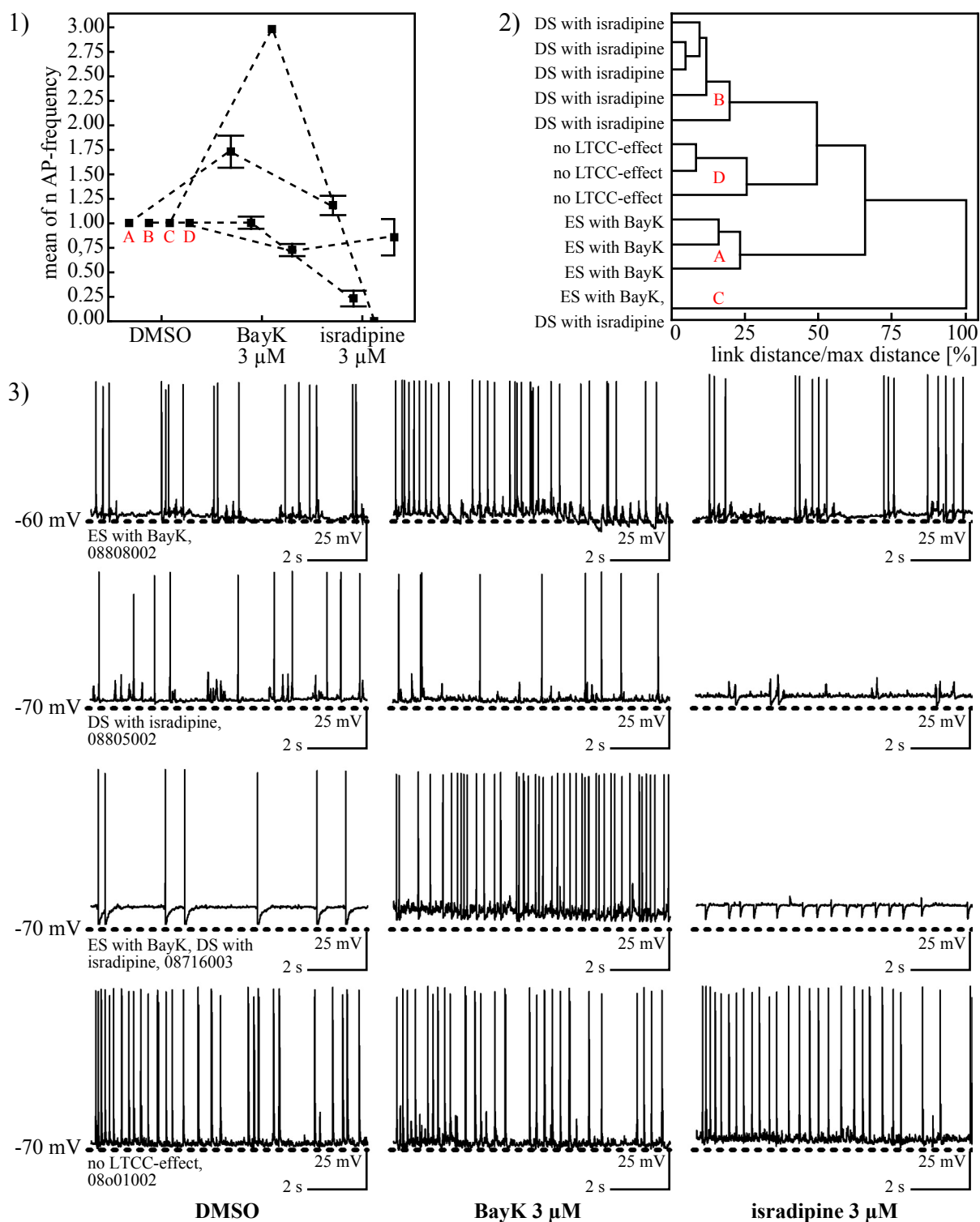


Fig. 24: Hippocampal neurons with an activity of consecutive APs (spiking). Activity-dependent clusters of cells (2) are represented by their means of normalized (n) AP-frequency (1). Four clusters with different activity-profiles were determined including cells with enhanced spiking (ES) with BayK 3 μ M (A), decreased spiking (DS) with isradipine 3 μ M (B) as well as with enhanced and decreased spiking with BayK 3 μ M and isradipine 3 μ M, respectively (C). (D) marks the neurons, which displayed no LTCC-mediated effect.

Tab. 4: Cells classified by their durations of event times using a cluster analysis (subclasses). The classes are defined by the absence or presence of AHPs under control conditions with DMSO (BP = burst prolongation, BS = burst shortening, PP = plateau potential, AHP = afterhyperpolarization)

class	subclass	N	mean of normalized (DMSO) median event times +/- SEM	
			BayK 3 μ M	isradipine 3 μ M
burster without AHP	BP with BayK	5/31	1.6 +/- 0.3	0.9 +/- 0.3
	PP with BayK	3/31	113.4 +/- 92.0	0.9 +/- 0.4
	BP with isradipine	3/31	0.8 +/- 0.1	2.1 +/- 0.6
burster with AHP	BP with BayK	3/31	2.3 +/- 0.4	1.1 +/- 0.2
	PP with BayK	2/31	69.1 +/- 64.3	1.4 +/- 0.4
	BS with BayK, BP with isradipine	3/31	0.6 +/- 0.2	1.6 +/- 0.2
class	subclass	N	mean of normalized (DMSO) median AHP areas +/- SEM	
			BayK 3 μ M	isradipine 3 μ M
burster with AHP		8/31	1.3 +/- 0.7	11.0 +/- 6.4

Tab. 5: Spiking cells, which were separated from burster (tab. 1), classified in subclasses by their spiking frequency (ES = enhanced spiking, DS = decreased spiking).

class	subclass	N	mean of normalized (DMSO) AP frequency +/- SEM	
			BayK 3 μ M	isradipine 3 μ M
spiker	ES with BayK	3/31	1.7 +/- 0.2	1.2 +/- 0.1
	DS with isradipine	5/31	1.0 +/- 0.1	0.2 +/- 0.1
	ES with BayK, DS with isradipine	1/31	2.9	0
	no LTCC effect	3/31	0.7 +/- 0.1	0.9 +/- 0.2

4. DISCUSSION

4.1. $\text{Ca}_v1.3\text{long}$ activates at more negative potentials than $\text{Ca}_v1.2\alpha1\text{C77}$

All constructs tested exhibited the principal characteristics of VGCCs, such as tail currents as well as Ca^{2+} - and voltage-dependent inactivation (fig. 8). Moreover, for all DHPi-mutants the insensitivity to BayK 3 μM and isradipine 3 μM could be verified (fig. 8).

Most importantly, by comparing the voltage-dependent activation, I confirmed that $\text{Ca}_v1.3\text{long}$ possess biophysical properties clearly distinct from those of $\text{Ca}_v1.2\alpha1\text{C77}$. Generally, activation-curves of $\text{Ca}_v1.3\text{long}$ were shifted by 10 - 15 mV to more negative potentials. Concerning the V_{50s} , V_{5s} and peak voltages, values obtained from my measurements were comparable to published data for $\text{Ca}_v1.3\text{long} = \text{Ca}_v1.3_{8A}$ ([Koschak et al. 2001], fig. 9) and for $\text{Ca}_v1.2\alpha1\text{C77}$ ([Liao et al. 2004], fig. 9).

4.2. $\text{Ca}_v1.3$ plays an important role in hippocampal neurons

In biophysical studies IV- or activation curves of different LTCC-subtypes are usually established from voltage clamp recordings in heterologous expression systems [Xu and Lipscombe 2001; Lipscombe et al. 2004; Helton et al. 2005; Singh 2006; Koschak et al. 2007]. I tried to address the question of LTCC-activation on a more physiological level and performed experiments on differentiated hippocampal neurons (20 to 30 days in culture, see chapter 2) in the perforated patch configuration. Due to enhanced space clamp effects as well as augmented access resistances under these conditions, I decided to use the current clamp technique, where both the space clamp and high access resistances play a minor role compared to the voltage clamp

(see chapter 2.8, 2.9, fig. 9.3). The activation thresholds measured in the current clamp were at ~ -44 mV (“MVA”-cells) and > -35 mV (“HVA”-cells) for the control experiments and ~ -54 mV (“MVA”-cells) and ~ -44 mV (“HVA”-cells) under application of BayK 3 μ M (fig. 9.1). This corresponds to the BayK-induced ~ 10 mV shift in voltage-dependent LTCC-activation to more negative potentials determined in voltage clamp experiments e.g. by [Hess et al. 1984] and [Xu and Lipscombe 2001].

In line with my results (chapter 3.1, fig. 8) there is no indication that $\text{Ca}_v1.2$ -variants can activate at potentials negative to -35 mV. This has even been not observed, when low $[\text{Ba}^{2+}]$ were used, which are known to shift the voltage-dependent activation of VGCCs to more negative potentials [Koschak et al. 2001; Xu and Lipscombe 2001; Helton et al. 2005]. Moreover, there is no evidence that $\text{Ca}_v1.2$ -activation thresholds can be shifted to potentials negative than -35 mV by any auxiliary subunit or splice-variation in the CNS [Liao et al. 2004; Yasuda et al. 2004]. In contrast to that, activation thresholds for various $\text{Ca}_v1.3$ -variants were determined at approximately -40 mV [Koschak et al. 2001; Xu and Lipscombe 2001; Gao et al. 2006] (fig. 8). Furthermore, a specific splice variant ($\text{Ca}_v1.3_{42A}$) was shown to activate at especially negative potentials [Singh et al. 2008]. Therefore, if the activation thresholds from my current clamp recordings are compared with those obtained from the voltage clamp using heterologous expression systems, I assume that LTCC-activation in the current clamp under control conditions occurring lower than -40 mV represent $\text{Ca}_v1.3$ -activation. Furthermore, I suggest that in “HVA”-cells there is no $\text{Ca}_v1.3$ -mediated impact on the membrane potential, whereas “MVA”-cells are thought to require a significant $\text{Ca}_v1.3$ -contribution in order to be able to activate at such negative potentials. However, I have no information about the impact of $\text{Ca}_v1.2$ in “MVA”-cells. Since “HVA”-cells represented a minority in our culture, I conclude that under control conditions in the majority of hippocampal neurons the activation of $\text{Ca}_v1.3$ substantially contributes to depolarization-induced, LTCC-mediated effects on the membrane potential (fig. 9.1 right). These findings stand in clear contrast to several publications reporting the lack of significant $\text{Ca}_v1.3$ -mediated activities in hippocampal neurons [Moosmang et al. 2005; Lacinova et al. 2008] or even stating a minor physiological role of $\text{Ca}_v1.3$ in the entire CNS [Clark et al. 2003].

If I_{LTCC} was enhanced by the application of BayK 3 μ M, the detectability of “HVA”-cells was improved leading to a bimodal distribution of the LTCC-activation threshold (fig. 9.1 middle). This could possibly be explained by an intrinsic limitation of my experimental setting. In my experiments the strength of the artificially induced depolarizations highly depended on the amount of active outward-conducting ion channels due to the fact that no blocking agents for delayed rectifier K^+ -channels (e.g. TEA) were used [Lee and Tepper 2007]. Moreover, I showed that the strength of outward rectification was dependent on the strength of the depolarizing current injection (fig. 21.4). As a consequence of using the current clamp method without substances blocking delayed rectifier K^+ -channels, it was impossible to depolarize a neuronal membrane above -30 to -25 mV. Therefore, I assume that only under BayK, which is known to shift LTCC-activation to more negative potentials by about 10 mV [Hess et al. 1984; Xu and

Lipscombe 2001], I could estimate the amount of cells without Ca_v1.3 actively contributing to the membrane potential. Hence, I postulate the existence of two functional subtypes of hippocampal neurons occurring in similar frequencies (fig. 9.1 left), but are clearly distinct by their Ca_v1.3-contribution to membrane depolarizations (Ca_v1.3-contribution missing in “HVA”-cells). These results were further supported in a supplementary approach carried out within the parent FWF project (P19710) by experiments using step- instead of ramp-shaped current injections (Geier et al. unpublished).

How do these functional findings correlate with published Ca_v1.2/Ca_v1.3-expression levels? Concerning the Ca_v1.2/Ca_v1.3-expression ratio, published data either suggest a strong divergence of 90 to 10 % [Sinnegger-Brauns et al. 2009], or no significant difference [Schlick et al. unpublished]. Both findings were obtained from qRT-PCR assays. However, mRNA-levels do not have to reflect protein-levels and expression levels of ion channels do not necessarily correlate with the current it mediates. Hence, the comparability of electrophysiological data with binding [Clark et al. 2003] or expression studies [Sinnegger-Brauns et al. 2009] and [Schlick et al. unpublished] is generally difficult to assess.

Irrespective of the Ca_v1.2/Ca_v1.3-expression ratio, my data indicate a more prominent role of Ca_v1.3 in the hippocampus than previously reported [Clark et al. 2003; Moosmang et al. 2005; Lacinova et al. 2008].

4.3. The regulation of hippocampal firing activities by LTCCs

4.3.1. The LTCC-SK-coupling forms

long-lasting AHPs in hippocampal neurons

With the exception of the KCNQ-mediated AHPs (N = 7), all other afterpotentials (N = 39) were significantly inhibited with isradipine 3 μM and were thus induced by LTCC-activation. LTCC-activated AHPs were significantly reduced by highly selective SK(K_(Ca)2.x)-antagonists apamin 100 nM (fig. 12, 13, 15) and UCL 1684 30 nM (fig. 14, 16) indicative of an AHP-forming functional interplay of LTCCs and SK-channels. Such an interaction has already been reported for several tissues including the hippocampus [Rascol et al. 1991; Moyer et al. 1992; Marrion and Tavalin 1998; Bowden et al. 2001]. The occurrence of certain AHPs sensitive to the selective KCNQ-antagonist XE991 10 μM (fig. 10) in the hippocampus is supported by the work of [Gu et al. 2005] and [Tzingounis et al. 2008] (tab. 2, 3).

Interestingly, the pharmacology-kinetics-profile of the AHPs does not correspond to what has been described in literature [Sah and Faber 2002]. Independent of their sensitivity to various antagonists, the AHPs measured showed durations in the range of seconds, which typically characterizes sAHPs [Sah and Faber 2002]. With an approximately 10-fold faster inactivation mAHPs usually decay within several hundreds of ms [Sah and Faber 2002]. However, many publications describe the I_{sAHP} as being insensitive to SK- and KCNQ-blockade, whereas I_{mAHP}

is widely accepted to be SK- or KCNQ-mediated (i.e. [Lancaster and Nicoll 1987; Kohler et al. 1996; Shah and Haylett 2000b; Bowden et al. 2001; Villalobos et al. 2004; Gu et al. 2005]. Additionally, the notion that SK-channels mediate the mAHP rather than the sAHP is supported by findings obtained from $K_{(Ca)}2.2^{-/-}$ -mice completely lacking mAHPs [Bond et al. 2004]. Furthermore, the channels suggested to underlie the sAHP have a slow activation phase, incompatible with the rapid activation of apamin-sensitive and thus SK-mediated currents [Sah and Faber 2002].

One possible explanation for this contradiction could be the difference in recording conditions, namely whole cell and perforated patch measurements. Most of the AHPs have been characterized by their respective currents recorded in the voltage clamp using the whole cell configuration and pipette solutions with ATP-concentrations in the range of 2 - 4 mM [Shah and Haylett 2000b; Villalobos et al. 2004]. However, it has been shown in recent years that SK2 forms multiprotein complexes with protein kinase CK2 and protein phosphatase PPA2 and that SK2-inactivation can be accelerated by CK2-activation via the application of MgATP 5 mM on the inside face of the excised patch [Allen et al. 2007]. Hence, the internal [ATP] is an important factor regulating $K_{(Ca)}2.2$ -kinetics. Thus, a possible explanation for the discrepancy between the results reported here and the apamin-sensitive I_{mAHP} could be that I_{mAHP} measured in the voltage clamp (whole cell) corresponds to sAHPs in the current clamp (perforated patch) due to different phosphorylation levels of SK2-channels. Indeed, in [Kato et al. 2006] it can be seen that I_{sAHP} is sensitive to apamin, when recorded in the perforated patch mode. Moreover, as I_{sAHP} was early reported to be neurotransmitter-modulated via direct phosphorylation [Sah and Isaacson 1995], SK-channels seem to be promising molecular candidates mediating I_{sAHP} . To summarize, my results indicate that LTCC-induced SK-activation leads to slow AHPs following long-lasting depolarizations of the hippocampal membrane.

4.3.2. CAN-channels functionally couple to LTCCs and underlie the ADPs in hippocampal neurons

As it has been described in several publications [Haj-Dahmane and Andrade 1997; Ghamari-Langroudi and Bourque 2002; Schiller 2004; Lee and Tepper 2007] I tried to inhibit ADPs by the application of flufenamic acid, which was shown to block CAN-channels in the hippocampus [Partridge and Valenzuela 1999]. This was done in several concentrations from 3 to 300 μ M, however a blocking effect on ADPs could not be observed (N = 3, data not shown). In contrast to this, the reduction of the external Na^+ -concentration from 140 to 1.5 mM by superfusing the cells with a choline-based buffer (chapter 2.3.), led to a significant reduction of the ADPs (fig. 17 - 20, tab. 2, 3) consistent with data shown by [Lee and Tepper 2007]. To sum up, these experiments reveal the physiological profile of a CAN-channel, namely a Ca^{2+} -dependent Na^+ -conducting channel, which is activated by LTCC-mediated Ca^{2+} -entry and underlies ADPs in

hippocampal neurons. Such a LTCC-CAN-interaction system has already been described in nigral GABAergic neurons [Lee and Tepper 2007].

Furthermore, experiments showing the sensitivity of LTCC-induced ADPs to 2-Aminoethoxydiphenyl borate (2-APB) revealed that TRPM-channels are possible molecular candidates for the LTCC-coupling CAN-channels in the hippocampus [Alexander et al. 2007] and [Geier et al. unpublished].

4.3.3. In hippocampal neurons the stimulus intensity determines the afterpotential modality

The blockade of one of the two LTCC-dependent afterpotential modalities occurring in the hippocampus (AHPs and ADPs) revealed that in the majority of the tested neurons AHP-forming $K_{(Ca)}2.x$ -channels and ADP-forming CAN-channels act in parallel after LTCC-activation (fig. 12.2, tab. 1). Which afterpotential modality predominated, was dependent on the stimulus intensity of the preceding depolarization. If the intensity was enhanced, either by prolonging the pulse duration, or by augmenting the strength of depolarization, ADPs were decreased and AHPs were increased (fig. 21.1, 21.2). Therefore, as $K_{(Ca)}2.x$ - and CAN-channels differently respond to varying pulse lengths and strengths, I obtained evidence that they differ in their efficiency of LTCC-coupling.

Moreover, I showed that (I) CAN-channels always activate at weaker stimuli in response to LTCC-mediated Ca^{2+} -influx than $K_{(Ca)}2.x$ -channels indicated by the lack of AHPs after short current injections (< 500 ms). The assumption of faster I_{fADP} - than $I_{K(Ca)2.x}$ -kinetics is supported by a publication describing I_{fADP} as a mechanism for delaying $K_{(Ca)}2.x$ -mediated spike-frequency adaptation by activating faster than $I_{K(Ca)2.x}$ [Haj-Dahmane and Andrade 1997]. Furthermore, (II) long-lasting depolarizations (> 2 s) substantially favor the hyperpolarizing afterpotential modality (fig. 21.1). Since the time range, where the excitatory coupling reverses into the inhibitory one (500 ms to 2 s, fig. 21.1), corresponds to the duration of physiological depolarizations (e.g. bursts or upstate potentials), I suggest that the coupling efficiency provides a possible mechanism for fine-tuning hippocampal firing (will be further discussed in the following chapter). This would concern a CAN-mediated enhanced integration of short subthreshold potentials, such as in LTCC-dependent and NMDA-independent hippocampal LTP [Moosmang et al. 2005], as well as the protection against long-lasting excitotoxic LTCC-mediated plateau potential. In accordance with the latter assumption, the up-regulation of I_{CAN} is discussed in terms of Parkinson's disease [Lee and Tepper 2007].

What is the mediator between the stimulus intensity and the difference in coupling efficiency? In order to address this question, I performed experiments with enhanced [BayK] and augmented Ca^{2+} -driving forces. As the AHP-area correlated with [BayK] (fig. 21.3) as well as with the Ca^{2+} -driving force [Geier et al. unpublished], I assume that differences in the efficiency of LTCC-coupling could be caused by varieties in molecular proximities, as reported for BK- and

SK-channels [Fakler and Adelman 2008] as well as by varieties in signaling cascades, e.g. concerning CICR, which was described to be involved in the sAHP-formation in hippocampal neurons [Tanabe et al. 1998]. Alternatively, varieties in Ca^{2+} -affinities could provide the basis for different coupling efficiencies too. However, for TRPM4- [Launay et al. 2002], TRPM5- [Ullrich et al. 2005], $\text{K}_{(\text{Ca})}2.1$ - [Kohler et al. 1996], $\text{K}_{(\text{Ca})}2.2$ - [Kohler et al. 1996] and $\text{K}_{(\text{Ca})}2.3$ -channels [Xia et al. 1998] rather similar Ca^{2+} -affinities ranging between 300 - 650 nM have been reported.

4.3.4. In hippocampal neurons LTCCs predominantly contribute to enhanced discharge activity

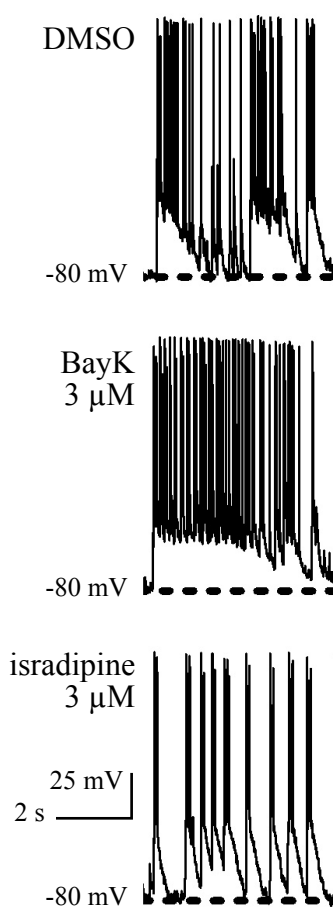


Fig. 25: Control discharge patterns (DMSO) of primary hippocampal neurons mainly consist of depolarizations with $t < 1$ s. For such a pulse duration the coupling model (fig. 21) predicts a predominance of the LTCC/CAN-coupling. This was confirmed as 80 % of the tested neurons responded with an increased excitation after enhancement of I_{LTCC} (BayK).

Regarding the described population of hippocampal neurons ($N = 31$), the investigation of their discharge activity in current clamp experiments revealed that in 80 % of the neurons LTCC-activation induced enhanced firing (fig. 22 - 24, tab 4, 5), which is in agreement with the repeatedly reported pro-epileptic [Sayer et al. 1993; Semyanov et al. 1997; Beck et al. 1998; Hassan et al. 1999] and rare appearance of the anti-epileptic role of LTCCs [Fragoso-Veloz et al. 1990; Yamada et al. 1991; Wielosz et al. 1995; van Luijtelaaar et al. 2000].

Since hippocampal discharge patterns mainly consist of rather short-lasting (< 1 s) depolarizations under control (fig. 25 DMSO), the LTCC-CAN-coupling is favored under these conditions (fig. 21.1). Therefore, if BayK is applied onto these cells, CAN-channels get further activated, which hence cause the prolongation of the depolarizing events (enhanced firing activity with BayK, fig. 25 BayK). This is in contrast to discharge patterns already displaying long-lasting depolarizations under control conditions, where the LTCC-SK-coupling is assumed to be predominant (fig. 21.1). Thus, I propose that under physiological conditions the depolarization-induced negative feed-back mechanism of the LTCC-SK-coupling limits the duration of depolarizations in order to prevent the neuron from excitotoxic Ca^{2+} -overloads. To sum up, I consider a certain balance between de- and hyperpolarizing LTCC-couplings as one of the pivotal points of excitation control in hippocampal neurons.

5. BIBLIOGRAPHY

- Aczel S, Kurka B, Hering S (1998) Mechanism of voltage- and use-dependent block of class A Ca²⁺ channels by mibefradil. *Br J Pharmacol* 125:447-454.
- Aktories K, Förstermann, U., Hofmann, F., B., Starke, K. (2009) *Allgemeine und spezielle Pharmakologie und Toxikologie*. München: Elsevier GmbH.
- Alberts B, Johnson, A., Lewis, J., Raff, M., Roberts., K., Walter, P. (2002) *Molecular Biology of the Cell*. New York: Garland Science.
- Alexander SP, Mathie A, Peters JA (2007) *Guide to Receptors and Channels (GRAC)*, 2nd edition (2007 Revision). *Br J Pharmacol* 150 Suppl 1:160-168.
- Allen D, Fakler B, Maylie J, Adelman JP (2007) Organization and regulation of small conductance Ca²⁺-activated K⁺ channel multiprotein complexes. *J Neurosci* 27:2369-2376.
- Armstrong C, M., Chow, R., H. (1987) Supercharging: A method for improving patch-clamp performance. *Biophys J* 52:133-136.
- Armstrong C, M, Gilly, W., F (1992) Access resistance and space-clamp problems associated with whole cell patch clamping. *Methods in Enzymology* 207.
- Barg S, Ma X, Eliasson L, Galvanovskis J, Gopel SO, Obermuller S, Platzer J, Renstrom E, Trus M, Atlas D, Striessnig J, Rorsman P (2001) Fast exocytosis with few Ca²⁺ channels in insulin-secreting mouse pancreatic B cells. *Biophys J* 81:3308-3323.
- Bhattacharjee A, Kaczmarek LK (2005) For K⁺ channels, Na⁺ is the new Ca²⁺. *Trends Neurosci* 28:422-428.
- Beck H, Steffens R, Elger CE, Heinemann U (1998) Voltage-dependent Ca²⁺ currents in epilepsy. *Epilepsy Res* 32:321-332.
- Ben-Ari Y (2002) Excitatory actions of gaba during development: the nature of the nurture. *Nat Rev Neurosci* 3:728-739.
- Ben-Ari Y (2006) Basic developmental rules and their implications for epilepsy in the immature brain. *Epileptic Disord* 8:91-102.
- Bentzen BH, Nardi A, Calloe K, Madsen LS, Olesen SP, Grunnet M (2007) The small molecule NS11021 is a potent and specific activator of Ca²⁺-activated big-conductance K⁺ channels. *Mol Pharmacol* 72:1033-1044.
- Berkefeld H, Fakler B (2008) Repolarizing responses of BKCa-Cav complexes are distinctly shaped by their Cav subunits. *J Neurosci* 28:8238-8245.

- Berkefeld H, Sailer CA, Bildl W, Rohde V, Thumfart JO, Eble S, Klugbauer N, Reisinger E, Bischofberger J, Oliver D, Knaus HG, Schulte U, Fakler B (2006) BKCa-Cav channel complexes mediate rapid and localized Ca²⁺-activated K⁺ signaling. *Science* 314:615-620.
- Biel M, Hullin R, Freundner S, Singer D, Dascal N, Flockerzi V, Hofmann F (1991) Tissue-specific expression of high-voltage-activated dihydropyridine-sensitive L-type calcium channels. *Eur J Biochem* 200:81-88.
- Birnbaumer L, Campbell KP, Catterall WA, Harpold MM, Hofmann F, Horne WA, Mori Y, Schwartz A, Snutch TP, Tanabe T, et al. (1994) The naming of voltage-gated calcium channels. *Neuron* 13:505-506.
- Bodi I, Yamaguchi H, Hara M, He M, Schwartz A, Varadi G (1997) Molecular studies on the voltage dependence of dihydropyridine action on L-type Ca²⁺ channels. Critical involvement of tyrosine residues in motif IIS6 and IVS6. *J Biol Chem* 272:24952-24960.
- Boehm S (1998) Selective inhibition of M-type potassium channels in rat sympathetic neurons by uridine nucleotide preferring receptors. *Br J Pharmacol* 124:1261-1269.
- Bond CT, Herson PS, Strassmaier T, Hammond R, Stackman R, Maylie J, Adelman JP (2004) Small conductance Ca²⁺-activated K⁺ channel knock-out mice reveal the identity of calcium-dependent afterhyperpolarization currents. *J Neurosci* 24:5301-5306.
- Bosse E, Regulla S, Biel M, Ruth P, Meyer HE, Flockerzi V, Hofmann F (1990) The cDNA and deduced amino acid sequence of the gamma subunit of the L-type calcium channel from rabbit skeletal muscle. *FEBS Lett* 267:153-156.
- Bourinet E, Mangoni ME, Nargeot J (2004) Dissecting the functional role of different isoforms of the L-type Ca²⁺ channel. *J Clin Invest* 113:1382-1384.
- Bourinet E, Soong TW, Sutton K, Slaymaker S, Mathews E, Monteil A, Zamponi GW, Nargeot J, Snutch TP (1999) Splicing of alpha 1A subunit gene generates phenotypic variants of P- and Q-type calcium channels. *Nat Neurosci* 2:407-415.
- Bowden SE, Fletcher S, Loane DJ, Marrion NV (2001) Somatic colocalization of rat SK1 and D class (Ca_v1.2) L-type calcium channels in rat CA1 hippocampal pyramidal neurons. *J Neurosci* 21:RC175.
- Bretschneider F, De Weille, J., R. (2006) *Electrophysiological Methods and Instrumentation*: Elsevier Ltd.
- Brown JP, Gee NS (1998) Cloning and deletion mutagenesis of the alpha2 delta calcium channel subunit from porcine cerebral cortex. Expression of a soluble form of the protein that retains [3H]gabapentin binding activity. *J Biol Chem* 273:25458-25465.
- Brown JP, Dissanayake VU, Briggs AR, Milic MR, Gee NS (1998) Isolation of the [3H]gabapentin-binding protein/alpha 2 delta Ca²⁺ channel subunit from porcine brain: development of a radioligand binding assay for alpha 2 delta subunits using [3H]leucine. *Anal Biochem* 255:236-243.
- Brown T, A. (1999) *Moderne Genetik*. Heidelberg, Berlin: Spektrum Akademischer Verlag GmbH.
- Burgess DL, Gefrides LA, Foreman PJ, Noebels JL (2001) A cluster of three novel Ca²⁺ channel gamma subunit genes on chromosome 19q13.4: evolution and expression profile of the gamma subunit gene family. *Genomics* 71:339-350.
- Büttner W, E. (2004) *Grundlagen der Elektrotechnik 1*: Oldenburg Wissenschaftsverlag GmbH.
- Byerly L, Hagiwara, S., ed (1988) *Calcium channel diversity*. New York.
- Campbell N, A., Reece, J., B. (2003) *Biologie*. Heidelberg, Berlin: Spektrum Akademischer Verlag GmbH.

- Castellano A, Wei X, Birnbaumer L, Perez-Reyes E (1993a) Cloning and expression of a third calcium channel beta subunit. *J Biol Chem* 268:3450-3455.
- Castellano A, Wei X, Birnbaumer L, Perez-Reyes E (1993b) Cloning and expression of a neuronal calcium channel beta subunit. *J Biol Chem* 268:12359-12366.
- Catterall WA (2000) Structure and regulation of voltage-gated Ca²⁺ channels. *Annu Rev Cell Dev Biol* 16:521-555.
- Cavalié A, Ochi R, Pelzer D, Trautwein W (1983) Elementary currents through Ca²⁺ channels in guinea pig myocytes. *Pflügers Arch* 398:284-297.
- Cens T, Restituito S, Galas S, Charney P (1999) Voltage and calcium use the same molecular determinants to inactivate calcium channels. *J Biol Chem* 274:5483-5490.
- Cha A, Snyder GE, Selvin PR, Bezanilla F (1999) Atomic scale movement of the voltage-sensing region in a potassium channel measured via spectroscopy. *Nature* 402:809-813.
- Chad JE, Eckert R (1986) An enzymatic mechanism for calcium current inactivation in dialysed Helix neurones. *J Physiol* 378:31-51.
- Chavis P, Ango F, Michel JM, Bockaert J, Fagni L (1998) Modulation of big K⁺ channel activity by ryanodine receptors and L-type Ca²⁺ channels in neurons. *Eur J Neurosci* 10:2322-2327.
- Chen L, Chetkovich DM, Petralia RS, Sweeney NT, Kawasaki Y, Wenthold RJ, Brecht DS, Nicoll RA (2000) Stargazin regulates synaptic targeting of AMPA receptors by two distinct mechanisms. *Nature* 408:936-943.
- Chen YH, Li MH, Zhang Y, He LL, Yamada Y, Fitzmaurice A, Shen Y, Zhang H, Tong L, Yang J (2004) Structural basis of the alpha1-beta subunit interaction of voltage-gated Ca²⁺ channels. *Nature* 429:675-680.
- Chin D, Means AR (2000) Calmodulin: a prototypical calcium sensor. *Trends Cell Biol* 10:322-328.
- Clark NC, Nagano N, Kuenzi FM, Jarolimek W, Huber I, Walter D, Wietzorrek G, Boyce S, Kullmann DM, Striessnig J, Seabrook GR (2003) Neurological phenotype and synaptic function in mice lacking the CaV1.3 alpha subunit of neuronal L-type voltage-dependent Ca²⁺ channels. *Neuroscience* 120:435-442.
- Congar P, Leinekugel X, Ben-Ari Y, Crepel V (1997) A long-lasting calcium-activated nonselective cationic current is generated by synaptic stimulation or exogenous activation of group I metabotropic glutamate receptors in CA1 pyramidal neurons. *J Neurosci* 17:5366-5379.
- Cox DH, Dunlap K (1994) Inactivation of N-type calcium current in chick sensory neurons: calcium and voltage dependence. *J Gen Physiol* 104:311-336.
- Davies PJ, Ireland DR, McLachlan EM (1996) Sources of Ca²⁺ for different Ca(2+)-activated K⁺ conductances in neurones of the rat superior cervical ganglion. *J Physiol* 495 (Pt 2):353-366.
- de Falco FA, Bartiromo U, Majello L, Di Geronimo G, Mundo P (1992) Calcium antagonist nimodipine in intractable epilepsy. *Epilepsia* 33:343-345.
- De Waard M, Pragnell M, Campbell KP (1994) Ca²⁺ channel regulation by a conserved beta subunit domain. *Neuron* 13:495-503.
- De Waard M, Gurnett, C.A., Campbell, K.P. (1996) Structural and functional diversity of voltage-gated calcium channels. New York: Plenum.
- Dilmac N, Hilliard N, Hockerman GH (2003) Molecular determinants of Ca²⁺ potentiation of diltiazem block and Ca²⁺-dependent inactivation in the pore region of cav1.2. *Mol Pharmacol* 64:491-501.

- Dilmac N, Hilliard N, Hockerman GH (2004) Molecular determinants of frequency dependence and Ca²⁺ potentiation of verapamil block in the pore region of Cav1.2. *Mol Pharmacol* 66:1236-1247.
- Ebihara S, Shirato, K., Harata, N., Akaike, N. (1995) Gramicidin-perforated patch recording: GABA response in mammalian neurones with intact intracellular chloride. *J Physiol* 484:77-86.
- Eckert E, Randall, D., Burggren, W., French, K., Apfelbach, R. (2002) *Tierphysiologie*: Georg Thieme Verlag.
- Ellis SB, Williams ME, Ways NR, Brenner R, Sharp AH, Leung AT, Campbell KP, McKenna E, Koch WJ, Hui A, et al. (1988) Sequence and expression of mRNAs encoding the alpha 1 and alpha 2 subunits of a DHP-sensitive calcium channel. *Science* 241:1661-1664.
- Ertel EA, Campbell KP, Harpold MM, Hofmann F, Mori Y, Perez-Reyes E, Schwartz A, Snutch TP, Tanabe T, Birnbaumer L, Tsien RW, Catterall WA (2000) Nomenclature of voltage-gated calcium channels. *Neuron* 25:533-535.
- Faber ES, Callister RJ, Sah P (2001) Morphological and electrophysiological properties of principal neurons in the rat lateral amygdala in vitro. *J Neurophysiol* 85:714-723.
- Fakler B, Adelman JP (2008) Control of K(Ca) channels by calcium nano/microdomains. *Neuron* 59:873-881.
- Fatt P, Katz B (1953) The electrical properties of crustacean muscle fibres. *J Physiol* 120:171-204.
- Felix R, Gurnett CA, De Waard M, Campbell KP (1997) Dissection of functional domains of the voltage-dependent Ca²⁺ channel alpha2delta subunit. *J Neurosci* 17:6884-6891.
- Fenwick EM, Marty A, Neher E (1982) Sodium and calcium channels in bovine chromaffin cells. *J Physiol* 331:599-635.
- Ferreira G, Yi J, Rios E, Shirokov R (1997) Ion-dependent inactivation of barium current through L-type calcium channels. *J Gen Physiol* 109:449-461.
- Fox AP, Nowycky MC, Tsien RW (1987) Kinetic and pharmacological properties distinguishing three types of calcium currents in chick sensory neurones. *J Physiol* 394:149-172.
- Fragoso-Veloz J, Massieu L, Alvarado R, Tapia R (1990) Seizures and wet-dog shakes induced by 4-aminopyridine, and their potentiation by nifedipine. *Eur J Pharmacol* 178:275-284.
- Frankenhaeuser B, Hodgkin AL (1957) The action of calcium on the electrical properties of squid axons. *J Physiol* 137:218-244.
- Galvez A, Gimenez-Gallego G, Reuben JP, Roy-Contancin L, Feigenbaum P, Kaczorowski GJ, Garcia ML (1990) Purification and characterization of a unique, potent, peptidyl probe for the high conductance calcium-activated potassium channel from venom of the scorpion *Buthus tamulus*. *J Biol Chem* 265:11083-11090.
- Ganitkevich V, Shuba MF, Smirnov SV (1986) Potential-dependent calcium inward current in a single isolated smooth muscle cell of the guinea-pig taenia caeci. *J Physiol* 380:1-16.
- Gao L, Blair LA, Salinas GD, Needleman LA, Marshall J (2006) Insulin-like growth factor-1 modulation of CaV1.3 calcium channels depends on Ca²⁺ release from IP₃-sensitive stores and calcium/calmodulin kinase II phosphorylation of the alpha1 subunit EF hand. *J Neurosci* 26:6259-6268.
- Garcia R, Carrillo E, Rebolledo S, Garcia MC, Sanchez JA (2002) The beta1a subunit regulates the functional properties of adult frog and mouse L-type Ca²⁺ channels of skeletal muscle. *J Physiol* 545:407-419.
- Gardos G (1958) The function of calcium in the potassium permeability of human erythrocytes. *Biochim Biophys Acta* 30:653-654.

- Gee NS, Brown JP, Dissanayake VU, Offord J, Thurlow R, Woodruff GN (1996) The novel anticonvulsant drug, gabapentin (Neurontin), binds to the alpha2delta subunit of a calcium channel. *J Biol Chem* 271:5768-5776.
- Ghamari-Langroudi M, Bourque CW (2002) Flufenamic acid blocks depolarizing afterpotentials and phasic firing in rat supraoptic neurones. *J Physiol* 545:537-542.
- Glauner KS, Mannuzzu LM, Gandhi CS, Isacoff EY (1999) Spectroscopic mapping of voltage sensor movement in the Shaker potassium channel. *Nature* 402:813-817.
- Glossmann H, Striessnig J (1990) Molecular properties of calcium channels. *Rev Physiol Biochem Pharmacol* 114:1-105.
- Grunnet M, Kaufmann WA (2004) Coassembly of big conductance Ca²⁺-activated K⁺ channels and L-type voltage-gated Ca²⁺ channels in rat brain. *J Biol Chem* 279:36445-36453.
- Gu N, Vervaeke K, Hu H, Storm JF (2005) Kv7/KCNQ/M and HCN/h, but not KCa2/SK channels, contribute to the somatic medium after-hyperpolarization and excitability control in CA1 hippocampal pyramidal cells. *J Physiol* 566:689-715.
- Guinamard R, Rahmati M, Lenfant J, Bois P (2002) Characterization of a Ca²⁺-activated nonselective cation channel during dedifferentiation of cultured rat ventricular cardiomyocytes. *J Membr Biol* 188:127-135.
- Guinamard R, Demion M, Magaud C, Potreau D, Bois P (2006) Functional expression of the TRPM4 cationic current in ventricular cardiomyocytes from spontaneously hypertensive rats. *Hypertension* 48:587-594.
- Hagiwara S (1983) Membrane Potential-Dependent Ion Channels in Cell Membrane. Phylogenetic and Developmental Approaches. New York: Raven Press.
- Hagiwara S, Takahashi K (1967) Surface density of calcium ions and calcium spikes in the barnacle muscle fiber membrane. *J Gen Physiol* 50:583-601.
- Hagiwara S, Ozawa S, Sand O (1975) Voltage clamp analysis of two inward current mechanisms in the egg cell membrane of a starfish. *J Gen Physiol* 65:617-644.
- Haj-Dahmane S, Andrade R (1997) Calcium-activated cation nonselective current contributes to the fast afterdepolarization in rat prefrontal cortex neurons. *J Neurophysiol* 78:1983-1989.
- Hassan H, Grecksch G, Ruthrich H, Krug M (1999) Effects of nicardipine, an antagonist of L-type voltage-dependent calcium channels, on kindling development, kindling-induced learning deficits and hippocampal potentiation phenomena. *Neuropharmacology* 38:1841-1850.
- Hayashida S, Katsura M, Torigoe F, Tsujimura A, Ohkuma S (2005) Increased expression of L-type high voltage-gated calcium channel alpha1 and alpha2/delta subunits in mouse brain after chronic nicotine administration. *Brain Res Mol Brain Res* 135:280-284.
- He M, Bodi I, Mikala G, Schwartz A (1997) Motif III S5 of L-type calcium channels is involved in the dihydropyridine binding site. A combined radioligand binding and electrophysiological study. *J Biol Chem* 272:2629-2633.
- Heinemann SH, Terlau H, Stuhmer W, Imoto K, Numa S (1992) Calcium channel characteristics conferred on the sodium channel by single mutations. *Nature* 356:441-443.
- Hell JW, Westenbroek RE, Warner C, Ahljianian MK, Prystay W, Gilbert MM, Snutch TP, Catterall WA (1993) Identification and differential subcellular localization of the neuronal class C and class D L-type calcium channel alpha 1 subunits. *J Cell Biol* 123:949-962.
- Helton TD, Xu W, Lipscombe D (2005) Neuronal L-type calcium channels open quickly and are inhibited slowly. *J Neurosci* 25:10247-10251.
- Hering S (2002) beta-Subunits: fine tuning of Ca(2+) channel block. *Trends Pharmacol Sci* 23:509-513.

- Herrington J, Lingle CJ (1992) Kinetic and pharmacological properties of low voltage-activated Ca^{2+} current in rat clonal (GH3) pituitary cells. *J Neurophysiol* 68:213-232.
- Hescheler J, Pelzer D, Trube G, Trautwein W (1982) Does the organic calcium channel blocker D600 act from inside or outside on the cardiac cell membrane? *Pflugers Arch* 393:287-291.
- Hess P, Lansman JB, Tsien RW (1984) Different modes of Ca channel gating behaviour favoured by dihydropyridine Ca agonists and antagonists. *Nature* 311:538-544.
- Hibino H, Pironkova R, Onwumere O, Rousset M, Charnet P, Hudspeth AJ, Lesage F (2003) Direct interaction with a nuclear protein and regulation of gene silencing by a variant of the Ca^{2+} -channel beta 4 subunit. *Proc Natl Acad Sci U S A* 100:307-312.
- Higashi H, Tanaka E, Inokuchi H, Nishi S (1993) Ionic mechanisms underlying the depolarizing and hyperpolarizing afterpotentials of single spike in guinea-pig cingulate cortical neurons. *Neuroscience* 55:129-138.
- Hille B (2001) *Ion Channels of Excitable Membranes*. Sunderland, MA, USA: Sinauer Associates, Inc.
- Hobom M, Dai S, Marais E, Lacinova L, Hofmann F, Klugbauer N (2000) Neuronal distribution and functional characterization of the calcium channel alpha2delta-2 subunit. *Eur J Neurosci* 12:1217-1226.
- Hodgkin AL, Huxley AF (1952) Currents carried by sodium and potassium ions through the membrane of the giant axon of *Loligo*. *J Physiol* 116:449-472.
- Hofmann T, Chubanov V, Gudermann T, Montell C (2003) TRPM5 is a voltage-modulated and Ca^{2+} -activated monovalent selective cation channel. *Curr Biol* 13:1153-1158.
- Horn R, Marty, A. (1988) Muscarinic activation of ionic currents measured by a new whole-cell recording method. *J Gen Physiol* 92:145-159.
- Horvath H (1999) *Biologische Physik*. Wien: Hölder-Pichler-Tempsky Verlag.
- Hullin R, Singer-Lahat D, Freichel M, Biel M, Dascal N, Hofmann F, Flockerzi V (1992) Calcium channel beta subunit heterogeneity: functional expression of cloned cDNA from heart, aorta and brain. *Embo J* 11:885-890.
- Ishii TM, Silvia C, Hirschberg B, Bond CT, Adelman JP, Maylie J (1997) A human intermediate conductance calcium-activated potassium channel. *Proc Natl Acad Sci U S A* 94:11651-11656.
- Ito H, Klugbauer N, Hofmann F (1997) Transfer of the high affinity dihydropyridine sensitivity from L-type to non-L-type calcium channel. *Mol Pharmacol* 52:735-740.
- Jacobo SM, Guerra ML, Hockerman GH (2009) Cav1.2 and Cav1.3 are differentially coupled to glucagon-like peptide-1 potentiation of glucose-stimulated insulin secretion in the pancreatic beta-cell line INS-1. *J Pharmacol Exp Ther* 331:724-732.
- Johnson BD, Byerly L (1994) Ca^{2+} channel Ca^{2+} -dependent inactivation in a mammalian central neuron involves the cytoskeleton. *Pflugers Arch* 429:14-21.
- Johnson BD, Hockerman GH, Scheuer T, Catterall WA (1996) Distinct effects of mutations in transmembrane segment IVS6 on block of L-type calcium channels by structurally similar phenylalkylamines. *Mol Pharmacol* 50:1388-1400.
- Jouveneau A, Giovannini F, Bath CP, Trotman E, Sher E (2000) Inactivation properties of human recombinant class E calcium channels. *J Neurophysiol* 83:671-684.
- Kamp TJ, Perez-Garcia MT, Marban E (1996) Enhancement of ionic current and charge movement by coexpression of calcium channel beta 1A subunit with alpha 1C subunit in a human embryonic kidney cell line. *J Physiol* 492 (Pt 1):89-96.
- Kandel E, R., Schwartz, J., H., Jesell T., M. (1996) *Neurowissenschaften. Eine Einführung.:* Spektrum Akademischer Verlag GmbH.

- Kang MG, Chen CC, Felix R, Letts VA, Frankel WN, Mori Y, Campbell KP (2001) Biochemical and biophysical evidence for gamma 2 subunit association with neuronal voltage-activated Ca²⁺ channels. *J Biol Chem* 276:32917-32924.
- Karnup S, Stelzer A (2001) Seizure-like activity in the disinhibited CA1 minislice of adult guinea-pigs. *J Physiol* 532:713-730.
- Kato M, Tanaka N, Usui S, Sakuma Y (2006) The SK channel blocker apamin inhibits slow afterhyperpolarization currents in rat gonadotropin-releasing hormone neurones. *J Physiol* 574:431-442.
- Kavalali ET, Plummer MR (1994) Selective potentiation of a novel calcium channel in rat hippocampal neurones. *J Physiol* 480 (Pt 3):475-484.
- Keen JE, Khawaled R, Farrens DL, Neelands T, Rivard A, Bond CT, Janowsky A, Fakler B, Adelman JP, Maylie J (1999) Domains responsible for constitutive and Ca(2+)-dependent interactions between calmodulin and small conductance Ca(2+)-activated potassium channels. *J Neurosci* 19:8830-8838.
- Kepplinger KJ, Forstner G, Kahr H, Leitner K, Pammer P, Groschner K, Soldatov NM, Romanin C (2000) Molecular determinant for run-down of L-type Ca²⁺ channels localized in the carboxyl terminus of the 1C subunit. *J Physiol* 529 Pt 1:119-130.
- Kim S, Yun HM, Baik JH, Chung KC, Nah SY, Rhim H (2007) Functional interaction of neuronal Cav1.3 L-type calcium channel with ryanodine receptor type 2 in the rat hippocampus. *J Biol Chem* 282:32877-32889.
- Klugbauer N, Lacinova L, Marais E, Hobom M, Hofmann F (1999) Molecular diversity of the calcium channel alpha2delta subunit. *J Neurosci* 19:684-691.
- Klugbauer N, Dai S, Specht V, Lacinova L, Marais E, Bohn G, Hofmann F (2000) A family of gamma-like calcium channel subunits. *FEBS Lett* 470:189-197.
- Kohler M, Hirschberg B, Bond CT, Kinzie JM, Marrion NV, Maylie J, Adelman JP (1996) Small-conductance, calcium-activated potassium channels from mammalian brain. *Science* 273:1709-1714.
- Koschak A, Obermair GJ, Pivotto F, Sinnegger-Brauns MJ, Striessnig J, Pietrobon D (2007) Molecular nature of anomalous L-type calcium channels in mouse cerebellar granule cells. *J Neurosci* 27:3855-3863.
- Koschak A, Reimer D, Huber I, Grabner M, Glossmann H, Engel J, Striessnig J (2001) alpha 1D (Cav1.3) subunits can form l-type Ca²⁺ channels activating at negative voltages. *J Biol Chem* 276:22100-22106.
- Kurokawa J, Adachi-Akahane S, Nagao T (1997) 1,5-benzothiazepine binding domain is located on the extracellular side of the cardiac L-type Ca²⁺ channel. *Mol Pharmacol* 51:262-268.
- Kyrozis A, Reichling D, B. (1995) Perforated patch recording with gramicidin avoids artifactual changes in the intracellular chloride concentration. *J Neurosci Meth* 57:27-35.
- Lacinova L, Hofmann F (2005) Ca²⁺- and voltage-dependent inactivation of the expressed L-type Ca(v)1.2 calcium channel. *Arch Biochem Biophys* 437:42-50.
- Lacinova L, Klugbauer N, Hofmann F (2000) Low voltage activated calcium channels: from genes to function. *Gen Physiol Biophys* 19:121-136.
- Lacinova L, Ludwig A, Bosse E, Flockerzi V, Hofmann F (1995) The block of the expressed L-type calcium channel is modulated by the beta 3 subunit. *FEBS Lett* 373:103-107.
- Lacinova L, Moosmang S, Langwieser N, Hofmann F, Kleppisch T (2008) Cav1.2 calcium channels modulate the spiking pattern of hippocampal pyramidal cells. *Life Sci* 82:41-49.

- Lammel S, Hetzel, A., Haeckel, O., Jones, I., Liss B., Roeper J. (2008) Unique Properties of Mesoprefrontal Neurons within a Dual Mesocorticolimbic Dopamine System. *Neuron* 57:760–773.
- Lancaster B, Nicoll RA (1987) Properties of two calcium-activated hyperpolarizations in rat hippocampal neurones. *J Physiol* 389:187-203.
- Launay P, Fleig A, Perraud AL, Scharenberg AM, Penner R, Kinet JP (2002) TRPM4 is a Ca²⁺-activated nonselective cation channel mediating cell membrane depolarization. *Cell* 109:397-407.
- Lee A, Scheuer T, Catterall WA (2000) Ca²⁺/calmodulin-dependent facilitation and inactivation of P/Q-type Ca²⁺ channels. *J Neurosci* 20:6830-6838.
- Lee A, Wong ST, Gallagher D, Li B, Storm DR, Scheuer T, Catterall WA (1999) Ca²⁺/calmodulin binds to and modulates P/Q-type calcium channels. *Nature* 399:155-159.
- Lee CR, Tepper JM (2007) A calcium-activated nonselective cation conductance underlies the plateau potential in rat substantia nigra GABAergic neurons. *J Neurosci* 27:6531-6541.
- Lee KS, Tsien RW (1984) High selectivity of calcium channels in single dialysed heart cells of the guinea-pig. *J Physiol* 354:253-272.
- Letts VA, Felix R, Biddlecome GH, Arikath J, Mahaffey CL, Valenzuela A, Bartlett FS, 2nd, Mori Y, Campbell KP, Frankel WN (1998) The mouse stargazer gene encodes a neuronal Ca²⁺-channel gamma subunit. *Nat Genet* 19:340-347.
- Liao P, Yu D, Lu S, Tang Z, Liang MC, Zeng S, Lin W, Soong TW (2004) Smooth muscle-selective alternatively spliced exon generates functional variation in Cav1.2 calcium channels. *J Biol Chem* 279:50329-50335.
- Lima PA, Marrion NV (2007) Mechanisms underlying activation of the slow AHP in rat hippocampal neurons. *Brain Res* 1150:74-82.
- Lipscombe D, Helton TD, Xu W (2004) L-type calcium channels: the low down. *J Neurophysiol* 92:2633-2641.
- Liu G, Dilmac N, Hilliard N, Hockerman GH (2003) Ca^v 1.3 is preferentially coupled to glucose-stimulated insulin secretion in the pancreatic beta-cell line INS-1. *J Pharmacol Exp Ther* 305:271-278.
- Llinas R, Yarom Y (1981) Electrophysiology of mammalian inferior olivary neurones in vitro. Different types of voltage-dependent ionic conductances. *J Physiol* 315:549-567.
- Llinas R, Sugimori M, Lin JW, Cherksey B (1989) Blocking and isolation of a calcium channel from neurons in mammals and cephalopods utilizing a toxin fraction (FTX) from funnel-web spider poison. *Proc Natl Acad Sci U S A* 86:1689-1693.
- Loane DJ, Lima PA, Marrion NV (2007) Co-assembly of N-type Ca²⁺ and BK channels underlies functional coupling in rat brain. *J Cell Sci* 120:985-995.
- Logothetis DE, Movahedi S, Satler C, Lindpaintner K, Nadal-Ginard B (1992) Incremental reductions of positive charge within the S4 region of a voltage-gated K⁺ channel result in corresponding decreases in gating charge. *Neuron* 8:531-540.
- Ludwig A, Flockerzi V, Hofmann F (1997) Regional expression and cellular localization of the alpha1 and beta subunit of high voltage-activated calcium channels in rat brain. *J Neurosci* 17:1339-1349.
- Marais E, Klugbauer N, Hofmann F (2001) Calcium channel alpha(2)delta subunits-structure and Gabapentin binding. *Mol Pharmacol* 59:1243-1248.
- Marrion NV, Tavalin SJ (1998) Selective activation of Ca²⁺-activated K⁺ channels by co-localized Ca²⁺ channels in hippocampal neurons. *Nature* 395:900-905.

- Masaki H, Sato Y, Luo W, Kranias EG, Yatani A (1997) Phospholamban deficiency alters inactivation kinetics of L-type Ca²⁺ channels in mouse ventricular myocytes. *Am J Physiol* 272:H606-612.
- McKinney BC, Sze W, Lee B, Murphy GG (2009) Impaired long-term potentiation and enhanced neuronal excitability in the amygdala of Ca(V)1.3 knockout mice. *Neurobiol Learn Mem* 92:519-528.
- McManus OB, Harris GH, Giangiacomo KM, Feigenbaum P, Reuben JP, Addy ME, Burka JF, Kaczorowski GJ, Garcia ML (1993) An activator of calcium-dependent potassium channels isolated from a medicinal herb. *Biochemistry* 32:6128-6133.
- Mitarai S, Kaibara M, Yano K, Taniyama K (2000) Two distinct inactivation processes related to phosphorylation in cardiac L-type Ca(2+) channel currents. *Am J Physiol Cell Physiol* 279:C603-610.
- Mitterdorfer J, Froschmayr M, Grabner M, Striessnig J, Glossmann H (1994) Calcium channels: the beta-subunit increases the affinity of dihydropyridine and Ca²⁺ binding sites of the alpha 1-subunit. *FEBS Lett* 352:141-145.
- Moosmang S, Haider N, Klugbauer N, Adelsberger H, Langwieser N, Muller J, Stiess M, Marais E, Schulla V, Lacinova L, Goebbels S, Nave KA, Storm DR, Hofmann F, Kleppisch T (2005) Role of hippocampal Cav1.2 Ca²⁺ channels in NMDA receptor-independent synaptic plasticity and spatial memory. *J Neurosci* 25:9883-9892.
- Mould J, Yasuda T, Schroeder CI, Beedle AM, Doering CJ, Zamponi GW, Adams DJ, Lewis RJ (2004) The alpha2delta auxiliary subunit reduces affinity of omega-conotoxins for recombinant N-type (Cav2.2) calcium channels. *J Biol Chem* 279:34705-34714.
- Moyer JR, Jr., Thompson LT, Black JP, Disterhoft JF (1992) Nimodipine increases excitability of rabbit CA1 pyramidal neurons in an age- and concentration-dependent manner. *J Neurophysiol* 68:2100-2109.
- Namkung Y, Skrypnik N, Jeong MJ, Lee T, Lee MS, Kim HL, Chin H, Suh PG, Kim SS, Shin HS (2001) Requirement for the L-type Ca(2+) channel alpha(1D) subunit in postnatal pancreatic beta cell generation. *J Clin Invest* 108:1015-1022.
- Neher E (1992) Correction of liquid junction potentials in patch-clamp experiments. In: *Methods in Enzymology*.
- Neher E (1998) Vesicle pools and Ca²⁺ microdomains: new tools for understanding their roles in neurotransmitter release. *Neuron* 20:389-399.
- Neher E, Sakmann, B. (1995) *Single-Channel Recording*. New York: Plenum.
- Nicoll RA (1988) The coupling of neurotransmitter receptors to ion channels in the brain. *Science* 241:545-551.
- Nilius B, Prenen J, Voets T, Droogmans G (2004) Intracellular nucleotides and polyamines inhibit the Ca²⁺-activated cation channel TRPM4b. *Pflugers Arch* 448:70-75.
- Nilius B, Prenen J, Tang J, Wang C, Owsianik G, Janssens A, Voets T, Zhu MX (2005) Regulation of the Ca²⁺ sensitivity of the nonselective cation channel TRPM4. *J Biol Chem* 280:6423-6433.
- Nowycky MC, Fox AP, Tsien RW (1985) Three types of neuronal calcium channel with different calcium agonist sensitivity. *Nature* 316:440-443.
- Numberger M, Draguhn, A. (1996) *Patch-clamp-technik*: Spektrum Akademischer Verlag GmbH.
- Obermair GJ, Kaufmann WA, Knaus HG, Flucher BE (2003) The small conductance Ca²⁺-activated K⁺ channel SK3 is localized in nerve terminals of excitatory synapses of cultured mouse hippocampal neurons. *Eur J Neurosci* 17:721-731.

- Obermair GJ, Szabo Z, Bourinet E, Flucher BE (2004) Differential targeting of the L-type Ca²⁺ channel alpha 1C (CaV1.2) to synaptic and extrasynaptic compartments in hippocampal neurons. *Eur J Neurosci* 19:2109-2122.
- Partridge LD, Valenzuela CF (1999) Ca²⁺ store-dependent potentiation of Ca²⁺-activated non-selective cation channels in rat hippocampal neurones in vitro. *J Physiol* 521 Pt 3:617-627.
- Partridge LD, Valenzuela CF (2000) Block of hippocampal CAN channels by flufenamate. *Brain Res* 867:143-148.
- Pedarzani P, Stocker M (2008) Molecular and cellular basis of small- and intermediate-conductance, calcium-activated potassium channel function in the brain. *Cell Mol Life Sci* 65:3196-3217.
- Peterson BZ, Catterall WA (1995) Calcium binding in the pore of L-type calcium channels modulates high affinity dihydropyridine binding. *J Biol Chem* 270:18201-18204.
- Peterson BZ, DeMaria CD, Adelman JP, Yue DT (1999) Calmodulin is the Ca²⁺ sensor for Ca²⁺-dependent inactivation of L-type calcium channels. *Neuron* 22:549-558.
- Peterson BZ, Johnson BD, Hockerman GH, Acheson M, Scheuer T, Catterall WA (1997) Analysis of the dihydropyridine receptor site of L-type calcium channels by alanine-scanning mutagenesis. *J Biol Chem* 272:18752-18758.
- Pinato G, Pegoraro S, Iacono G, Ruaro ME, Torre V (2009) Calcium control of gene regulation in rat hippocampal neuronal cultures. *J Cell Physiol* 220:727-747.
- Ping HX, Shepard PD (1999) Blockade of SK-type Ca²⁺-activated K⁺ channels uncovers a Ca²⁺-dependent slow afterdepolarization in nigral dopamine neurons. *J Neurophysiol* 81:977-984.
- Podlogar M, Dietrich D (2006) Firing pattern of rat hippocampal neurons: a perforated patch clamp study. *Brain Res* 1085:95-101.
- Pusch M, Neher, E. (1988) Rates of diffusional exchange between small cells and a measuring patch pipette. *Pflügers Arch* 411:204-211.
- Qin N, Yagel S, Momplaisir ML, Codd EE, D'Andrea MR (2002) Molecular cloning and characterization of the human voltage-gated calcium channel alpha(2)delta-4 subunit. *Mol Pharmacol* 62:485-496.
- Rae J, Cooper, K., Gates, P., Watsky, M. (1991) Low access resistance perforated patch recordings using amphotericin B. *B J Neurosci Meth* 37:15-26.
- Rascol O, Potier B, Lamour Y, Dutar P (1991) Effects of calcium channel agonist and antagonists on calcium-dependent events in CA1 hippocampal neurons. *Fundam Clin Pharmacol* 5:299-317.
- Reuter H, Scholz H (1977) The regulation of the calcium conductance of cardiac muscle by adrenaline. *J Physiol* 264:49-62.
- Richard S, Charnet P, Nerbonne JM (1993) Interconversion between distinct gating pathways of the high threshold calcium channel in rat ventricular myocytes. *J Physiol* 462:197-228.
- Roberts WM (1994) Localization of calcium signals by a mobile calcium buffer in frog saccular hair cells. *J Neurosci* 14:3246-3262.
- Rousset M, Cens T, Restituito S, Barrere C, Black JL, 3rd, McEnery MW, Charnet P (2001) Functional roles of gamma2, gamma3 and gamma4, three new Ca²⁺ channel subunits, in P/Q-type Ca²⁺ channel expressed in *Xenopus* oocytes. *J Physiol* 532:583-593.
- Sachs L (2002) *Angewandte Statistik*: Springer Verlag.
- Sah P, Isaacson JS (1995) Channels underlying the slow afterhyperpolarization in hippocampal pyramidal neurons: neurotransmitters modulate the open probability. *Neuron* 15:435-441.
- Sah P, Faber ES (2002) Channels underlying neuronal calcium-activated potassium currents. *Prog Neurobiol* 66:345-353.

- Salkoff L, Butler A, Ferreira G, Santi C, Wei A (2006) High-conductance potassium channels of the SLO family. *Nat Rev Neurosci* 7:921-931.
- Sanchez M, McManus OB (1996) Paxilline inhibition of the alpha-subunit of the high-conductance calcium-activated potassium channel. *Neuropharmacology* 35:963-968.
- Sayer RJ, Brown AM, Schwindt PC, Crill WE (1993) Calcium currents in acutely isolated human neocortical neurons. *J Neurophysiol* 69:1596-1606.
- Schiller Y (2004) Activation of a calcium-activated cation current during epileptiform discharges and its possible role in sustaining seizure-like events in neocortical slices. *J Neurophysiol* 92:862-872.
- Schreiber M, Salkoff L (1997) A novel calcium-sensing domain in the BK channel. *Biophys J* 73:1355-1363.
- Schulla V, Renstrom E, Feil R, Feil S, Franklin I, Gjinovci A, Jing XJ, Laux D, Lundquist I, Magnuson MA, Obermuller S, Olofsson CS, Salehi A, Wendt A, Klugbauer N, Wollheim CB, Rorsman P, Hofmann F (2003) Impaired insulin secretion and glucose tolerance in beta cell-selective Ca(v)1.2 Ca²⁺ channel null mice. *Embo J* 22:3844-3854.
- Semyanov A, Godukhin O (1997) Kindling-like state in rat hippocampal CA1 slices induced by the repeated short-term extracellular K⁺ increases: the role of L-type Ca(2⁺)-channels. *Neurosci Lett* 223:177-180.
- Shah M, Haylett DG (2000a) The pharmacology of hSK1 Ca²⁺-activated K⁺ channels expressed in mammalian cell lines. *Br J Pharmacol* 129:627-630.
- Shah M, Haylett DG (2000b) Ca(2⁺) channels involved in the generation of the slow afterhyperpolarization in cultured rat hippocampal pyramidal neurons. *J Neurophysiol* 83:2554-2561.
- Shah MM, Miscony Z, Javadzadeh-Tabatabaie M, Ganellin CR, Haylett DG (2001) Clotrimazole analogues: effective blockers of the slow afterhyperpolarization in cultured rat hippocampal pyramidal neurones. *Br J Pharmacol* 132:889-898.
- Shah MM, Javadzadeh-Tabatabaie M, Benton DC, Ganellin CR, Haylett DG (2006) Enhancement of hippocampal pyramidal cell excitability by the novel selective slow-afterhyperpolarization channel blocker 3-(triphenylmethylaminomethyl)pyridine (UCL2077). *Mol Pharmacol* 70:1494-1502.
- Sham JS (1997) Ca²⁺ release-induced inactivation of Ca²⁺ current in rat ventricular myocytes: evidence for local Ca²⁺ signalling. *J Physiol* 500 (Pt 2):285-295.
- Sham JS, Cleemann L, Morad M (1995) Functional coupling of Ca²⁺ channels and ryanodine receptors in cardiac myocytes. *Proc Natl Acad Sci U S A* 92:121-125.
- Shaw T, Lee RJ, Partridge LD (1995) Action of diphenylamine carboxylate derivatives, a family of non-steroidal anti-inflammatory drugs, on [Ca²⁺]_i and Ca(2⁺)-activated channels in neurons. *Neurosci Lett* 190:121-124.
- Sherman-Gold R (1993) *The Axon Guide*: Axon Instruments.
- Shirokov R (1999) Interaction between permeant ions and voltage sensor during inactivation of N-type Ca²⁺ channels. *J Physiol* 518 (Pt 3):697-703.
- Shistik E, Ivanina T, Puri T, Hosey M, Dascal N (1995) Ca²⁺ current enhancement by alpha 2/delta and beta subunits in *Xenopus* oocytes: contribution of changes in channel gating and alpha 1 protein level. *J Physiol* 489 (Pt 1):55-62.
- Shitak R, Sahai AK, Hota D, Chakrabarti A (2007) Evaluation of the modulatory role of nimodipine in seizures induced by kainic acid and pentylenetetrazole in mice. *Methods Find Exp Clin Pharmacol* 29:11-17.
- Singer D, Biel M, Lotan I, Flockerzi V, Hofmann F, Dascal N (1991) The roles of the subunits in the function of the calcium channel. *Science* 253:1553-1557.

- Singh A, Gebhart M, Fritsch R, Sinnegger-Brauns MJ, Poggiani C, Hoda JC, Engel J, Romanin C, Striessnig J, Koschak A (2008) Modulation of voltage- and Ca²⁺-dependent gating of CaV1.3 L-type calcium channels by alternative splicing of a C-terminal regulatory domain. *J Biol Chem* 283:20733-20744.
- Singh A, Hamedinger, D., Hoda, J-C., Gebhart, M., Koschak, A., Romanin, C., Striessnig, J. (2006) C-terminal modulator controls Ca²⁺-dependent gating of Cav1.4 L-type Ca²⁺ channels. *Nat Neurosci* 9.
- Sinnegger-Brauns MJ, Huber IG, Koschak A, Wild C, Obermair GJ, Einzinger U, Hoda JC, Sartori SB, Striessnig J (2009) Expression and 1,4-dihydropyridine-binding properties of brain L-type calcium channel isoforms. *Mol Pharmacol* 75:407-414.
- Sinnegger-Brauns MJ, Hetzenauer A, Huber IG, Renstrom E, Wietzorrek G, Berjukov S, Cavalli M, Walter D, Koschak A, Waldschutz R, Hering S, Bova S, Rorsman P, Pongs O, Singewald N, Striessnig JJ (2004) Isoform-specific regulation of mood behavior and pancreatic beta cell and cardiovascular function by L-type Ca²⁺ channels. *J Clin Invest* 113:1430-1439.
- Snutch TP, Leonard JP, Gilbert MM, Lester HA, Davidson N (1990) Rat brain expresses a heterogeneous family of calcium channels. *Proc Natl Acad Sci U S A* 87:3391-3395.
- Stephens GJ, Page KM, Bogdanov Y, Dolphin AC (2000) The alpha1B Ca²⁺ channel amino terminus contributes determinants for beta subunit-mediated voltage-dependent inactivation properties. *J Physiol* 525 Pt 2:377-390.
- Stotz SC, Barr W, McRory JE, Chen L, Jarvis SE, Zamponi GW (2004) Several structural domains contribute to the regulation of N-type calcium channel inactivation by the beta 3 subunit. *J Biol Chem* 279:3793-3800.
- Striessnig J, Koschak A, Sinnegger-Brauns MJ, Hetzenauer A, Nguyen NK, Busquet P, Pelster G, Singewald N (2006) Role of voltage-gated L-type Ca²⁺ channel isoforms for brain function. *Biochem Soc Trans* 34:903-909.
- Suh-Kim H, Wei X, Birnbaumer L (1996) Subunit composition is a major determinant in high affinity binding of a Ca²⁺ channel blocker. *Mol Pharmacol* 50:1330-1337.
- Sun X, Gu XQ, Haddad GG (2003) Calcium influx via L- and N-type calcium channels activates a transient large-conductance Ca²⁺-activated K⁺ current in mouse neocortical pyramidal neurons. *J Neurosci* 23:3639-3648.
- Takahashi Y, Jeong SY, Ogata K, Goto J, Hashida H, Isahara K, Uchiyama Y, Kanazawa I (2003) Human skeletal muscle calcium channel alpha1S is expressed in the basal ganglia: distinctive expression pattern among L-type Ca²⁺ channels. *Neurosci Res* 45:129-137.
- Tanabe M, Gahwiler BH, Gerber U (1998) L-Type Ca²⁺ channels mediate the slow Ca²⁺-dependent afterhyperpolarization current in rat CA3 pyramidal cells in vitro. *J Neurophysiol* 80:2268-2273.
- Triggle DJ (2003) 1,4-Dihydropyridines as calcium channel ligands and privileged structures. *Cell Mol Neurobiol* 23:293-303.
- Tsien RW, Lipscombe D, Madison DV, Bley KR, Fox AP (1988) Multiple types of neuronal calcium channels and their selective modulation. *Trends Neurosci* 11:431-438.
- Tzingounis AV, Nicoll RA (2008) Contribution of KCNQ2 and KCNQ3 to the medium and slow afterhyperpolarization currents. *Proc Natl Acad Sci U S A* 105:19974-19979.
- Ullrich ND, Voets T, Prenen J, Vennekens R, Talavera K, Droogmans G, Nilius B (2005) Comparison of functional properties of the Ca²⁺-activated cation channels TRPM4 and TRPM5 from mice. *Cell Calcium* 37:267-278.
- Vacher H, Mohapatra DP, Trimmer JS (2008) Localization and targeting of voltage-dependent ion channels in mammalian central neurons. *Physiol Rev* 88:1407-1447.

- Vamos E, Pardutz A, Klivenyi P, Toldi J, Vecsei L (2009) The role of kynurenines in disorders of the central nervous system: Possibilities for neuroprotection. *J Neurol Sci*.
- van Luijtelaar G, Wiaderna D, Elants C, Scheenen W (2000) Opposite effects of T- and L-type Ca(2+) channels blockers in generalized absence epilepsy. *Eur J Pharmacol* 406:381-389.
- Van Petegem F, Clark KA, Chatelain FC, Minor DL, Jr. (2004) Structure of a complex between a voltage-gated calcium channel beta-subunit and an alpha-subunit domain. *Nature* 429:671-675.
- Varadi G, Lory P, Schultz D, Varadi M, Schwartz A (1991) Acceleration of activation and inactivation by the beta subunit of the skeletal muscle calcium channel. *Nature* 352:159-162.
- Vergara C, Latorre R, Marrion NV, Adelman JP (1998) Calcium-activated potassium channels. *Curr Opin Neurobiol* 8:321-329.
- Villalobos C, Shakkottai VG, Chandy KG, Michelhaugh SK, Andrade R (2004) SKCa channels mediate the medium but not the slow calcium-activated afterhyperpolarization in cortical neurons. *J Neurosci* 24:3537-3542.
- Volsen SG, Day NC, McCormack AL, Smith W, Craig PJ, Beattie RE, Smith D, Ince PG, Shaw PJ, Ellis SB, Mayne N, Burnett JP, Gillespie A, Harpold MM (1997) The expression of voltage-dependent calcium channel beta subunits in human cerebellum. *Neuroscience* 80:161-174.
- Watanabe T, Kalasz H, Yabana H, Kuniyasu A, Mershon J, Itagaki K, Vaghy PL, Naito K, Nakayama H, Schwartz A (1993) Azidobutyryl cleftiazem, a new photoactivatable diltiazem analog, labels benzothiazepine binding sites in the alpha 1 subunit of the skeletal muscle calcium channel. *FEBS Lett* 334:261-264.
- Wei X, Pan S, Lang W, Kim H, Schneider T, Perez-Reyes E, Birnbaumer L (1995) Molecular determinants of cardiac Ca²⁺ channel pharmacology. Subunit requirement for the high affinity and allosteric regulation of dihydropyridine binding. *J Biol Chem* 270:27106-27111.
- Wei XY, Perez-Reyes E, Lacerda AE, Schuster G, Brown AM, Birnbaumer L (1991) Heterologous regulation of the cardiac Ca²⁺ channel alpha 1 subunit by skeletal muscle beta and gamma subunits. Implications for the structure of cardiac L-type Ca²⁺ channels. *J Biol Chem* 266:21943-21947.
- Welling A, Lacinova L, Donatin K, Ludwig A, Bosse E, Flockerzi V, Hofmann F (1995) Expression of the L-type calcium channel with two different beta subunits and its modulation by Ro 40-5967. *Pflugers Arch* 429:400-411.
- West AE, Griffith EC, Greenberg ME (2002) Regulation of transcription factors by neuronal activity. *Nat Rev Neurosci* 3:921-931.
- Wicher D, Penzlin H (1997) Ca²⁺ currents in central insect neurons: electrophysiological and pharmacological properties. *J Neurophysiol* 77:186-199.
- Wielosz M, Mlynarczyk M, Kleinrok Z (1995) Effect of nifedipine on lithium-pilocarpine-induced seizures in the rats. *Pol J Pharmacol* 47:279-284.
- Williams ME, Feldman DH, McCue AF, Brenner R, Velicelebi G, Ellis SB, Harpold MM (1992) Structure and functional expression of alpha 1, alpha 2, and beta subunits of a novel human neuronal calcium channel subtype. *Neuron* 8:71-84.
- Xia XM, Fakler B, Rivard A, Wayman G, Johnson-Pais T, Keen JE, Ishii T, Hirschberg B, Bond CT, Lutsenko S, Maylie J, Adelman JP (1998) Mechanism of calcium gating in small-conductance calcium-activated potassium channels. *Nature* 395:503-507.

- Xu W, Lipscombe D (2001) Neuronal Ca(V)1.3alpha(1) L-type channels activate at relatively hyperpolarized membrane potentials and are incompletely inhibited by dihydropyridines. *J Neurosci* 21:5944-5951.
- Yamada N, Bilkey DK (1991) Nifedipine has paradoxical effects on the development of kindling but not on kindled seizures in amygdala-kindled rats. *Neuropharmacology* 30:501-505.
- Yasuda T, Chen L, Barr W, McRory JE, Lewis RJ, Adams DJ, Zamponi GW (2004) Auxiliary subunit regulation of high-voltage activated calcium channels expressed in mammalian cells. *Eur J Neurosci* 20:1-13.
- Zhen XG, Xie C, Yamada Y, Zhang Y, Doyle C, Yang J (2006) A single amino acid mutation attenuates rundown of voltage-gated calcium channels. *FEBS Lett* 580:5733-5738.
- Zhou Z, Bers DM (2000) Ca²⁺ influx via the L-type Ca²⁺ channel during tail current and above current reversal potential in ferret ventricular myocytes. *J Physiol* 523 Pt 1:57-66.
- Zong X, Hofmann F (1996) Ca(2+)-dependent inactivation of the class C L-type Ca²⁺ channel is a property of the alpha 1 subunit. *FEBS Lett* 378:121-125.
- Zuhlke RD, Pitt GS, Deisseroth K, Tsien RW, Reuter H (1999) Calmodulin supports both inactivation and facilitation of L-type calcium channels. *Nature* 399:159-162.
- www.uniprot.org/uniprot/Q13936 (30.10.2009)

Erklärung zu den Quellenangaben:

„Ich habe mich bemüht, sämtliche Inhaber der Bildrechte ausfindig zu machen und ihre Zustimmung zur Verwendung der Bilder eingeholt. Sollte dennoch eine Urheberrechtsverletzung bekannt werden, ersuche ich um Meldung bei mir.“

Michael Lagler, am 31.10.2009

6. APPENDIX

6.1. Kurzfassung

L-type spannungsabhängige Ca^{2+} -Kanäle (LTCC) erfüllen verschiedene Aufgaben in erregbaren Zellen. Unter anderem wurde gezeigt, dass LTCCs zur Erregungs-Transkription Kopplung betragen [Pinato et al. 2009, West et al. 2002]. Darüberhinaus hat die Aktivierung von LTCCs sowohl einen direkten, als auch indirekten Einfluss auf die Membranspannung. Letzteres erfolgt z.B. über die Aktivierung von Ca^{2+} -abhängigen K^{+} - [Lima and Marion 2007] und Kationen-Kanäle [Lee and Tepper 2007].

Im Zuge dieser Diplomarbeit wurde der Einfluss von LTCCs auf das Entladungsverhalten von hippocampalen Neuronen *in vitro* untersucht. Um das Membranpotential abzuleiten wurden „current clamp“-Experimente in der „perforated patch“-Konfiguration durchgeführt. I_{LTCC} wurde durch die Applikation von den Dihydropyridine BayK 8644 (Agonist) und isradipine (Antagonist) verstärkt bzw. verringert. Um spannungsaktivierte Na^{+} -Kanäle zu blockieren, deren Ströme die LTCC-induzierten Effekte überlagern würden, wurde bei allen „current clamp“-Experimenten TTX 500 nM zusätzlich appliziert. Die spannungsinduzierte Aktivierung der LTCCs erfolgte mittels 5 aufeinander folgender Strominjektionen ansteigender Stromstärke, die entweder eine Rechteck- oder Rampenform aufwiesen. Das Ziel dieser Experimente war es (I) den Schwellenwert der LTCC-Aktivierung zu bestimmen und (II) die LTCC-induzierte Kopplung zu Ca^{2+} -aktivierten Ionenkanälen zu untersuchen.

Die Analyse der Aktivierungsschwelle des L-type Ca^{2+} -Kanals ergab eine Population von Neuronen, deren Schwellenwerte größtenteils deutlich negativer als -35 mV lagen. Da bis dato keine neuronalen $\text{Ca}_v1.2$ -Kanalvarianten beschrieben worden sind, die negativer als -35 mV aktivieren würden, verweisen meine Daten auf einen bedeutenden Beitrag von $\text{Ca}_v1.3$ -Kanälen, deren Aktivierung allgemein um 10 - 15 mV negativer liegt als die der $\text{Ca}_v1.2$ -Kanäle. Dieses Ergebnis steht im krassen Gegensatz zu Untersuchungen an transgenen Tieren, deren Daten auf eine untergeordnete Rolle von $\text{Ca}_v1.3$ -Kanälen im ZNS verwiesen [Clark et al. 2003, Lacinova et al. 2008, Moosmang et al. 2005].

Nachpotentiale traten in meinen Ergebnissen in zwei unterschiedlichen Modalitäten auf: Nachhyperpolarisationen (AHPs) und Nachdepolarisationen (ADPs). Diesen wurden typischerweise schon unter Kontrollbedingungen (DMSO) ausgelöst und durch I_{LTCC} -Erhöhung mit BayK noch weiter verstärkt. Im Falle von 8 s andauernden depolarisierenden Strompulsen, überwiegte die Häufigkeit der AHPs klar. Aus pharmakologischer Sicht, konnten die AHPs als Apamin- und UCL 1684-sensitive und somit $K_{(Ca)}2.x/SK$ -vermittelt charakterisiert werden. Mittels Blockade von SK-Kanäle konnten zwei unterschiedliche AHP-Typen ausgemacht werden. Dies betraf das gleichzeitige Auftreten von AHPs und ADPs, was nur in einer Teilpopulation von hippocampalen Neuronen (50 %) nachgewiesen wurde (N = 5, Nachpotentialsfläche normalisiert auf DMSO mit BayK: -3.25, 8.05 oder BayK + apamin: 18.99, 22.72, $p < 0.01$). In der anderen Hälfte von Neuronen führte SK-Blockade lediglich zu einer Reduktion des AHPs (N = 10, Nachpotentialsfläche normalisiert auf DMSO mit BayK: -1.37, 1.30 oder BayK + apamin: 0.11, 1.00, $p < 0.001$). Mit Hilfe einer Außenlösung mit stark reduzierter $[Na^+]$ zusammen mit Isradipine konnte nachgewiesen werden, dass es sich bei I_{ADP} um einen Ca^{2+} -aktivierten Na^+ -leitenden Ionenkanal handelt (N = 7, Nachpotentialsfläche normalisiert auf DMSO mit BayK + apamin = 2.22, 3.99 oder low Na^+ /BayK + apamin = 0.34, 0.68, $p < 0.01$, alle Werte sind dargestellt als Median und dem Interquartilabstand). Nach der Identifizierung der zugrunde liegenden Kanäle wurden die LTCC-induzieren Nachpotentiale in Abhängigkeit von der Stimulusintensität untersucht. Zu diesem Zweck wurden sowohl Pulslängen, als auch -stärken variiert. Daraus resultierende Ergebnisse weisen darauf hin, dass es zwischen SK- und CAN-Kanälen Unterschied in der Kopplungseffizienz gibt. Im Speziellen wurden ADPs bei kürzeren Pulsen (< 500 ms) ausgelöst, wogegen AHPs erst bei langanhaltenden Pulse (> 2 s) entstanden.

Anschließend wurde die Validität des Kopplungs-Modells im Bezug auf die physiologische Feueraktivität von Hippocampus-Neuronen getestet. Da das Entladungsverhalten von hippocampalen Neuronen in der Regel aus eher kurzen Depolarisationen (< 1 s) besteht, würde man anhand des Kopplungsmodells für diese Neurone eine stärkere LTCC-CAN- als LTCC-SK-Kopplung erwarten. Diese Vorhersage stimmte in der Tat mit den experimentellen Beobachtungen in unserer Kultur überein, indem 80 % der Neurone mit BayK ihre Feueraktivität verstärkten.

Daraus schlussfolgere ich, dass die funktionale Kopplung von L-type Ca^{2+} -Kanälen an ADP-bildende CAN-Kanäle sowie AHP-bildende SK-Kanäle einen wichtigen Mechanismus zur Regulation hippocampal Entladungsaktivität darstellt. Etwaige physiologische Implikationen sind im Falle der ADPs die Verstärkung von unterschwelligen Potentialen und im Falle der AHPs ein negativer Rückkopplungsmechanismus zur Unterbindung excitoxischer Plateaupotentiale [Ping and Sheppard 1999]. Zusammenfassend weisen meine Ergebnisse darauf hin, dass in primären hippocampalen Neuronen sowohl $Ca_v1.2$, als auch $Ca_v1.3$ aktiv sind und zeigen, dass (I) SK- und CAN-Kanäle funktional an L-type Ca^{2+} -Kanäle koppeln, dass (II) in den meisten getesteten Neuronen eine Überlagerung beider Nachpotential-Modalitäten stattfindet und dass (III) sich diese beiden Nachpotentiale in der Effizienz der LTCC-Kopplung unterscheiden.

6.2. Calculations of the LJP

6.2.1. For whole cell configuration (fig. 6, left)

- 1) bath, offset correction U_{offset} , without LJP corrected:
pipette offset potentials $1/2 + \text{LJP} - U_{\text{offset}} = 0 \text{ mV}$ (fig. 5.1)
- 2) cell attached mode, without LJP corrected:
Upipette offset $1/2 - U_{\text{offset}} = -\text{LJP} = -17.6 \text{ mV} \rightarrow \text{LJP} = 17.6 \text{ mV}$ (fig. 5.2)
- 3) bath, theoretical correction of LJP: $U_{\text{offset}} - (U_{\text{offset}} - \text{LJP}) = \text{LJP}$ (fig. 5.4)
- 4) cell attached, theoretical correction of LJP:
Upipette offset $1/2 - (U_{\text{offset}} - \text{LJP}) = 0 \text{ mV}$ (fig. 5.5)
- 5) theoretical assumption for E_{Cl} with $7 \text{ mM } [\text{Cl}]_i$: $-78.6 \text{ mV} + 17.6 \text{ mV} = -61.0 \text{ mV}$
(without LJP corrected, fig. 5.3) or $-78.6 \text{ mV} + 17.6 \text{ mV} - 17.6 \text{ mV} = -78.6 \text{ mV}$
(with LJP corrected, fig. 5.6)
- 6) measured E_{Cl} with $7 \text{ mM } [\text{Cl}]_i$ and without corrected LJP: -70.5 mV
- 7) experimentally determined LJP: $-70.5 - (-78.6 \text{ mV}) = 8.1 \text{ mV}$,
which is comparable with the value published by [Podlogar and Dietrich 2006]
- 8) difference between theoretically and experimentally determined LJP:
 $17.6 \text{ mV} - 8.1 \text{ mV} = 9.5 \text{ mV}$, 9) theoretically assumed E_{Cl} with $x \text{ mM } [\text{Cl}]_i$
and with LJP corrected: $-70.5 \text{ mV} - 17.6 \text{ mV} = -88.1 \text{ mV}$, 10)
experimentally assumed $[\text{Cl}]_i$: $[\text{Cl}]_i = 4.9 \text{ mM}$

6.2.2. For perforated Patch configuration (fig. 6, right)

- 1) cell 1: LJP (if $[\text{Cl}]_i = 7 \text{ mM}$) = $-93.7 \text{ mV} - (-78.6 \text{ mV}) = -15.1 \text{ mV}$
- 2) cell 1: E_{Cl} (if LJP = 17.6 mV) = $-93.7 \text{ mV} - 17.6 \text{ mV} = -111.3 \text{ mV} \rightarrow [\text{Cl}]_i = 2.0 \text{ mM}$
- 3) cell 2: LJP (if $[\text{Cl}]_i = 7 \text{ mM}$) = $-89.7 \text{ mV} - (-78.6 \text{ mV}) = -11.1 \text{ mV}$
- 4) cell 2: E_{Cl} (if LJP = 17.6 mV) = $-89.7 \text{ mV} - 17.6 \text{ mV} = -107.3 \text{ mV} \rightarrow [\text{Cl}]_i = 2.3 \text{ mM}$
- 5) cell 3: LJP (if $[\text{Cl}]_i = 7 \text{ mM}$) = $-54.4 \text{ mV} - (-78.6 \text{ mV}) = 24.2 \text{ mV}$
- 6) cell 3: E_{Cl} (if LJP = 17.6 mV) = $-54.4 \text{ mV} - 17.6 \text{ mV} = -72.0 \text{ mV} \rightarrow [\text{Cl}]_i = 9.2 \text{ mM}$.

6.3. Statistics for Chapter 3.2.1.1. and 3.2.1.2.

All values are given as median/interquartile range normalized to DMSO and tested by a Kruskal Wallis H test and Dunn's post hoc test.

Afterpotential-area: "AHP↓"-AHP-forming cells: BayK: -1.37/1.30, BayK + apamin: -0.11/1.00, isradipine: -0.03/0.61, isradipine + apamin: -0.01/0.57; N = 10: H = 16.46, $p < 0.001$. Post hoc test: DMSO vs. BayK: $p > 0.05$, DMSO vs. BayK + apamin: $p < 0.05$, DMSO vs. isradipine: $p > 0.05$, DMSO vs. isradipine + apamin: $p < 0.05$, BayK vs. BayK + apamin: $p < 0.001$, BayK vs. isradipine: $p < 0.001$, BayK vs. isradipine + apamin: $p < 0.001$, BayK + apamin vs. isradipine: $p > 0.05$, BayK + apamin vs. isradipine + apamin: $p > 0.05$, isradipine vs. isradipine + apamin: $p > 0.05$

Afterpotential-amplitude: "AHP↓"-AHP-forming cells: BayK: -1.29/0.58, BayK + apamin: -0.51/0.52, isradipine: -0.76/1.17, isradipine + apamin: -0.55/1.65; N = 10: H = 28.30, $p < 0.001$; Post hoc test: DMSO vs. BayK: $p > 0.05$, DMSO vs. BayK + apamin: $p > 0.05$, DMSO vs. isradipine: $p > 0.05$, DMSO vs. isradipine + apamin: $p > 0.05$, BayK vs. BayK + apamin: $p < 0.001$, BayK vs. isradipine: $p < 0.01$, BayK vs. isradipine + apamin: $p < 0.001$, BayK + apamin vs. isradipine: $p > 0.05$, BayK + apamin vs. isradipine + apamin: $p > 0.05$, isradipine vs. isradipine + apamin: $p > 0.05$

Afterpotential-area: "ADP"-AHP-forming cells: BayK: -3.25/8.05, BayK + apamin: 18.99/22.72, isradipine: 0.38/2.74, isradipine + apamin: 0.08; N = 5: H = 16.46, $p < 0.01$; Post hoc test: DMSO vs. BayK: $p > 0.05$, DMSO vs. BayK + apamin: $p > 0.05$, DMSO vs. isradipine: $p > 0.05$, DMSO vs. isradipine + apamin: $p > 0.05$, BayK vs. BayK + apamin: $p < 0.01$, BayK vs. isradipine: $p > 0.05$, BayK vs. isradipine + apamin: $p > 0.05$, BayK + apamin vs. isradipine: $p > 0.05$, BayK + apamin vs. isradipine + apamin: $p > 0.05$, isradipine vs. isradipine + apamin: $p > 0.05$

Afterpotential-amplitude: "ADP"-AHP-forming cells: BayK: -1.22/1.32, BayK + apamin: 1.92/2.19, isradipine: -0.26/1.83, isradipine + apamin: 0.54/2.14; N = 5: H = 24.14, $p < 0.001$; Post hoc test: DMSO vs. BayK: $p > 0.05$, DMSO vs. BayK + apamin: $p < 0.01$, DMSO vs. isradipine: $p > 0.05$, DMSO vs. isradipine + apamin: $p > 0.05$, BayK vs. BayK + apamin: $p < 0.001$, BayK vs. isradipine: $p > 0.05$, BayK vs. isradipine + apamin: $p > 0.05$, BayK + apamin vs. isradipine: $p > 0.05$, BayK + apamin vs. isradipine + apamin: $p > 0.05$, isradipine vs. isradipine + apamin: $p > 0.05$

Afterpotential-area: "ADP"-AHP-forming cells: BayK: -0.71/1.97, BayK + UCL 1684: 0.35/0.53, isradipine: -0.03/0.14, isradipine + UCL 1684: -0.01/0.29; N = 5: H = 18.33, $p < 0.01$; Post hoc test: DMSO vs. BayK: $p > 0.05$, DMSO vs. BayK + UCL 1684: $p < 0.001$, DMSO vs. isradipine: $p > 0.05$, DMSO vs. isradipine + UCL 1684: $p > 0.05$, BayK vs. BayK + UCL 1684: $p < 0.05$, BayK vs. isradipine: $p > 0.05$, BayK vs. isradipine + UCL 1684: $p > 0.05$, BayK + UCL 1684 vs. isradipine: $p > 0.05$, BayK + UCL 1684 vs. isradipine + UCL 1684: $p > 0.05$, isradipine vs. isradipine + UCL 1684: $p > 0.05$

Afterpotential-amplitude: “ADP”-AHP-forming cells: BayK: -0.62/0.96, BayK + UCL 1684: 0.85/1.06, isradipine: -0.36/0.20, isradipine + UCL 1684: -0.31/0.11; N = 5: H = 18.63, $p < 0.001$; Post hoc test: DMSO vs. BayK: $p > 0.05$, DMSO vs. BayK + UCL 1684: $p < 0.001$, DMSO vs. isradipine: $p > 0.05$, DMSO vs. isradipine + UCL 1684: $p > 0.05$, BayK vs. BayK + UCL 1684: $p > 0.05$, BayK vs. isradipine: $p > 0.05$, BayK vs. isradipine + UCL 1684: $p > 0.05$, BayK + UCL 1684 vs. isradipine: $p > 0.05$, BayK + UCL 1684 vs. isradipine + UCL 1684: $p > 0.05$, isradipine vs. isradipine + UCL 1684: $p > 0.05$

Afterpotential-area: ADP-forming cells: BayK: 1.48/137, BayK + apamin: 2.87/3.39, isradipine: -0.03/0.07, isradipine + apamin: -0.08

Afterpotential-amplitude: ADP-forming cells: BayK: 1.09/0.14, BayK + apamin: 1.30/0.66, isradipine: -0.12/0.31, isradipine + apamin: -0.10

Afterpotential-area: ADP-forming cells: BayK: 1.50/0.63, BayK + apamin: 2.22/3.99, low Na^+ - BayK + apamin: 0.34/0.68, BayK + apamin wash out: 1.85/0.87, isradipine: 0.02/0.13, isradipine + apamin: 0.02/0.12, low Na^+ - isradipine + apamin: 0.21/0.42; N = 7: H = 47.64, $p < 0.001$; Post hoc test: BayK + apamin vs. low Na^+ - BayK + apamin: $p < 0.01$, BayK + apamin vs. BayK + apamin wash out: $p > 0.05$, low Na^+ - BayK + apamin vs. BayK + apamin wash out: $p < 0.01$

Afterpotential-amplitude: ADP-forming cells: BayK: 1.04/0.20, BayK + apamin: 1.13/0.25, low Na^+ - BayK + apamin: 0.62/0.29, BayK + apamin wash out: 1.10/0.2, isradipine: 0.18/0.50, isradipine + apamin: 0.18/0.50, low Na^+ - isradipine + apamin: 0.29/0.92, N = 7: H = 40.14, $p < 0.001$; Post hoc test: BayK + apamin vs. low Na^+ - BayK + apamin: $p < 0.01$, BayK + apamin vs. BayK + apamin wash out: $p > 0.05$, low Na^+ - BayK + apamin vs. BayK + apamin wash out: $p > 0.05$

ACKNOWLEDGEMENTS

First of all, I want to thank Helmut Kubista for the opportunity of working in his FWF project (P19710) and writing this diploma thesis.

Also, I want to thank Petra Geier who prepared most of the cell cultures for me and taught me how to prepare them myself.

Special thanks go to Klaus Schicker for always having time for my problems and questions and for providing his expertise in electrophysiology.

Moreover, I want to thank Xaver König for the helpful discussions and comments on my diploma thesis and Nina Krako who generated the DHP-insensitive constructs.

Besides that I want to thank everybody in the lab for helping me and especially Stefan Boehm for being able to work in his lab.

Finally, I want to thank my sister for her support and help and my parents for making everything possible.

MICHAEL LAGLER



1100 Vienna, Troststraße 74/2/4
0676/5423525
michael.lagler@gmx.at

Personal Data

Date of Birth	December 14, 1984
Place of Birth	St. Poelten (Lower Austria)
Nationality	Austria
Marital status	single, no children

Education

2008 - 2009	Diploma thesis at the Pharmacological Institute of the Medical University of Vienna with focus on "The role of voltage activated calcium channels in hippocampal discharge activity" in the lab of Univ-Prof. Dr. Stefan Boehm, supervised by Univ-Prof. Dr. Karlheinz Hilber and Univ-Prof. Dr. Steffen Hering (University of Vienna)
2006 - 2008	Study of Zoology at the University of Vienna with main focus on neurobiology and the diploma subject "Pharmacology and Toxicology"
2004 - 2006	Study of Biology at the University of Vienna
1995 - 2003	Grammar school in Lilienfeld (Lower Austria)
1991 - 1995	Elementary school in Wilhelmsburg (Lower Austria)

Special Training Courses

Neurobiological courses	Different electrophysiological and microscopic methods, measurement technology, neuroanatomy, sensory physiology, biomechanics, biology of cognition and behavioral biology
Pharmacological courses	Toxicology, pharmakogenetics and cell biology
Others	Biostatistics

Scholarships

2005, 2006, 2008	Academic excellence Scholarship given by the University of Vienna
2008	Diploma Scholarship given by the FWF

MICHAEL LAGLER 1100 VIENNA, TROSTSTRASSE 74/2/4
 0676/5423525
 MICHAEL.LAGLER@GMX.AT

Skills

Language skills English fluent in spoken and written, basics in French
 Computer skills Software knowledge (MS-Office, Adobe Creative Suite, Endnote, Statistica, GraphPad Prism, SPSS, SigmaPlot, pClamp, Leica Confocal Software, Philips XL20 microscope control and Scandium)

Scientific skills

Electrophysiology One and two electrode voltage clamp, one electrode current clamp, intra- and extracellular recordings
 Neuroanatomy Neurobiotin labeling
 Microscopy Fluorescence microscopy, confocal microscopy, electron microscopy
 Cell biology, molecular biology Primary cultures (e.g. hippocampus) of mice and rats, stable cell lines, *Xenopus* oocytes, DNA amplification, transfections, PCR, RFLP
 Statistics Univariate, multivariate and explorative methods

Congress attendance

2009 ANA meeting, poster presentation: Opposing LTCC-Couplings regulate hippocampal discharge activity
 2008 Retreat of Center of Biomolecular Medicine and Pharmacology, poster presentation: L-type voltage gated calcium channels differently contribute to electrical activity of hippocampal neurons

Employment history

2008 - 2009 Diploma student at the Pharmacological Institute of the Medical University of Vienna
 2007 Teaching assistant at the University of Vienna
 2004 Salzer Papier GmbH
 2003 - 2004 Austria Armed Forces (rank: Lance-Corporal)
 2002 GW St. Poelten GmbH (work with mentally disordered people)

Outside interests

Sports, hobbies Tennis, hiking, diving, snowboarding, photography
 Reading Daily newspaper, scientific magazines, literature
 Travelling Get to know new cultures, landscapes and languages